

QUANTIFYING HUMAN IMPACTS ON NATURAL RATES OF  
EROSION ALONG CONTINENTAL MARGINS

A Dissertation Presented

by

Lucas Jonathan Reusser

to

The Faculty of the Graduate College

of

The University of Vermont

In Partial Fulfillment of the Requirements  
for the Degree of Doctor of Philosophy specializing  
Natural Resources

May, 2014



Accepted by the Faculty of the Graduate College, The University of Vermont, in partial fulfillment of the requirements for the degree of Doctor of Philosophy, specializing in Natural Resources.

Thesis Examination Committee:

\_\_\_\_\_  
Paul R. Bierman, Ph.D. Advisor

\_\_\_\_\_  
Beverley C. Wemple, Ph.D.

\_\_\_\_\_  
Austin R. Troy, Ph.D.

\_\_\_\_\_  
Donna M. Rizzo, Ph. D. Chairperson

\_\_\_\_\_  
Cynthia J. Forehand, Ph.D. Dean, Graduate College,

Date: December 2<sup>nd</sup>, 2013

## ABSTRACT

Human activities such as agriculture, development, mineral extraction, and land clearance, move more material at Earth's surface than any natural process. Quantifying natural, or background rates of landscape erosion is prerequisite to understanding the impact of human landuse practices on natural process rates. Through the clearance of hillslopes, human activities have profoundly altered the source areas of sediment in drainage basins, and the mixing of sediment in river networks around the globe. Traditional approaches used to quantify the mass of sediment moving through fluvial systems (such as contemporary sediment yield data) are typically uncertain and often biased, and thus do not reflect background rates of erosion.

This research utilizes concentrations of both meteoric and *in situ*  $^{10}\text{Be}$  measured in samples of river sediment to locate source areas of disproportionately high sediment production and to estimate rates of long-term background erosion in order to quantify human-impacts on natural erosion rates in two locations; 1) the east coast of New Zealand's North Island, and 2) the southern Appalachian Piedmont draining the North American Atlantic passive margin. While these two regions represent very different geologic and climate conditions, they share a common history of intensive land clearance for agriculture, peaking in the early 1900's, and the ensuing erosional consequences.

In the Waipaoa River Basin, New Zealand, concentrations of meteoric  $^{10}\text{Be}$  in river sediment trace the mixing of sediment from tributary basins characterized by different erosion styles as they mix downstream. A simple mixing model indicates that the heavily gullied headwater regions of the Waipaoa river system produce sediment at a rate  $\sim 20$  times that of the eastern and western tributaries. A limited number of *in situ*  $^{10}\text{Be}$  measurement suggest that the Waipaoa landscape erodes naturally at a rate of  $\sim 300$  m/My, nearly 10 times slower than the modern, human-induced sediment output from the catchment.

*In situ*  $^{10}\text{Be}$  data from the southern Appalachian Piedmont suggest that the region naturally erodes more than 100 times more slowly ( $\sim 9$  vs.  $\sim 950$  m/My) than during the period of peak agricultural use. Further, a carefully designed sampling strategy robustly characterizes background erosion rates at the landscape-scale, and allows for the prediction of background erosion rates at any point across the Piedmont with a simple yet strong ( $R^2 = 0.88$ ) average basin slope-based regression model.

Findings from both studies provide valuable information for improving our ability to manage landscapes affected by human activities. Meteoric  $^{10}\text{Be}$ -based mixing models, such as those generated in the Waipaoa Basin, can apportion the relative contribution of sediment from different regions on non-uniformly eroding landscapes, while landscape-based predictive erosion models, such as that produced for the southern Piedmont, can inform total maximum daily load values for sediment and associated pollutants.

## CITATIONS

Material from this dissertation has been published in the following forms:

Reusser, L.J. and Bierman, P.R.. (2010). Using meteoric  $^{10}\text{Be}$  to track fluvial sand through the Waipaoa River basin, New Zealand. *Geology*, 38, 1, 47-50, doi: 10.1130/G30395.1.

Reusser, L.J., Graly, J., Bierman, P.R., and Rood, D.. (2010). Calibrating a long-term meteoric  $^{10}\text{Be}$  accumulation rate in soil. *Geophysical Research Letters*, 37, 19, L19403, doi: 10.1029/2010GL044751.

## ACKNOWLEDGEMENTS

There are a great many individuals and organizations that deserve my sincere gratitude for their support and contribution to this research. I would of course like to thank the National Science Foundation and the U.S. Geological Survey for funding this research, and also the University of Vermont for their support following the burning of the Cosmogenic Laboratory toward the beginning of my dissertation work.

I would especially like to thank Matthew Jungers and William Hackett for their endless help with fieldwork in places as far away as the Tarndale Slip in New Zealand, to the coastlines of the Pacific Northwest, to the sleepy towns of the Blue Ridge Mountains. I would further like to thank Basil Gomez for introducing us to the Waipaoa Field area and providing many hours of useful discussions while interpreting cosmogenic data from this complex landscape. I thank Kelin Whipple and Benjamin Crosby for many days of tromping through streams of the Waipaoa Basin. Mike Marden of Landcare Research constituted not only an inexhaustible source of knowledge concerning the history of the Waipaoa Landscape, but also provided logistical support during several long and wet field seasons. Finally, I would like to sincerely thank Jenny and Gindy for providing us with a home away from home at Te Hau station.

The laboratory work for this research would not have been possible without the generosity of several key researchers and institutions. I offer my deepest gratitude to both Dr. John Stone at the University of Washington and Dr. Ari Matmon at Hebrew University, Israel, for opening their laboratories to me. I would like to again thank Matthew Jungers for assisting me in processing nearly one hundred meteoric samples in

Ari Matmon's laboratory in only three weeks. I of course thank Dylan Rood at CAMS for his time and help measuring countless meteoric and *in situ* <sup>10</sup>Be samples resulting from this research. And where would I be without my graduate student cohorts. I thank them all for their friendship, support, good times, and many fruitful geologic discussions.

I offer my deepest gratitude to my advisor Dr. Paul Bierman for his never ceasing help, guidance, knowledge, and more than anything his professional and personal support. Over the course of working with him for more than ten years, he has proven himself time and time again to be an exceptional and incisive scientist, an advisor that all graduate students could only hope to be lucky enough to have, and a wonderful father. I could never hope to repay him for all he has given; instead I will look for opportunities to pay forward these lessons I have learned to others I encounter in my life. In addition to Paul, I offer my sincere thanks to the rest of my committee members, Dr. Donna Rizzo, Dr. Beverley Wemple, and Dr. Austin Troy for all of their time, help and guidance over the course of my dissertation work.

Finally, and most of all, I thank my family and friends. My parents, Jonathan and Christina and my sister Meghan as well as her new husband Jono for all of their love and support. They are each exceptional individuals without whom I could never have made it through this experience.

## TABLE OF CONTENTS

ACKNOWLEDGEMENTS .....	iii
LIST OF TABLES .....	viii
LIST OF FIGURES .....	ix
CHAPTER 1: INTRODUCTION .....	1
1.1. Human impacts on background rates of landscape erosion .....	2
1.2. Utility of meteoric $^{10}\text{Be}$ in landscape erosion studies .....	4
1.3. Modeling background erosion rates from concentration of <i>in situ</i> $^{10}\text{Be}$ .....	5
1.4. Study areas and research objectives .....	6
1.6. Structure of Dissertation .....	9
CHAPTER 2: (PUBLISHED IN <i>GEOLOGY</i> ) USING METEORIC $^{10}\text{Be}$ TO TRACK FLUVIAL SAND THROUGH THE WAIPAEOA RIVER BASIN, NEW ZEALAND ...	11
2.1. Abstract .....	12
2.2. Introduction .....	13
2.3. Meteoric $^{10}\text{Be}$ .....	14
2.4. Waipaoa River basin .....	15
2.5. Methods .....	16
2.6. Results .....	17
2.7. Meteoric $^{10}\text{Be}$ as a useful tracer of fluvial sediment sources .....	18
2.8. Implications and future research .....	20
2.9. Acknowledgements .....	20
2.10. Referenced cited .....	21
2.11. Figure captions .....	25
2.12. Data Repository .....	30
CHAPTER 3: (PUBLISHED IN <i>GEOPHYSICAL RESEARCH LETTERS</i> ) CALIBRATING A LONG-TERM METEORIC $^{10}\text{Be}$ ACCUMULATION RATE IN SOIL .....	37
3.1. Abstract .....	38
3.2. Introduction .....	38
3.3. Behavior of meteoric $^{10}\text{Be}$ .....	39
3.4. Geologic setting .....	41
3.5. Age of sampled profile .....	42
3.6. Sampling and analysis techniques .....	43
3.7. Long-term meteoric $^{10}\text{Be}$ delivery rate .....	44
3.8. Discussion .....	46
3.9. Implications .....	47

3.10. References cited .....	49
3.11. Figure captions .....	55
3.12. Auxiliary Information .....	58
CHAPTER 4: (FOR SUBMISSION TO <i>GSA BULLETIN</i> ) USING $^{10}\text{Be}$ AS A TRACER OF LANDSCAPE PROCESSES IN AN EXTREME GEOMORPHIC ENVIRONMENT, WAIPAUA RIVER BASIN, NORTH ISLAND, NEW ZEALAND .....	60
4.1. Abstract .....	61
4.2. Introduction .....	62
4.3. Geologic and Geographic setting .....	64
4.4. Methods .....	65
4.5. Data .....	66
4.6. Discussion .....	72
4.7. References Cited: .....	77
4.8. Figure Captions: .....	81
CHAPTER 5: (FOR SUBMISSION TO <i>NATURE GEOSCIENCE</i> ) QUANTIFYING HUMAN IMPACTS ON RATES OF EROSION AND SEDIMENT TRANSPORT AT A LANDSCAPE-SCALE .....	104
5.1. Introductory paragraph .....	105
5.2. Article text .....	105
5.3. Methods .....	111
5.4. Acknowledgements .....	112
5.5. Author contributions .....	112
5.6. References cited .....	112
5.7. Figure captions .....	118
5.8. Supplemental information .....	122
CHAPTER 6: (FOR SUBMISSION TO <i>JOURNAL OF GEOPHYSICAL RESEARCH: EARTH SURFACE</i> ) ROBUSTLY CHARACTERIZING LANDSCAPE-SCALE EROSION WITH <i>IN SITU</i> $^{10}\text{Be}$ .....	123
6.1. Abstract .....	124
6.2. Introduction .....	125
6.3. Background .....	126
6.4 Methods .....	127
6.5. Results .....	132
6.6. Discussion .....	135
6.7. Conclusions .....	140
6.8. References cited .....	141
6.9. Acknowledgments .....	146
6.10. Figure captions .....	147
CHAPTER 7: CONCLUSIONS AND FUTURE RESEARCH .....	160
7.1. Summary of findings .....	160

7.2. Suggestion for future research .....	164
COMPREHENSIVE BIBLIOGRAPHY .....	168

## LIST OF TABLES

Table 2 - 1 (DR-1) Summary information for all samples presented in the New Zealand, meteoric $^{10}\text{Be}$ article published in <i>Geology</i> . .....	34
Table 2 - 2 (DR-2) Soil profile from the Te Arai basin, SW Waipaoa basin. ....	35
Table 3 - 1 (Auxiliary Table 1) Summary information for all sample in the Waipaoa 1 Terrace depth profile published in <i>Geophysical Research Letters</i> . ....	58
Table 4 - 1 <i>In situ</i> $^{10}\text{Be}$ laboratory replication results.....	98
Table 4 - 2 Meteoric $^{10}\text{Be}$ laboratory replication results.....	99
Table 4 - 3 <i>In situ</i> $^{10}\text{Be}$ temporal variability results.....	100
Table 4 - 4 Meteoric $^{10}\text{Be}$ temporal variability results .....	101
Table 4 - 5 Distribution of <i>in situ</i> $^{10}\text{Be}$ concentrations .....	102
Table 4 - 6 Distribution of meteoric $^{10}\text{Be}$ concentrations.....	103
Table 5 - 1 (Supplemental Table S1) Summary data table for data presented in Nature Geoscience paper. ....	122
Table 6 - 1 (Supplemental Table S1) Summary information for all large-scale basins from the southern Appalachian Piedmont.....	158
Table 6 - 2 (Supplemental Table S2) Summary information for all 37 small-scale slope-test samples. ....	159

## LIST OF FIGURES

Figure 2 - 1	Location map for the Waipaoa River Basin, North Island New Zealand. ....	27
Figure 2 - 2	Schematic representation of sediment sourcing.....	28
Figure 2 - 3	Synthesis of data presented in this study.....	29
Figure 2 - 4 (DR-1)	Map depicts the four samples used in the mixing model used to determine proportionally how much sediment originates in the northern headwater regions of the Waipaoa basin vs. the eastern and western regions of the basin. ....	33
Figure 3 - 1	Calibration profile located in the middle Waipaoa River basin, North Island, New Zealand. ....	56
Figure 3 - 2	Meteoric $^{10}\text{Be}$ concentration results for the depth profile.....	57
Figure 3 - 3 (Auxiliary Figure 1)	Calibrated age for depth profile in the Waipaoa 1 Terrace. ....	59
Figure 4 - 1	Location map for the Waipaoa River Basin showing the influence of gullies on channel sediments .....	85
Figure 4 - 2	<i>In situ</i> $^{10}\text{Be}$ laboratory replicates.....	86
Figure 4 - 3	Meteoric $^{10}\text{Be}$ laboratory replicates .....	87
Figure 4 - 4	<i>In situ</i> $^{10}\text{Be}$ temporal variability.....	88
Figure 4 - 5	Meteoric $^{10}\text{Be}$ temporal variability.....	89
Figure 4 - 6	Map depicting points of interest along the Waipaoa River mainstem from figure 7 and discussed in the text.....	90
Figure 4 - 7	Temporal variance in meteoric $^{10}\text{Be}$ concentrations as a function of drainage basin area .....	91
Figure 4 - 8	Depth-distribution of meteoric $^{10}\text{Be}$ concentrations within soil samples from the Waimata hillslope .....	92
Figure 4 - 9	Distribution of <i>in situ</i> $^{10}\text{Be}$ across the study area.....	93

Figure 4 - 10 Distribution of meteoric $^{10}\text{Be}$ concentration across the landscape.....	94
Figure 4 - 11 <i>In situ</i> and meteoric $^{10}\text{Be}$ concentrations from the 18 comparison samples .....	95
Figure 4 - 12 Normalized concentrations of <i>in situ</i> an meteoric $^{10}\text{Be}$ concentrations .....	96
Figure 4 - 13 Estimates of background erosion made with concentrations of <i>in situ</i> $^{10}\text{Be}$ compared to other previously proxy estimates .....	97
Figure 5 - 1 Location map for the Southern Appalachian Piedmont, USA .....	119
Figure 5 - 2 Conceptual diagram of measurement integration times, land clearance conditions, landcover conditions, hillslope conditions, sediment loads, and sediment storage .....	120
Figure 5 - 3 Compilation of hillslope erosion rates, sediment yield rates, and background $^{10}\text{Be}$ background erosion rates. ....	121
Figure 6 - 1 Location map for the southern Appalachian Piedmont draining the North American Atlantic Passive Margin .....	150
Figure 6 - 2 The four basins out of ten Piedmont drainages summarized and used to generate the slope-test.....	151
Figure 6 - 3 Frequency distribution of average basin slopes for all sub-basin with the four large basins in Figure 2 used to select the 40 slope-test samples .....	152
Figure 6 - 4 Results from the small-basin slope test. The avererage basin slope vs. erosion rate relationship is used to predict rates in basin without $^{10}\text{Be}$ data.....	153
Figure 6 - 5 Relationships between our measured $^{10}\text{Be}$ erosion rates, and the aggregated $E_{ps}$ predicted erosion rates for large basins.....	154
Figure 6 - 6 A: compilation of $^{10}\text{Be}$ erosion rates and $E_{ps}$ predicted erosion rates for all large-scale outlet basins, and B: basin-by-basin average values several morphometric and meteorological variables.....	155
Figure 6 - 7 Effects of spatial scaling on $E_{ps}$ predicted erosion rate using the amalgamated approach vs. the whole-basin approach.....	156
Figure 6 - 8 Example of sample site located below a large hydroelectric dam along the Savannah River showing the eroding bluff in the background.....	157

## CHAPTER 1: INTRODUCTION

The issue of how quickly, in what manner, and why those portions of our planet standing above the sea erode has been studied extensively by earth scientists for far longer than a century (e.g. Gilbert, 1877; Davis, 1889). The concept of erosion is multifaceted and can be studied from a number of different spatial and/or temporal perspectives depending upon what “erosion” actually constitutes in regard to the questions being asked. For example, erosion can encompass the redistribution of material from one area to another across a landscape (e.g. Gomez et al., 2003; Hicks et al., 2000; Marden et al., 2005; Phillips, 2003; Trimble, 1977), the mass of sediment drained from continental landmasses to the sea (e.g. Syvitski et al., 2005; Wilkinson and McElroy, 2007), and/or the gradual lowering of mean elevations across broad geographic regions, a condition ironically often accompanied by the uplift of mountain peaks (e.g. England and Molnar, 1990; Montgomery, 1994). Operating over geologic timeframes and at continental to regional scales, landscape erosion, global climate, and tectonics are intricately interconnected (e.g. Harris and Mix, 2002; Molnar and England, 1990). However, for the work I present here, I investigate erosion at the regional- to drainage basin-scale, over timeframes ranging from years to millennia, in order to quantify the impacts that human landuse practices have had on background or “natural” rates of landscape erosion as well as on the sourcing of river sediment during the historic era.

### **1.1. Human impacts on background rates of landscape erosion**

Human activities such as agriculture, development, mineral extraction, and land clearance, move more material at Earth's surface than any other natural process (e.g. Hooke, 1994, 2000). Human activities affect how quickly landscapes erode today, and the pace at which sediment moves down hillslopes and into river channels. Human landuse practices have the ability to disrupt and often fundamentally change the natural processes and rates that have governed landscape evolution over much longer timeframes (e.g. Wilkinson and McElroy, 2007). Land clearance for agriculture can accelerate rates of hillslope erosion and increase the load of sediment carried by streams by several orders of magnitude (Meade, 1969), often resulting in channel aggradation and massive flooding on downstream floodplains (Hicks et al., 2000; Team, 1994). In tectonically active regions underlain by weak rocks, land clearance can cause detrimental erosional features (i.e. large amphitheater gullies), that continuously shed large quantities of sediment that can alter entire fluvial networks even though these features may only represent several percent of a landscape as a whole (Gomez et al., 2003; Hicks et al., 2000; Marden, 2004; Marden et al., 2008). Even if efforts to stabilize the landscape have been made following episodes of landscape disturbance, the volume of sediment carried by rivers no longer represents natural conditions (Kirchner et al., 2001; Meade, 1969). Disproportionately high rates of hillslope erosion during brief periods of human-induced landscape disturbance can result in large volumes of sediment going into storage across the landscape (Gomez et al., 2003; Meade, 1982; Phillips, 2003). This legacy sediment can take decades to centuries to be evacuated from fluvial systems, and may cause sediment

loads to remain elevated long after landscape stabilization and recovery have occurred (e.g. Marden, 2004; Marden et al., 2005; Meade, 1982; Walter and Merritts, 2008). One further complication is that most large rivers around the globe harbor dams designed either for flood control or power generation. Dams impound not only water but also sediment, in turn further extending the recovery time of landscapes following past disturbances. While human activities have substantially elevated the load of sediment transported by major river systems worldwide (Wilkinson and McElroy, 2007), artificially constructed reservoirs have actually reduced the amount of sediment that reaches the sea (Syvitski et al., 2005).

Quantifying natural, or background rates of landscape erosion, is prerequisite to understanding the impact of human activities on natural process rates (National Research Council, 2010). Over human time scales, one of the most commonly employed methods for estimating the mass of material carried off landscapes is the measurement of river sediment loads (Judson and Ritter, 1964; Menard, 1961; Walling, 1999). However, contemporary sediment yield data rarely reflect long-term background rates of erosion (e.g. Ahnert, 1970; Meade, 1969). Human-landscape interactions can generate sediment yields and inferred erosion rates that are elevated by more than an order of magnitude over background rates (Meade, 1969). Alternatively, sediment yield records are often short (years to decades) and thus may miss large volumes of sediment delivered to rivers during high-magnitude, low frequency events (Kirchner et al., 2001; Wolman and Miller, 1960). Further, if the erosion following human-disturbance outpaces the rate at which streams can transport the material fed to them, sediment yield data represent neither

natural erosion nor the maximum degree of upstream erosion. Instead, such streams are transport-limited systems in which sediment yield data represent the maximum carrying capacity of the rivers; much of the eroded material remains trapped on the landscape (e.g. Walling, 1999; Wilkinson and McElroy, 2007). Quantitatively determining background rates of erosion remains a difficult but critical task worldwide. Knowing such rates well is imperative for making important environmental decisions, such as the regulation of suspended sediment as a pollutant.

In summary, with the ultimate aim of providing informative and useful information for the management of landscape erosion, understanding the disparity between natural and human-induced erosion is crucial. Also of importance, in the case of non-uniformly eroding landscapes, is allocating what proportion of sediment loads measured at the outlets of large river systems originates from different tributary regions comprising the basins as a whole. This dissertation aims to both trace sediment sources and to quantify the differences between human and natural erosion rates across two different landscapes using the comogenically produced isotope,  $^{10}\text{Be}$ .

## **1.2. Utility of meteoric $^{10}\text{Be}$ in landscape erosion studies**

Meteoritic  $^{10}\text{Be}$  is produced in the atmosphere through the spallation of N and O (Lal and Peters, 1967). At the drainage basin scale,  $^{10}\text{Be}$  rains down on the landscape, adheres to soil particles on hillslopes of all lithologies (Nyffeler et al., 1984), and is transported with them into and down river channels. For most mid-latitude humid regions, on average  $\sim 1.2$  to  $1.3 \times 10^6$  atoms  $^{10}\text{Be} \text{ cm}^{-2}$  are delivered annually (Brown et

al., 1988; Monaghan et al., 1986; Pavich et al., 1986; Pavich, 1985); on the North Island, New Zealand, the delivery rate integrated over ~18 ka is somewhat higher ( $\sim 1.7 \times 10^6$  atoms  $^{10}\text{Be cm}^{-2} \cdot \text{yr}^{-1}$ ; (Reusser et al., 2010).

Most meteoric  $^{10}\text{Be}$  resides within the upper meters of Earth's surface (Graly et al., 2010; Pavich et al., 1984; Pavich, 1985). Because soils in slowly eroding landscapes have a greater residence time in the near surface than soils in rapidly eroding environments, sediment shed from more stable hillslopes will on average have higher concentrations of meteoric  $^{10}\text{Be}$ . Exceedingly low  $^{10}\text{Be}$  concentrations measured in fluvial sediment are indicative of material sourced from deeply penetrating gullies or deep-seated landslides active within a sampled catchment (Brown et al., 1988). Although such features may be small in aerial extent, if the amount of sediment they contribute is large, they can profoundly lower the overall  $^{10}\text{Be}$  concentration of sediment leaving a drainage basin. As such, meteoric  $^{10}\text{Be}$  in fluvial sediment can be used to trace the origin and mixing of isotopically distinct material (Reusser and Bierman, 2010).

### **1.3. Modeling background erosion rates from concentration of *in situ* $^{10}\text{Be}$**

Concentrations of *in situ*-produced  $^{10}\text{Be}$  measured in fluvial sediments can be used to estimate spatially-averaged, millennial-scale rates of sediment production and landscape erosion (Bierman et al., 1996; Brown et al., 1995; Granger et al., 1996). The concentration of  $^{10}\text{Be}$  is homogenized in the upper ~1 m of Earth's surface as hillslope materials are stirred by bioturbation (Jungers et al., 2009) making erosion rate estimates insensitive to all but the most deeply penetrating forms of mass wasting (Niemi et al.,

2005). Thus, in most instances, erosion rates modeled from  $^{10}\text{Be}$  measurements in river sediments still record the isotopic signature of longer-term erosion ( $10^3 - 10^4$  years) and constitute a useful metric for comparison to human-induced rates of erosion (von Blackenburg et al., 2004). Cosmogenic  $^{10}\text{Be}$  data allow us to quantify the erosive effects of human land-use practices in a region with a profound and well documented history of disturbance and compare erosion rates calculated from sediment yields to long-term, background rates of erosion determined using  $^{10}\text{Be}$  (Costa, 1975; Dole and Stabler, 1909; Meade, 1969; Trimble, 1977; Walter and Merritts, 2008; Wolman, 1967).

#### **1.4. Study areas and research objectives**

This dissertation research focuses on two different landscapes draining continental margins separated by >15,000 km. While the climate and geology of these two regions differ dramatically (Hatcher, 1978; Hessell, 1980; Mazengarb and Speden, 2000; Trimble, 1974), they share common histories of pervasive and well-documented human-induced landscape disturbance, primarily for agricultural purposes (Hicks et al., 2000; Trimble, 1977).

The first study area is located along the East Cape region of New Zealand's North Island, where my work focuses on the Waipaoa River basin. The East Cape region is located along an active subduction margin (Berryman et al., 2000; Mazengarb and Speden, 2000) and is typified by steep slopes that experience periodic intense cyclonic activity (Hessell, 1980; Hicks et al., 2000). These conditions, acting in concert with the heavily fractured and weakly cemented rocks that underlie the landscape render the

region susceptible to erosion. Beginning in the 1800's and peaking around 1920, widespread land clearance for agriculture in the Waipaoa river basin resulted in extensive hillslope erosion from gullying and landsliding as well as rapid and substantial aggradation of river channels (e.g. Hicks et al., 2000). The northern headwaters of the Waipaoa River are underlain by particularly weak and faulted rocks (Mazengarb and Speden, 2000) that, following land clearance, proved to be especially vulnerable to the formation of large amphitheater gully complexes. Sediment from these gullies swamped the mainstem channel, all the way to the coast, with an overwhelming and continual supply of deeply sourced sediment. Other parts of the basin are dominated by shallow landsliding typically triggered only during large precipitation events.

Prior to this research, it remained uncertain what proportion of sediment originated from the gullied headwaters versus other more stable parts of the basin, or what the natural pace of erosion was prior to human-induced landscape disturbance. Because the Waipaoa landscape is so severely and non-uniformly eroding, my research pushes the boundaries of, as well as challenges many of the assumptions underlying the use of  $^{10}\text{Be}$  for modeling geomorphic process rates. Further, because the majority of lithologies comprising the landscape are virtually devoid of coarse-grained quartz (the mineral phase from which  $^{10}\text{Be}$  is typically isolated) this work relies heavily on meteoric  $^{10}\text{Be}$  adhered to the surface of particles of sediment. The differences between these two methods (touched upon above) will become clear in the ensuing chapters.

My second study area is located along the largely stable North American Atlantic passive margin and focuses on the expansive southern Appalachian Piedmont. In stark

contrast to the Waipaoa landscape, the southern Piedmont is characterized by a humid-temperate climate, and generally subdued rolling topography. Despite the relatively low-slopes of the region, the southern Piedmont also experienced the deleterious erosional effects of land clearance for agriculture beginning in the 1700's and peaking in the early 1900's (Meade and Trimble, 1974; Trimble, 1975, 1977). During this episode of intensive human-induced disturbance, rates of hillslope erosion increased dramatically, inundating rivers channels with sediment (Meade and Trimble, 1974; Trimble, 1977). Because the rivers at the time were incapable of transporting the majority of the agriculturally sourced sediment off the Piedmont (Trimble, 1977), today much of it still remains spread across the landscape at the bottom of hillslopes and in river channels (Meade, 1982; Meade and Trimble, 1974; Trimble, 1977). In contrast to meteoric  $^{10}\text{Be}$  used in the Waipaoa, my work here utilizes exclusively *in situ*  $^{10}\text{Be}$  produced within the crystal lattice of grains of the mineral quartz. Although the erosional consequences of land clearance have been studied extensively for decades, comparisons of human-induced and background rates of erosion have remained elusive. My work along the southern Appalachian Piedmont using  $^{10}\text{Be}$  aims to quantify the difference between background rates of erosion and those representing peak agricultural disturbance.

In addition, because erosion along the southern Piedmont is spatially uniform (i.e. not punctuated by discrete features yielding disproportionately large volumes of sediment) compared to many regions around the globe, I attempt to create a statistically robust representation of landscape-scale background erosion in order to generate mean basin slope-based models capable of predicting erosion rates for drainage basins without

$^{10}\text{Be}$  data. These predictions will inform management strategies, such as total maximum daily load (TMDL) values for sediment and associated pollutants (Whiting, 2006).

## **1.6. Structure of Dissertation**

Chapter 1 is an introductory chapter providing a basic overview of the importance of quantifying the difference between human-induced rates of erosion and much longer-term background rates of erosion (integrated over  $10^3$  to  $10^4$  years). In addition, the systematics of both meteoric and *in situ*  $^{10}\text{Be}$ , and their utility for identifying sediment sources and estimating background erosion rates are introduced. Finally, the two field areas where this research was conducted and the specific research objective for each are introduced.

Chapter 2 is a paper published in the peer-reviewed journal *Geology* on January 6<sup>th</sup>, 2010. This paper presents meteoric  $^{10}\text{Be}$  data from the Waipaoa River basin along the east coast of New Zealand's North Island. These data were used to track the mixing of sediment throughout the Waipaoa River network, and to generate a mixing model capable of apportioning the relative contribution of sediment from various parts of the basin that are governed by different styles of erosion.

Chapter 3 is a paper published in *Geophysical Research Letters* on October 15<sup>th</sup>, 2010. This paper presents meteoric  $^{10}\text{Be}$  data also from the Waipaoa River Basin. These samples, collected from the vertical face of a river terrace of known age, represent the depth-distribution of meteoric  $^{10}\text{Be}$ , and are used to calculate a long-term (~18 ka) accumulation rate of the isotope within soil.

Chapter 4 is a working draft of a intended for submission the peer-reviewed journal *GSA Bulletin* describing additional work I conducted in the Waipaoa River Basin, New Zealand. The paper presents temporally replicate sampling from this geomorphically complex landscape, as well as a set of *in situ* and meteoric  $^{10}\text{Be}$  comparisons, each isolated from the same sample.

Chapter 5 is a manuscript for submission to Nature Geosciences. The paper presents a subset of the *in situ*  $^{10}\text{Be}$  data I collected along the southern Appalachian Piedmont. The primary focus of the manuscript is to explicitly quantify the difference between human-induced and background rates of erosion. A secondary focus of the work is to demonstrate that sediment yield data are unreliable representations of either rates of background erosion or rates of erosion resulting from human landuse practices.

Chapter 6 is a manuscript for submission to Journal of Geophysical Research: Earth Surface. This paper presents the entire *in situ*  $^{10}\text{Be}$  dataset collected from the southern Appalachian Piedmont. There are two motivations for this work; first, to develop a detailed strategy for characterizing background erosion rates using *in situ*  $^{10}\text{Be}$  that are statistically representative at the landscape-scale, and second, to create models capable of predicting background erosion rates for drainage basin without  $^{10}\text{Be}$  data.

Chapter 7 is a brief synopsis of the overall findings of my research from the Waipaoa Basin, New Zealand and the southern Appalachian Piedmont, U.S.A., as well as avenues for future research. This chapter is followed by a comprehensive bibliography.

**CHAPTER 2: (PUBLISHED IN *GEOLOGY*) USING METEORIC  $^{10}\text{Be}$  TO  
TRACK FLUVIAL SAND THROUGH THE WAIPAQA RIVER BASIN, NEW  
ZEALAND**

**Using meteoric  $^{10}\text{Be}$  to track fluvial sand through the Waipaoa River Basin, New  
Zealand**

Lucas J. Reusser\*  
Paul R. Bierman

Rubenstein School of Environment and Natural Resources and Department of Geology  
University of Vermont, Burlington, VT 05405

*\*Corresponding author: [lreusser@uvm.edu](mailto:lreusser@uvm.edu)  
(802) 656-3398 ph. (802) 656-0045 fax.*

Keywords: Meteoric  $^{10}\text{Be}$ , sediment mixing, sediment sources, gully erosion, Waipaoa  
River Basin, land management, cosmogenic.

## 2.1. Abstract

We use meteoric  $^{10}\text{Be}$  measured in 24 fluvial sand samples collected along the mainstem and from prominent tributaries within the tectonically active Waipaoa River Basin, New Zealand, to identify sediment sources and monitor the mixing of sediment as it travels from headwater basins to the sea. Deforestation for agriculture beginning in the early 1900's resulted in severe, but non-uniformly distributed erosion. Tributaries in the northern headwaters, where large amphitheater gullies that continually feed prodigious amounts of deeply sourced sediment to the mainstem are prevalent, yield exceptionally low concentrations of meteoric  $^{10}\text{Be}$  ( $\sim 1.5 \times 10^6$  atoms  $\text{g}^{-1}$ ). In the more stable eastern and western tributaries, concentrations of meteoric  $^{10}\text{Be}$  are nearly an order of magnitude greater ( $\sim 14 \times 10^6$  atoms  $\text{g}^{-1}$ ). Meteoric  $^{10}\text{Be}$  concentrations in samples collected along the mainstem above and below tributary confluences steadily and regularly increase downstream ( $R^2 = 0.92$ ) as large amounts of low concentration gully-derived sediments are augmented with higher concentration sediment from more stable tributaries, providing strong evidence that meteoric  $^{10}\text{Be}$  concentrations reflect sediment sourcing in this fluvial network. A two component mixing model indicates that the gullied northern region of the Waipaoa basin produces sediment at a rate  $\sim 20$  times that of the eastern and western regions. These results suggest that meteoric  $^{10}\text{Be}$ , in contrast to the widely applied *in situ* technique that is limited by the availability and distribution of quartz, is an effective tool for the rapid assessment of sediment dynamics and movement within a wide range of fluvial networks.

## 2.2. Introduction

Humans have become the dominant geomorphic force on our planet today (e.g. Hooke, 1994, 2000). Our activities affect how quickly landscapes erode and the pace sediments move across hillslopes and into river systems. For land managers attempting to restore watersheds, determining the degree to which human actions have impacted landscapes and the specific locations and magnitudes of such impacts are critical (e.g. Wilkinson and McElroy, 2007).

Quantifying the mass and source of sediment moving through fluvial systems remains difficult; results are typically uncertain and may be biased (Meade, 1969; Trimble and Crosson, 2000) because contemporary sediment yield records are often short and thus may not incorporate high-magnitude, low-frequency events (e.g. Kirchner et al., 2001; Wolman and Miller, 1960). The concentration of  $^{10}\text{Be}$  produced *in situ* by cosmic ray bombardment, has been used to monitor erosion and determine sediment sources (e.g. Clapp et al., 2000; Cox et al., 2009), but the method has several limitations; its applicability is restricted to landscapes with quartz-bearing lithologies, it presumes homogenous quartz distribution throughout the sampled basin (Bierman and Steig, 1996), and samples are time consuming and expensive to prepare.

Here, we present a new rapid method for identifying sediment sources and for tracking sediment downstream - the measurement of meteoric  $^{10}\text{Be}$  concentrations in river sand. Our work, building on Brown *et al.* (1988), identifies major sediment sources within a 2,200 km<sup>2</sup> catchment, the Waipaoa River Basin (Fig. 2 - 1b). The basin drains a rapidly eroding landscape of predominately fine-grained calcareous mud and siltstones

(Mazengarb and Speden, 2000), making *in situ*  $^{10}\text{Be}$  analysis nearly impossible. The basin is tectonically active and has been severely impacted by land clearance for agriculture. The approach we detail enables the study of sediment dynamics in landscapes previously beyond the reach of cosmogenic techniques.

### 2.3. Meteoric $^{10}\text{Be}$

Meteoritic  $^{10}\text{Be}$  is produced in the atmosphere through the spallation of N and O (Lal and Peters, 1967). At the drainage basin scale,  $^{10}\text{Be}$  rains evenly across the landscape, adheres to soil particles on hillslopes of all lithologies (Nyffeler et al., 1984), and is transported with them into and down river channels. For mid-latitude humid regions, on average  $\sim 1.2$  to  $1.3 \times 10^6$  atoms  $^{10}\text{Be} \text{ cm}^{-2}$  are delivered annually (Brown et al., 1988; Monaghan et al., 1986; Pavich et al., 1984; Pavich, 1985).

Most meteoric  $^{10}\text{Be}$  resides within the upper meters of Earth's surface (Pavich et al., 1984; Pavich, 1985). Because soils in slowly eroding landscapes have a greater residence time in the near surface than soils in rapidly eroding environments, sediment shed from more stable hillslopes will have higher concentrations of meteoric  $^{10}\text{Be}$ . Exceedingly low  $^{10}\text{Be}$  concentrations measured in fluvial sediment are indicative of material sourced from deeply penetrating gullies or deep-seated landslides active within a sampled catchment (Brown, *et al.*, 1988). Although such features may be small in aerial extent, if the amount of sediment they contribute is large, they can profoundly lower the overall  $^{10}\text{Be}$  concentration of sediment leaving a drainage basin (Fig. 2 - 2). As such,

meteoric  $^{10}\text{Be}$  in fluvial sediment can be used to trace the origin and mixing of isotopically distinct material.

#### **2.4. Waipaoa River basin**

The Waipaoa is one of several meso-scale catchments draining the northeast coast of New Zealand's North Island (Fig. 2 - 1b). Rapid uplift along the subduction margin ( $\sim 1$  to  $4 \text{ mm yr}^{-1}$ ; Berryman et al., 2000; Mazengarb and Speden, 2000), heavily fractured and weakly cemented rocks (Black, 1980; Mazengarb and Speden, 2000), and periodic intense cyclonic activity (Hessell, 1980; Hicks et al., 2000) render the East Cape region of the North Island exceptionally susceptible to erosion. In the Waipaoa River Basin, these natural conditions, acting in concert with widespread deforestation, have resulted in some of the most dramatic erosional features in the world (Fig. 2 - 1a and c). The Waipaoa River's sediment yield ( $\sim 6800 \text{ t km}^{-2} \text{ yr}^{-1}$ ) is among the highest recorded around the globe for basins of its size (Gomez et al., 2003; Hicks et al., 2000; Milliman and Robert, 1983).

The region was first settled by Polynesians  $\sim 700$  ybp; however, widespread land clearance did not begin until the early 1800's following European settlement. By 1880, the downstream portion of the Waipaoa Basin was largely cleared, and by the 1920's most of the headwaters were cleared, resulting in extensive hillslope erosion from gullying and landsliding accompanied by rapid and substantial aggradation in river channels (Hicks et al., 2000). The northern headwaters, underlain by heavily faulted and crushed allochthonous lithologies (Mazengarb and Speden, 2000) were especially

vulnerable to the formation of large amphitheater gully complexes, which swamped the mainstem channel with a continual supply of deeply sourced gully sediment (Figs. 1 and 2). Although reforestation efforts have been implemented (Allsop, 1973; Marden et al., 2005), in-channel aggradation, downstream sedimentation, and flooding continue today. Despite extensive study of Waipaoa Basin erosion (e.g. Gomez et al., 2003; Hicks et al., 2000; Kettner et al., 2007; Marden et al., 2005; Marden et al., 2008; Reid and Page, 2002), it remains uncertain what proportion of sediment delivered to the sea is derived from the heavily gullied northern headwaters vs. the more stable eastern and western portions of the basin. The uneven distribution of discrete, deep-seated sediment sources (gully complexes) in the Waipaoa Basin provides an ideal setting to test the utility of meteoric  $^{10}\text{Be}$  as a monitor of sediment sourcing and mixing through a fluvial network.

## 2.5. Methods

In May 2004 and March 2005, we collected samples of fluvial sediment down the mainstem of the Waipaoa River (n=10), and from prominent tributaries (n=8) for meteoric  $^{10}\text{Be}$  analysis. At each sampling station, we collected several kg of well-mixed active channel sediment, field sieved to a grain size of 250-850  $\mu\text{m}$ . Here, we present and discuss  $^{10}\text{Be}$  concentration from 24 isotopic analyses, made on 21 samples collected at 18 locations, including 3 process replicates and 3 temporal replicates. At the University of Vermont, samples were dried and milled, then prepared for isotopic analysis at three separate laboratories. Meteoric  $^{10}\text{Be}$  was isolated from ~0.75 g aliquots

using the method of Stone (1998), and measured at the Center for Accelerator Mass Spectrometry, Livermore National Laboratory.

## 2.6. Results

Concentrations of meteoric  $^{10}\text{Be}$  vary by more than an order of magnitude across the Waipaoa Basin ( $1.44 \pm 0.06$  to  $14.64 \pm 0.46 \times 10^6$  atoms  $\text{g}^{-1}$ ; Table DR-1). Tight agreement between all process replicates (2.2, 4.3, and 1.3 percent; Table DR-1) indicates that our laboratory procedures and  $^{10}\text{Be}$  concentrations are reproducible. The lowest  $^{10}\text{Be}$  concentrations were measured in both mainstem and tributary samples located in the heavily disturbed headwaters of the basin ( $\sim 1.5 \times 10^6$  atoms  $\text{g}^{-1}$ ; Fig. 2 - 3a). The highest concentrations of  $^{10}\text{Be}$  ( $\sim 14.5 \times 10^6$  atoms  $\text{g}^{-1}$ ) were measured in samples from the prominent western and eastern tributaries that enter the Waipaoa River approximately half way down the mainstem channel (Figs. 1b and 3a). Samples along the mainstem, collected both upstream and downstream of tributary confluences, show a regular increase in  $^{10}\text{Be}$  concentration ( $R^2 = 0.92$ ,  $p < 0.001$ ) as tributaries contribute sediment containing higher concentrations of  $^{10}\text{Be}$  to the mainstem (Fig. 2 - 3a).

In landscapes, such as the Waipaoa, where delivery of sediment by mass wasting is common, the isotopic concentrations of fluvial sediment may not be constant over time (Niemi et al., 2005). To assess the temporal reproducibility of meteoric  $^{10}\text{Be}$  concentrations, we re-collected sediment in March 2005 at three locations sampled  $\sim 9$  months previously (Table DR-1). Two temporal replicates along the mainstem reproduce well, with percent differences of 2.7% (WA1met and WA21met;  $1560 \text{ km}^2$ ) and 2.1%

(WA8met and WA19met; 237 km<sup>2</sup>), well within both average analytic error ( $\pm 3.6\%$ ) and average process replication differences (2.6%; Table DR-1). These results indicate that over our replication interval, the isotopic concentration of the primarily gully-derived sediment carried by the mainstem is constant, and, by inference, that sediment is well mixed within the mainstem channel. In contrast to the mainstem samples, one temporal replicate from a small tributary basin (130 km<sup>2</sup>; WA2met and WA23met; Fig. 2 - 1) yields a greater difference in meteoric <sup>10</sup>Be concentration between the two points in time (~19%). While the mainstem channel is wide (~1 km in the mid-basin) and appears to be well mixed, this particular small tributary channel is narrow (~1 m) and deeply entrenched. We attribute its higher degree of variability to the reworking of material from frequent bank collapses and/or episodic delivery of material to the channel by shallow landsliding upstream.

### **2.7. Meteoric <sup>10</sup>Be as a useful tracer of fluvial sediment sources**

The strong increasing downstream trend ( $R^2 = 0.92$ ,  $p < 0.001$ ; Fig. 2 - 3a) in meteoric <sup>10</sup>Be along the mainstem channel reflects the augmentation of low-concentration, gully-derived sediment originating in the northern headwaters, by higher-concentration sediment sourced from regions where erosion is shallow and slower. In the headwaters, the vast majority of sediment that reaches the channel originates from gullies etched deep into hillsides (Fig. 2 - 1a,b and c) where, in the most severely impacted tributary basins, >75% of the landscape is classified as “gully-prone” (Fig. 2 - 1b; Table DR-1; Waipaoa Catchment Study Project Team, 1994). Because this sediment is rapidly

eroded from deep below the surface, it has had little chance to accumulate meteoric  $^{10}\text{Be}$ . Samples collected from gullied terrain do not reflect the isotopic inventory contained in the landscape; rather, they predominately reflect the isotopic concentration of material sourced from the deep gullies (Fig. 2 - 2). The Te Weraroa Basin (WA52met; Figs. 1b and 3a) harbors one of the largest gully complexes in the Waipaoa Basin, the Tarndale Slip. The low  $^{10}\text{Be}$  concentration in sediment from this sample ( $1.62 \pm 0.05 \times 10^6$  atoms  $\text{g}^{-1}$ ) sets the initial concentration of the downstream mainstem trend. Farther downstream, the more stable eastern and western tributaries mix sediment with  $^{10}\text{Be}$  concentrations nearly an order of magnitude greater than the primarily gully-derived mainstem sediment. Strong inverse relationships between the percent of the landscape that is gully-prone and basin area (Fig. 2 - 3b), as well as meteoric  $^{10}\text{Be}$  concentration ( $R^2 = 0.88, p < 0.001$ ; Fig. 2 - 3c) demonstrate just how well  $^{10}\text{Be}$  tracks the mixing of gully and non-gully derived sediment in the mainstem Waipaoa River. We use a two component, isotope and mass mixing model to estimate the proportion of sediment originating from the northern regions of the basin relative the eastern and western regions with the following equation:

$$[N_{up}][m_{up}] + [N_{trib}][m_{trib}] = [N_{dn}][m_{up} + m_{trib}] ; [m_{up}] + [m_{trib}] = 100\% \quad (1)$$

where  $[N]$  is meteoric  $^{10}\text{Be}$  concentration,  $[m]$  is mass proportion, and (*up*), (*trib*), and (*dn*) denote the upstream mainstem sample, incoming tributary, and downstream sample respectively (refer to the Data Repository for further detail). We find that the gullied northern regions of the Waipaoa Basin (765  $\text{km}^2$ ) produce sediment at a rate  $\sim 20$  times that of the more stable eastern and western regions (717  $\text{km}^2$ ).

## 2.8. Implications and future research

Measuring the concentration of meteoric  $^{10}\text{Be}$  in fluvial sand provides a spatially and temporally integrated view into the sourcing, movement, and mixing of sediment in the disturbed and rapidly eroding Waipaoa River system. Our results are analytically reproducible, and particularly for the mainstem, temporally reproducible. The method demonstrated here has the potential to address questions such as ‘where does sediment come from?’ and ‘proportionally how much sediment is generated in different parts of a basin?’ providing information that will allow land managers to more effectively target remediation strategies. Measuring meteoric  $^{10}\text{Be}$  is particularly useful because quartz need not be present and preparation is many times faster than the widely applied *in situ* technique. While careful analysis of sediment yield data, repeat channel surveys, and DEM differencing offer critical information, these efforts are spatially limited and often take decades to complete (e.g. Gomez et al., 2003; Hicks et al., 2000; Marden et al., 2008; Reid and Page, 2002). This study suggests that fluvial network analysis with meteoric  $^{10}\text{Be}$  can be used as a rapid assessment tool for understanding sediment dynamics within appropriate watersheds.

## 2.9. Acknowledgements

We thank B. Gomez and M. Marden for introducing us to the Waipaoa field area, M. Jungers for field assistance, M. Marden for use of the Landcare Research facility, and R. Finkel and D. Rood for AMS measurement. We thank J. Stone and A. Matmon for the

use of their laboratory facilities, and the 2009 Critical Writing seminar for ms review.  
Project funded by NSF BCS-0317530 to Gomez and Bierman.

### **2.10. Referenced cited**

Allsop, F., 1973, The Story of Mangatu: the forest which healed the land: Wellington, New Zealand, New Zealand Forest Service, 99 p.

Berryman, K.R., Marden, M., Eden, D., Mazengarb, C., Ota, Y., and Moriya, I., 2000, Tectonic and paleoclimatic significance of Quaternary river terraces of the Waipaoa River, east coast, North Island, New Zealand: New Zealand Journal of Geology and Geophysics, v. 43, p. 229-245.

Bierman, P., and Steig, E., 1996, Estimating rates of denudation and sediment transport using cosmogenic isotope abundances in sediment: Earth Surface Processes and Landforms, v. 21, p. 125-139.

Black, R.D., 1980, Upper Cretaceous and Tertiary geology of Mangatu State Forest, Raukumara Peninsula, New Zealand: New Zealand Journal of Geology and Geophysics, v. 23, p. 293-312.

Brown, L.J., Pavich, M., Hickman, R.E., Klein, J., and Middleton, R., 1988, Erosion in the eastern United States observed with  $^{10}\text{Be}$ : Earth Surface Processes and Landforms, v. 13, p. 441-457.

- Clapp, E.M., Bierman, P.R., Schick, A.P., Lekack, J., Enzel, Y., and Caffee, M., 2000, Sediment yield exceeds sediment production in arid region drainage basins: *Geology*, v. 28, p. 995-998.
- Cox, R., Bierman, P., and Jungers, M., Rakotondranzafy, M. 2009, Erosion rates and sediment sources in Madagascar inferred from  $^{10}\text{Be}$  analysis of lavaka, slope, and river sediment: *Journal of Geology*, v. 117, p. 363-376.
- Gomez, B., Banbury, K., Marden, M., Trustrum, N.A., Peacock, D., and Hoskin, P., 2003, Gully erosion and sediment production: Te Weraroa Stream, New Zealand: *Water Resources Research*, v. 39, p. ESG 3-1 to ESG 3-7.
- Hessell, J.W., 1980, The climate and weather of the Gisborne region: New Zealand Meteorological Service, Misc. Publ, v. 115, p. 29p.
- Hicks, D.M., Gomez, B., and Trustrum, N.A., 2000, Erosion thresholds and suspended sediment yields, Waipaoa River Basin, New Zealand: *Water Resources Research*, v. 36, p. 1129-1142.
- Hooke, R.L., 1994, On the efficacy of humans as geomorphic agents: *GSA Today*, v. 4, p. 224-225.
- , 2000, On the history of humans as geomorphic agents: *Geology*, v. 28, p. 843-846.
- Jungers, M., Bierman, P., Matmon, A., Cox, R., Pavich, M., Larsen, J., and Finkel, R., 2006, Tracking soil transport downslope using in-situ produced  $^{10}\text{Be}$ : *Geological Society of America - Abstracts with Programs*, v. 38, p. 283.

- Kettner, A.J., Gomez, B., and Syvitski, J.P.M., 2007, Modeling suspended sediment discharge from the Waipaoa River system, New Zealand: The last 3000 years: *Water Resources Research*, v. 43, p. doi: 10.1029/2006WR005570.
- Kirchner, J.W., Finkel, R., Reibe, C., Granger, D.E., Clayton, J., King, J., and Megahan, W., 2001, Mountain erosion over 10 yr, 10 k.y., and 10 m.y. time scales: *Geology*, v. 29, p. 591-594.
- Lal, D., and Peters, B., 1967, Cosmic ray produced radioactivity on the Earth, *in* Sitte, K., ed., *Handbuch der Physik*: New York, Springer-Verlag, p. 551-612.
- Marden, M., Arnold, G., Gomez, B., and Rowan, D., 2005, Pre- and post-reforestation gully development in Mangatu Forest, East Coast, North Island, New Zealand: *River Research and Applications*, v. 21, p. 757-771.
- Marden, M., Betts, H., Arnold, G., and Hambling, R., 2008, Gully erosion and sediment load: Waipaoa, Waiapu and Uawa rivers, eastern North Island, New Zealand, *Sediment Dynamics in Changing Environments*, Volume 325, IAHS, p. 339-350.
- Mazengarb, C., and Speden, I., 2000, Geology of the Raukumara Area, Map 6, *in* Heron, D.W., and Isaac, M.J., eds.: Lower Hutt, New Zealand, Institute of Geological & Nuclear Sciences, p. 1 sheet 1:250,000, 60 pp.
- Meade, R.H., 1969, Errors in using modern stream-load data to estimate natural rates of denudation: *Geological Society of America Bulletin*, v. 80, p. 1265-1274.
- Milliman, J., and Robert, M., 1983, World-wide delivery of river sediment to the oceans: *The Journal of Geology*, v. 91, p. 1-21.

- Monaghan, M.C., Krishnaswami, S., and Turekian, K.K., 1986, The global-average production rate of  $^{10}\text{Be}$ : *Earth and Planetary Science Letters*, v. 76 (1985/86), p. 279-287.
- Niemi, N., Oskin, M., Burbank, D.W., Heimsath, A.M., and Gabet, E., 2005, Effects of bedrock landslides on cosmogenically determined erosion rates: *Earth and Planetary Science Letters*, v. 237, p. 480-498.
- Nyffeler, U.P., Li, Y.-H., and Santschi, P.H., 1984, A kinetic approach to describe trace-element distribution between particles and solution in natural aquatic systems: *Geochemica et Cosmochemica Acta*, v. 48, p. 1513-1522.
- Pavich, M., Brown, E.T., Klein, J., and Middleton, R., 1984, Beryllium-10 accumulations in a soil chronosequence: *Earth and Planetary Science Letters*, v. 69, p. 198-204.
- Pavich, M.J., Brown, L., Valette-Silver, J.N., Klein, J. & Middleton, R., 1985,  $^{10}\text{Be}$  analysis of a Quaternary weathering profile in the Virginia piedmont: *Geology*, v. 13, p. 39-41.
- Reid, L.M., and Page, M.J., 2002, Magnitude and frequency of landsliding in a large New Zealand catchment: *Geomorphology*, v. 49, p. 71-88.
- Stone, J., 1998, A rapid fusion method for separation of beryllium-10 from soils and silicates: *Geochemica et Cosmochemica Acta*, v. 62, p. 555-561.
- Trimble, S.W., and Crosson, P., 2000, U.S. soil erosion rates - Myth and reality: *Science*, v. 289, p. 248-250.
- Waipaoa Catchment Study Project Team, 1994, *Waipaoa Catchment Study: Literature Review*, 122 p, Manaaki Whenua-Landcare Research, Palmerston North.

Wilkinson, B.H., and McElroy, B.J., 2007, The impact of humans on continental erosion and sedimentation: GSA Bulletin, v. 119, p. 140-156.

Wolman, M.G., and Miller, J.P., 1960, Magnitude and frequency of forces in geomorphic processes: Journal of Geology, v. 68, p. 54-74.

## 2.11. Figure captions

**Figure 2 - 1.** A. Air photo of the Tarndale Slip. B. Location map of the Waipaoa River Basin. Map shows all data points included in this study. For clarity, sample IDs have been abbreviated (i.e. 10 stands for WA10met in Table DR-1). Temporal replicate ID's are separated with a slash (i.e. 1/21). (X) denotes the location of the soil profile presented in figure 2. C. Photo oriented NW looking up the channel exiting the Tarndale Slip. D. Gully-derived sediments in the mainstem ~2 km downstream from the Tarndale Slip.

**Figure 2 - 2.** Schematic representation of sediment sources in a gullied basin. Large amounts of deeply sourced gully sediment, containing little meteoric  $^{10}\text{Be}$ , overwhelm the relatively small amounts of higher-concentration sediment issuing from non-gullied portions of the landscape. Sediment ultimately leaving the catchment predominately reflects the isotopic signature of gully-derived sediment. Inset shows meteoric  $^{10}\text{Be}$  concentrations from a single depth profile along a stable nose in the southwestern portion of the Waipaoa basin (Fig. 2 - 1b; Table DR-2).

**Figure 2 - 3.** Synthesis of data presented in this study. A. Basin area vs. meteoric  $^{10}\text{Be}$  concentrations for all samples. The horizontal length of the grey triangles equals the contributing area of each tributary (x-axis) as it mixes into the mainstem. B. Basin area vs. the percent of land area classified as “gully prone” for all mainstem samples. C. Meteoric  $^{10}\text{Be}$  vs. percent of gully prone land area for all mainstem samples.

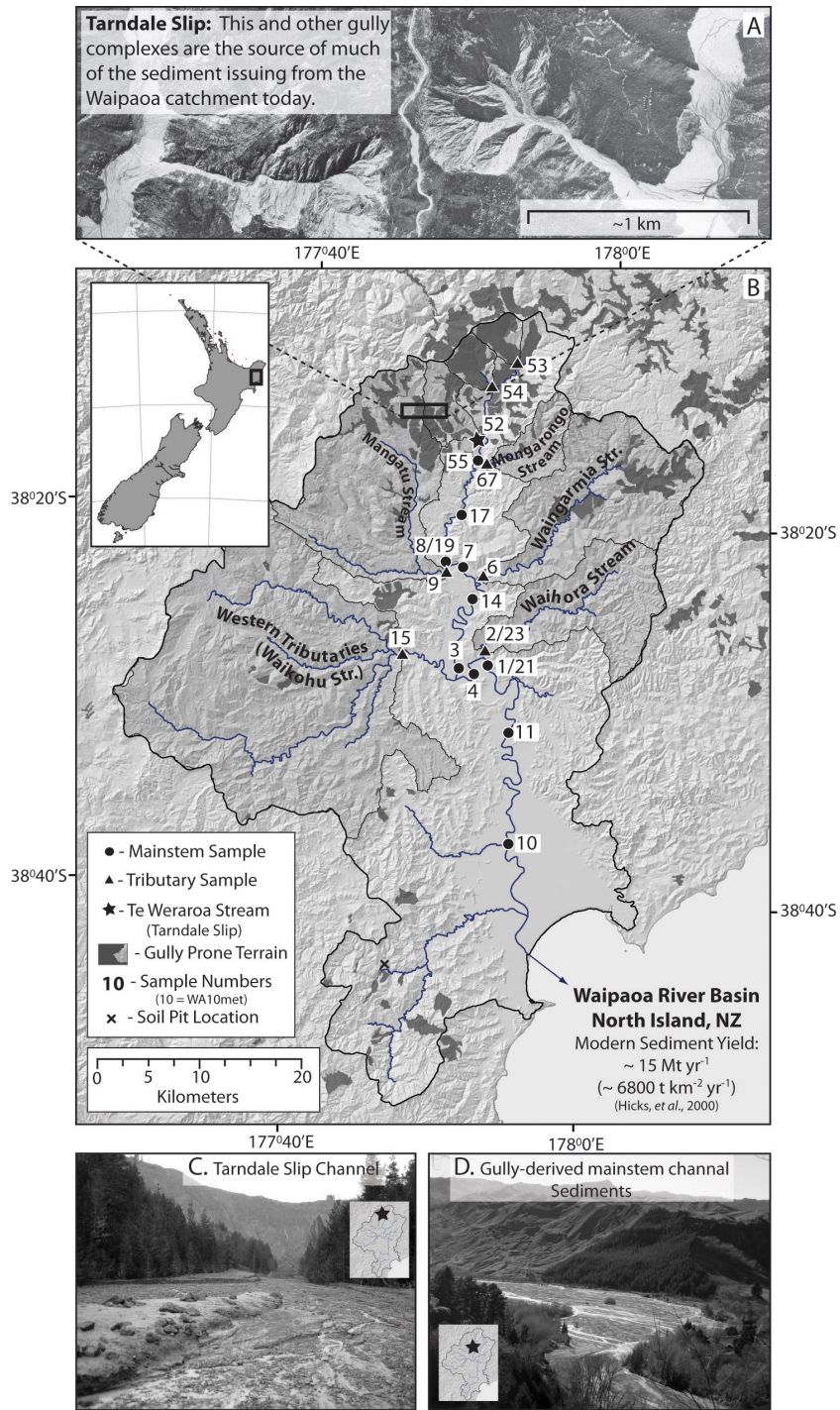


Figure 2 - 1 Location map for the Waipaoa River Basin, North Island New Zealand.

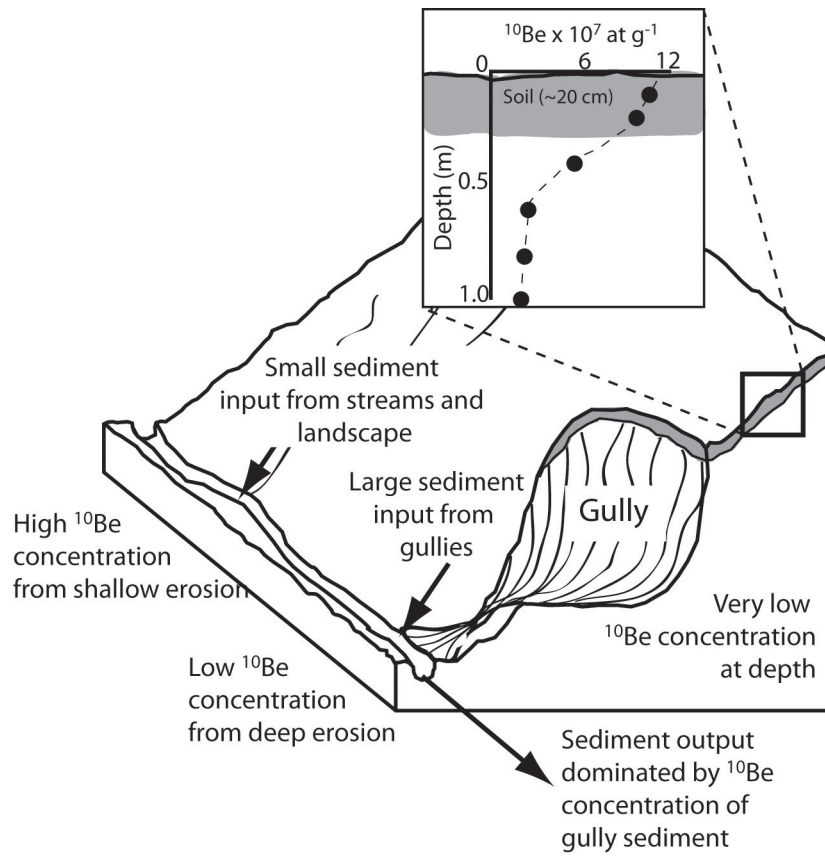


Figure 2 - 2 Schematic representation of sediment sourcing

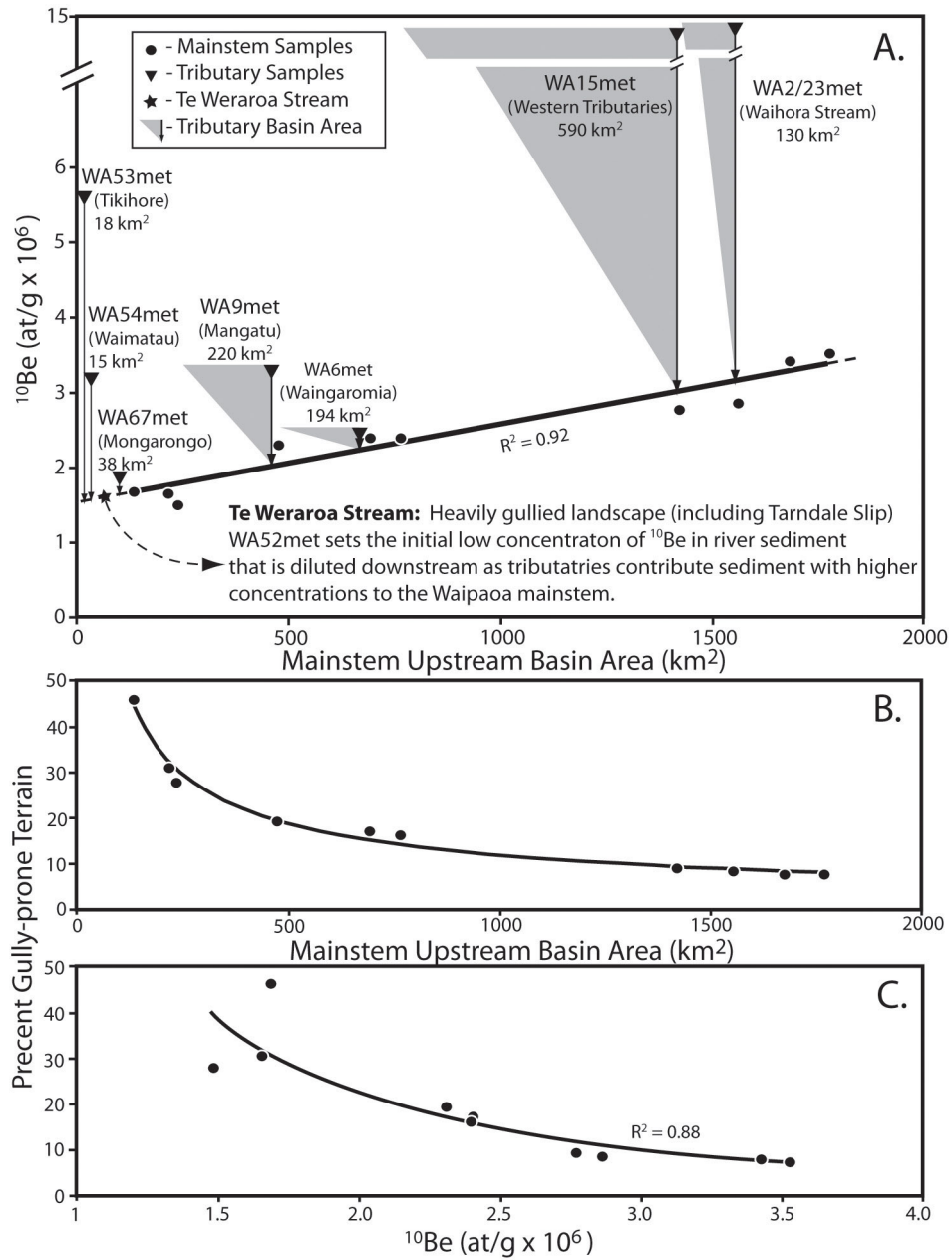


Figure 2 - 3 Synthesis of data presented in this study.

## 2.12. Data Repository

Ms. No. G30395

Using meteoric  $^{10}\text{Be}$  to track fluvial sand through the  
Waipaoa River Basin, New Zealand

L. Reusser and P. Bierman

---

### **Sample preparation and measurement:**

Upon arrival at the University of Vermont, we thoroughly dried each sample, then milled a well mixed ~20g aliquot in a SPEX Centriprep 8500 Shatterbox to a fine powder. We further prepared samples in three separate cosmogenic isotope laboratories located at the University of Vermont in Burlington, VT, the University of Washington in Seattle, WA, and Hebrew University in Jerusalem, IS. Meteoric  $^{10}\text{Be}$  was isolated from a ~0.75 g aliquot through the rapid fusion method presented in Stone (1998), precipitated as a hydroxide, burned to produce BeO, packed into cathodes mixed with Nb powder, and measured at the Center for Accelerator Mass Spectrometry (CAMS), Lawrence Livermore National Laboratory. We normalized measured ratios of  $^{10}\text{Be}/^9\text{Be}$  to the 07KNSTD3110 standard (Nishiizumi *et al.*, 2007) to arrive at our final  $^{10}\text{Be}$  concentrations.

### **Process and temporal replication:**

We calculate the percent difference between process and temporal replicates by dividing the absolute difference between  $^{10}\text{Be}$  concentrations of the two analyses by the average of the two analyses.

### **Mid-basin mixing model:**

In order to quantify the proportion of sediment originating in the upper basin, which contains nearly all of the gully complexes in the Waipaoa system, versus the more stable eastern and western tributaries, we generated a simple mixing model using meteoric  $^{10}\text{Be}$  concentrations:

$$[N_{up}][m_{up}] + [N_{trib}][m_{trib}] = [N_{down}][m_{up} + m_{trib}]$$

*and*

$$[m_{up}] + [m_{trib}] = 100 \%$$

where  $[N_{up}]$  is the meteoric  $^{10}\text{Be}$  concentration measured in WA3met, upstream of the confluence of the eastern and western tributaries,  $[N_{trib}]$  is the average meteoric  $^{10}\text{Be}$  concentration measured in sediment from the eastern and western tributaries (WA15met and WA2/23met),  $[N_{down}]$  is the average  $^{10}\text{Be}$  concentration measured in WA1/21met,

downstream of the confluence of the tributaries,  $[m_{up}]$  is the percent of total mass delivered from upstream,  $[m_{trib}]$  is the percent of total mass contributed by the two incoming tributaries, and  $[m_{up} + m_{trib}]$  is the total mass at the downstream mainstem sample site. Refer to Fig. 2 - DR-1 and Table DR-1 for sample locations and concentrations.

The model suggests that, at this prominent tributary confluence, ~95% of the sediment originates upstream, from the gully-impacted landscape. Because the area upstream of the confluence (765 km<sup>2</sup>) and the area represented by the incoming tributaries (717 km<sup>2</sup>) are roughly equal, this suggests that the northern Waipaoa basin is producing sediment at a proportional rate approximately 20 times greater relative to the more stable eastern and western tributaries.

In Table DR-1, note that for this mixing scenario, the combined areas of WA3met, WA15met and WA2/23met (1482 km<sup>2</sup>) do not exactly match the “mixed” area at WA1/21met (1560 km<sup>2</sup>). This discrepancy is due to the fact that we collected samples a sufficient distance from the actual confluence in order to ensure that no backwater mixing of sediment occurred during extreme discharge events.

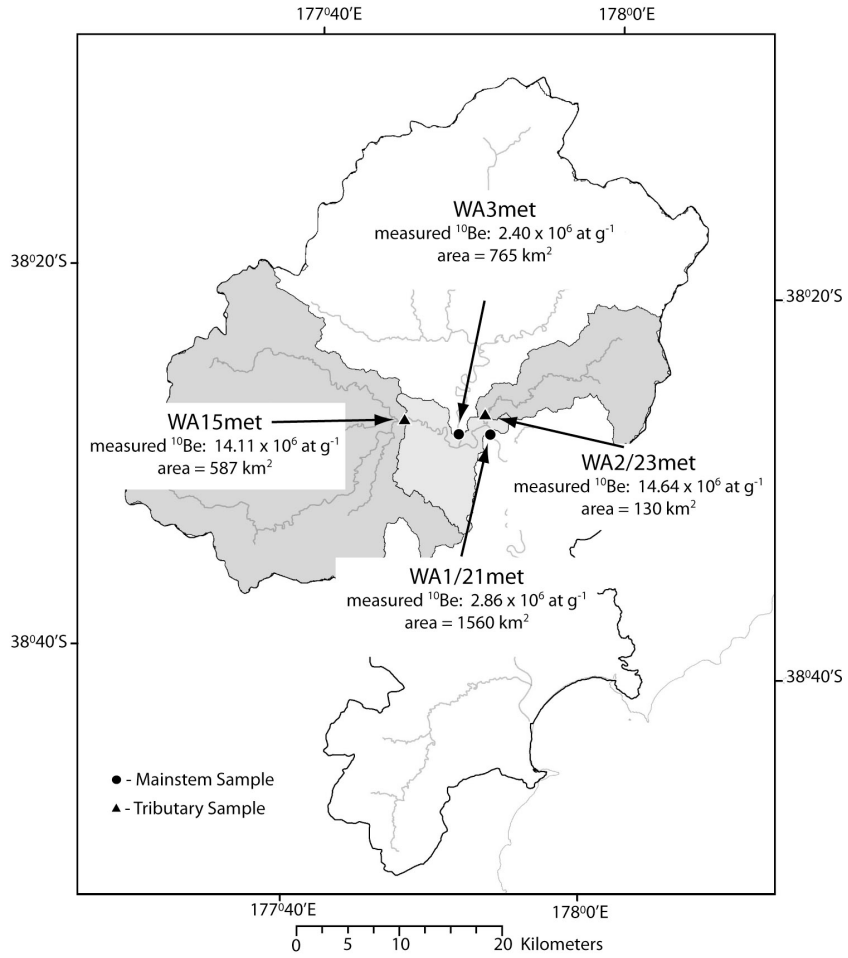


Figure 2 - 4 (DR-1) Map depicts the four samples used in the mixing model used to determine proportionally how much sediment originates in the northern headwater regions of the Waipaoa basin vs. the eastern and western regions of the basin.

Table 2 - 1 (DR-1) Summary information for all samples presented in the New Zealand, meteoric <sup>10</sup>Be article published in *Geology*.

Sample ID#	Collection Date	Type†	Basin	Dominant Lithologies‡	Basin Area (km²)	Area After Mix (km²)#	Gully-prone Area (km²)*	Percent Gully-prone Area	Easting††	Northing††	<sup>10</sup> Be (at/g x 10 <sup>6</sup> )§§	Percent Analytic Error (±)	Laboratory Percent Difference	Temporal Percent Difference
wa5metis	March 2005	Mainstem	Waipaoa	Mix	135	-	62.7	46.6	2934482	6313167	1.68 ± 0.07	4.1	-	-
wa17metis	March 2005	Mainstem	Waipaoa	Mix	215	-	66.3	30.8	2932852	6307866	1.66 ± 0.07	4.4	-	-
wa8metis	May 2004	Mainstem	Waipaoa	Mix	237	-	66.3	28.0	2931309	6303207	1.52 ± 0.07	4.4	-	-
wa19metis	March 2005	Mainstem	Waipaoa	Mix	237	-	66.3	28.0	2931320	6303196	1.44 ± 0.06	4.1	-	-
wa819met_ave##	na		Waipaoa	Mix	237	-	66.3	28.0	2931315	6303202	1.48 ± 0.06	4.2	-	2.7
wa7metis	May 2004	Mainstem	Waipaoa	Mix	476	-	92.6	19.5	2933052	6302712	2.31 ± 0.08	3.5	-	-
wa14metis	May 2004	Mainstem	Waipaoa	Mix	692	-	119.4	17.2	2933907	6299582	2.40 ± 0.08	3.5	-	-
wa3metis	May 2004	Mainstem	Waipaoa	Mix	765	-	125.2	16.4	2932576	6292861	2.40 ± 0.09	3.6	-	-
wa4metis	May 2004	Mainstem	Waipaoa	Mix	1422	-	133.3	9.4	2934089	6292248	2.77 ± 0.09	3.4	-	-
wa1metis	May 2004	Mainstem	Waipaoa	Mix	1560	-	133.3	8.5	2935404	6293113	2.89 ± 0.10	3.4	-	-
wa21metis	March 2005	Mainstem	Waipaoa	Mix	1560	-	133.3	8.5	2935397	6293012	2.83 ± 0.10	3.4	-	-
wa121met_ave	na		Waipaoa	Mix	1560	-	133.3	8.5	2935401	6293063	2.86 ± 0.10	3.4	-	1.2
wa11metuw	May 2004	Mainstem	Waipaoa	Mix	1682	-	133.3	7.9	2937417	6286506	3.43 ± 0.11	3.1	-	-
wa10metis	May 2004	Mainstem	Waipaoa	Mix	1777	-	133.3	7.5	2937490	6275586	3.53 ± 0.13	3.8	-	-
wa53metuw	March 2005	Prom Trib	Tikihoro	Gullied ss	18	18	14	79.1	2938834	6320513	5.65 ± 0.17	3.1	-	-
wa54metis	March 2005	Prom Trib	Waimatau	Gullied ss	15	33	11.7	76.0	2938264	6322674	3.28 ± 0.10	3.0	-	-
wa54metvt	March 2005	Prom Trib	Waimatau	Gullied ss	15	33	11.7	76.0	2938264	6322674	3.14 ± 0.18	5.8	-	-
wa5met_ave	March 2005	Prom Trib	Waimatau	Gullied ss	15	33	11.7	76.0	2938264	6322674	3.21 ± 0.14	4.4	2.2	-
wa52metuw	March 2005	Prom Trib	Te Werarua	Gullied ss	29	62	12.6	43.2	2934448	6315280	1.62 ± 0.05	3.3	-	-
wa67metis	March 2005	Prom Trib	Mongourongo	Gullied ms, ss, mel	38	100	1.1	2.9	2935332	6312973	1.86 ± 0.07	3.6	-	-
wa9metis	May 2004	Prom Trib	Mangatu	Gullied ms, ln	220	451	26.4	12.0	2931396	6302380	3.34 ± 0.14	4.1	-	-
wa10metis	May 2004	Prom Trib	Wangaromia	Gullied ms	194	667	26.9	13.9	2934984	6301871	2.51 ± 0.09	3.7	-	-
wa15metuw	May 2004	Prom Trib	Waikohu	Ungullied ms, ss	587	1397	7.4	1.3	2927098	6294320	14.72 ± 0.45	3.0	-	-
wa15metvt	May 2004	Prom Trib	Waikohu	Ungullied ms, ss	587	1397	7.4	1.3	2927098	6294320	13.50 ± 0.45	3.3	-	-
wa15met_ave	May 2004	Prom Trib	Waikohu	Ungullied ms, ss	587	1397	7.4	1.3	2927098	6294320	14.11 ± 0.45	3.2	4.3	-
wa2metuw	May 2004	Prom Trib	Waihora	Ungullied ms	130	1535	0	0.0	2935145	6294576	12.01 ± 0.37	3.1	-	-
wa2metvt	May 2004	Prom Trib	Waihora	Ungullied ms	130	1535	0	0.0	2935145	6294576	11.70 ± 0.37	3.2	-	-
wa2met_ave	May 2004	Prom Trib	Waihora	Ungullied ms	130	1535	0	0.0	2935145	6294576	11.85 ± 0.37	3.1	1.3	-
wa23metis	March 2005	Prom Trib	Waihora	Ungullied ms	130	1535	0	0.0	2935145	6294576	17.43 ± 0.56	3.2	-	-
wa223met_ave	na		Waihora	Ungullied ms	130	1535	0	0.0	2935145	6294576	14.64 ± 0.46	3.2	-	19.1

\* The last two letters on sample IDs indicate the lab in which they were prepared; vt = University of Vermont, uw = University of Washington, and is = Hebrew University.

† Mainstem = samples collected along the mainstem Waipaoa channel. Prom trib = samples collected from prominent tributaries mixing into the mainstem Waipaoa channel.

‡ Lithology abbreviations are as follows: ss = sandstone, ms = mudstone, ln = limestone, and mel = melange.

# Area after mix is the total basin area after a given tributary has mixed with the mainstem channel.

\*\* Gully-prone areas were calculated in ArcGIS® using the East Cape Terrain Geographic coverage (Team, 1994).

†† All coordinates are listed in NZ Grid, 1949.

§§ Errors in nuclide concentrations include propagated laboratory and measurement uncertainties. Measured ratios of <sup>10</sup>Be normalized to the new 07KNSTD3110 standard (Nishiizumi, et al., 2007).

## IDs ending in "ave" are the average of the indicated process or temporal replicates.

Table 2 - 2 (DR-2) Soil profile from the Te Arai basin, SW Waipaoa basin.

Table DR-2. Soil profile from the Te Arai basin, SW Waipaoa Basin.

Sample ID*	Collection Date	Type	Basin	Depth (cm)	$^{10}\text{Be}$ (at/g x $10^7$ )†	Percent Analytic Error (±)
MJNZ5met	March 2005	Soil Profile	Te Arai	10	10.81 ± 0.29	2.7
MJNZ6met	March 2005	Soil Profile	Te Arai	20	9.90 ± 0.26	2.6
MJNZ7met	March 2005	Soil Profile	Te Arai	40	5.65 ± 0.14	2.5
MJNZ8met	March 2005	Soil Profile	Te Arai	60	2.48 ± 0.09	3.5
MJNZ9met	March 2005	Soil Profile	Te Arai	80	2.28 ± 0.06	2.8
MJNZ10met	March 2005	Soil Profile	Te Arai	100	1.97 ± 0.06	3.2

\* All samples prepared at the Hebrew University in Jerusalem, Israel, and measured at CAMS, LLNL.

† Errors in nuclide concentrations include propagated laboratory and measurement uncertainties.

Measured ratios of  $^{10}/^9\text{Be}$  normalized to the new 07KNSTD3110 standard (Nishiizumi, et al., 2007).

**References Cited:**

Nishiizumi, K., Imamura, M., Caffee, M., Southon, J., Finkel, R., and McAninch, J., 2007, Absolute calibration of  $^{10}\text{Be}$  AMS standards: Nuclear Instruments and Methods in Physics Research B, v. 258, p. 403-413.

Stone, J., 1998, A rapid fusion method for separation of beryllium-10 from soils and silicates: *Geochemica et Cosmochemica Acta*, v. 62, p. 555-561.

Waipaoa Catchment Study Project Team, 1994, Waipaoa Catchment Study: Literature Review, 122 p, Manaaki Whenua-Landcare Research, Palmerston North.

**CHAPTER 3: (PUBLISHED IN *GEOPHYSICAL RESEARCH LETTERS*)**  
**CALIBRATING A LONG-TERM METEORIC  $^{10}\text{Be}$  ACCUMULATION RATE IN**  
**SOIL**

**Calibrating a long-term meteoric  $^{10}\text{Be}$  accumulation rate in soil**

Lucas Reusser<sup>1\*</sup>,

Joseph Graly<sup>2</sup>,

Paul Bierman<sup>1</sup>,

Dylan Rood<sup>3</sup>

<sup>1</sup> Rubenstein School of Environment and Natural Resources, and Department of Geology,  
University of Vermont, Burlington, VT 05405

<sup>2</sup> Department of Geology, University of Vermont, Burlington, VT 05405

<sup>3</sup> Center for Accelerator Mass Spectrometry, Livermore National Laboratory, CA 94550

\*Corresponding Author: [lreusser@uvm.edu](mailto:lreusser@uvm.edu) - (802) 656-3398

Keywords: isotope, calibration, surface process, soils

### 3.1. Abstract

Using 13 samples collected from a 4.1 meter profile in a well-dated and stable New Zealand fluvial terrace, we present the first long-term accumulation rate for meteoric  $^{10}\text{Be}$  in soil ( $1.68$  to  $1.72 \times 10^6$  at/( $\text{cm}^2 \cdot \text{yr}$ )) integrated over the past  $\sim 18$  ka. Site-specific accumulation data, such as these, are prerequisite to the application of meteoric  $^{10}\text{Be}$  in surface process studies. Our data begin the process of calibrating long-term meteoric  $^{10}\text{Be}$  delivery rates across latitude and precipitation gradients. Our integrated rate is lower than contemporary meteoric  $^{10}\text{Be}$  fluxes measured in New Zealand rainfall, suggesting that long-term average precipitation, dust flux, or both, at this site were less than modern values. With accurately calibrated long-term delivery rates, such as this, meteoric  $^{10}\text{Be}$  will be a powerful tool for studying rates of landscape change in environments where other cosmogenic nuclides, such as in situ  $^{10}\text{Be}$ , cannot be used.

### 3.2. Introduction

The concentration of meteoric  $^{10}\text{Be}$  in soils and sediment can be used as a geochronometer [e.g., *Egil et al.*, 2010; *Pavich et al.*, 1984; *Pavich et al.*, 1986] and a tracer of Earth surface processes [e.g., *Brown et al.*, 1988; *Reusser and Bierman*, 2010; *Valette-Silver et al.*, 1986, *Willenbring and von Blackenburg*, 2010]. Critical to both of these geomorphic applications is constraining the delivery rate of meteoric  $^{10}\text{Be}$  to landscapes over geomorphically meaningful time-scales ( $10^3$  to  $10^5$  yrs). To date, no

study has explicitly and deliberately attempted to constrain the long-term accumulation rate of meteoric  $^{10}\text{Be}$  in soil. Most geomorphic applications of meteoric  $^{10}\text{Be}$  measure concentrations in soil and base their interpretations on globally averaged contemporary delivery rates [e.g., *Jungers et al., 2009; Reusser et al., 2008*]; yet, contemporary, short-term data clearly indicate that the total flux of meteoric  $^{10}\text{Be}$  to the soil surface varies over time and space [e.g., *Graham et al., 2003; Heikkilä et al., 2008; Monaghan et al., 1986*].

Because of documented long-term changes in primary meteoric  $^{10}\text{Be}$  production [*Frank et al., 1997*], climate (primarily precipitation) [*Dore, 2005*], and the source and volume of allochthonous dust [*Baumgartner et al., 1997*], there are differences between long- and short-term meteoric  $^{10}\text{Be}$  delivery rates. These complexities suggest the importance of calibrating site-specific, long-term delivery rates by measuring the accumulation of meteoric  $^{10}\text{Be}$  in geologic archives. Such work has been done in lake deposits, deep-sea sediments, and glacial ice [e.g., *Finkel and Nishiizumi, 1997; Frank et al., 1997*] but not in soils, the basis for most geomorphic studies. Here, we quantify the meteoric  $^{10}\text{Be}$  inventory in a 4.1 m depth profile collected from a stable and well-dated alluvial surface on New Zealand's North Island and estimate a long-term accumulation rate for meteoric  $^{10}\text{Be}$  in soil.

### **3.3. Behavior of meteoric $^{10}\text{Be}$**

Meteoritic  $^{10}\text{Be}$  is a valuable tool for studying surface process rates because, once deposited, it adsorbs tenaciously to near-surface materials in all but the most acidic soils

[*You et al.*, 1989]. Unlike shorter-lived radionuclides, such as  $^{210}\text{Pb}$  and  $^{137}\text{Cs}$  [e.g., *Walling et al.*, 2003], the longer half-life of  $^{10}\text{Be}$  (1.36 Myr; [*Nishiizumi et al.*, 2007]) increases the period of time over which the nuclide accumulates in soils and penetrates to depth before decay, thus extending the timeframe over which the method is applicable. Because measurements of meteoric  $^{10}\text{Be}$  are made on bulk samples, the presence or absence of a specific mineral phase is irrelevant, making the isotope useful across a wide variety of landscapes.

The flux of meteoric  $^{10}\text{Be}$  to terrestrial environments comes from two sources:  $^{10}\text{Be}$  produced in the atmosphere by spallation of nitrogen and oxygen and delivered to earth's surface by precipitation and dryfall (primary component), and  $^{10}\text{Be}$  adhered to airborne dust (recycled component) [*Monaghan et al.*, 1986].

Primary production of meteoric  $^{10}\text{Be}$  is controlled by solar activity and magnetic field intensity [*Masarik and Beer*, 2009], both of which vary over time [*Beer*, 1994; *Frank et al.*, 1997]. The subsequent distribution of primary meteoric  $^{10}\text{Be}$  is controlled by atmospheric circulation, with annual precipitation being a strong predictor of total meteoric  $^{10}\text{Be}$  fallout at any one location [*Heikkilä et al.*, 2009].

Delivery of recycled meteoric  $^{10}\text{Be}$  is controlled by the flux, and  $^{10}\text{Be}$  concentration, of dust. Recycled meteoric  $^{10}\text{Be}$  is usually <20% of total meteoric  $^{10}\text{Be}$  flux [*Graham et al.*, 2003; *Monaghan et al.*, 1986]; in high-dust environments, such as in regions of loess accumulation, the flux of recycled meteoric  $^{10}\text{Be}$  can be far greater [*Baumgartner et al.*, 1997; *Zhou et al.*, 2007]. Aridity sufficient to promote topsoil loss

by wind [Zhou *et al.*, 2007] and land-use practices that disrupt topsoil [Brown *et al.*, 1988] increase recycled meteoric  $^{10}\text{Be}$  flux from dust.

Because geochemical processes in soils rapidly meld primary and recycled meteoric  $^{10}\text{Be}$ , constraining the spatial and temporal variation in the rate of accumulation of both components is required when measurements of meteoric  $^{10}\text{Be}$  are used for modeling surface processes. Most contemporary  $^{10}\text{Be}$  flux measurements exclude dust influence to determine the primary  $^{10}\text{Be}$  flux. In this study, both components are critical and not explicitly separable.

### 3.4. Geologic setting

We sampled a soil profile within the Waipaoa River Basin, a 2,200 km<sup>2</sup> catchment draining the eastern margin of New Zealand's North Island (Figure 3 - 1) [Mazengarb and Speden, 2000]. At ~38°S Latitude, this site receives ~110 cm of rain annually [Hessell, 1980].

Within the basin, an extensive flat-lying fluvial terrace (termed Waipaoa-1) stands up to ~100 m above the mainstem and many of the tributary channels of the Waipaoa River. This terrace surface is capped by ~10 m of coarse fluvial gravel deposited during the last glacial maximum [Berryman *et al.*, 2000]. Atop the gravel, lie several meters of overbank silty clay-rich flood deposits laid down as this river level was rapidly abandoned in response to a combination of tectonic uplift and a switch in the fluvial system from aggradation to rapid incision, most likely in response to changing climate following the glacial maximum at ~18 ka [Berryman *et al.*, 2000; Eden *et al.*, 2001].

Evidence from other dated terrace surfaces suggest that the cessation of aggradation at ~18 ka was a regional event across the eastern and southern North Island [Eden *et al.*, 2001]. Where we sampled the Waipaoa-1 terrace, it stands ~50 m above the modern channel, is extensive, flat, far from any nearby slopes, well-preserved, and lacks any surface drainage, indicating that little net erosion or deposition have occurred since the emplacement of the overbank deposits shortly after ~18 ka. Land clearance and agriculture have at most reworked the upper several dm of the sampled site.

### 3.5. Age of sampled profile

The overbank deposits contain age-constrained tephra used to estimate the timing of the Waipaoa-1 terrace abandonment and emplacement of the sediment we sampled. The Rerewhakaaitu Tephra is located at or near the base of the Waipaoa-1 overbank deposits that cap the fluvial gravels [Berryman *et al.*, 2000; Eden *et al.*, 2001; Froggatt and Lowe, 1990]. The stratigraphic position of this tephra indicates that it fell coincidentally with the initiation of rapid incision [Berryman *et al.*, 2000; Eden *et al.*, 2001]. The overlying flood deposits were emplaced relatively quickly (perhaps over the course of decades; [Eden *et al.*, 2001]) until the river had incised far enough to isolate the terrace surface from further aggradation. The age of the Rerewhakaaitu Tephra is constrained with multiple radiocarbon ages (n=4) of organic material directly overlying the tephra in a bog core collected nearby [Lowe *et al.*, 1999]. We calibrated the radiocarbon age of  $14,700 \pm 95$   $^{14}\text{C}$  yrs with CALIB REV6.0 [Stuiver and Reimer, 1993], yielding a  $1\sigma$  age range of 17,659 to 18,030 cal. yr.

The Waipaoa-1 terrace is ideal for constraining the long-term delivery rate of meteoric  $^{10}\text{Be}$  because: 1) the airfall deposition of the Rerewhakaaitu Tephra within the overbank deposits constrains the integration time of  $^{10}\text{Be}$  accumulation, 2) an intact younger capping tephra bed argues against either surface erosion or deposition, 3) the fine texture of the soil and the buffering capacity of the carbonate-bearing source rocks [Black, 1980; Mazengarb and Speden, 2000] ensure retention of meteoric  $^{10}\text{Be}$  and, 4) the ~5 m of overbank deposits above the basal tephra at the location we sampled is thick enough to retain the inventory of meteoric  $^{10}\text{Be}$  delivered since 18 ka.

### 3.6 Sampling and analysis techniques

We sampled the Waipaoa-1 overbank sequence from a recent excavation at 2931760 E, 6297492 N (NZ Grid 1949; Figure 3 - 1). The sequence consists of fluvial silty clay-rich sediment containing small amounts of reworked tephra. The overbank sediment is capped by a discrete younger tephra bed (presumably the widespread ~3500 cal. ybp Waimihia Tephra) [Eden *et al.*, 2001], the upper ~15 cm of which has developed an organic-rich A/O-horizon. We collected a total of thirteen, 15 to 37 cm thick amalgamated samples. In addition, we collected several undisturbed samples of profile sediment for dry density determination.

We dried and milled samples and isolated meteoric  $^{10}\text{Be}$  from ~0.5 g aliquots using a modification of the method of Stone [1998], then calculated meteoric  $^{10}\text{Be}$  concentrations from  $^{10}\text{Be}/^9\text{Be}$  ratios measured at Lawrence Livermore National Laboratory. Data were normalized to the 07KNSTD3110 standard with an assumed ratio

of  $2850 \cdot 10^{-15}$  [Nishiizumi *et al.*, 2007]. All measured sample isotopic ratios were corrected using process blanks prepared from acid-leached fluvial sediment collected in the Waipaoa Basin; blank corrections ranged from 2.1 to 0.3 % of measured ratios.

### 3.7. Long-term meteoric $^{10}\text{Be}$ delivery rate

In general, meteoric  $^{10}\text{Be}$  concentrations decrease regularly down section (Figure 3 - 2; Table 3 - 1 (S1)), with a maximum concentration of  $16.27 \pm 0.40 \times 10^7$  atoms/g in the uppermost sample, and a minimum concentration of  $3.12 \pm 0.07 \times 10^7$  atoms/g near the bottom of the profile. When deposited, the overbank sediment carried some meteoric  $^{10}\text{Be}$ , its inherited concentration. Following the abandonment of the Waipaoa-1 terrace and the emplacement of the overbank sequence, additional atmospherically-derived meteoric  $^{10}\text{Be}$  accumulated, adsorbed to fine sediment, was bioturbated, and translocated downward through macropores, resulting in the profile shape we see today (Figure 3 - 2). We consider the relatively uniform and low concentration of meteoric  $^{10}\text{Be}$  in the bottom ~0.6 m of the profile (samples WA102l and n; Figure 3 - 2) as representative of the inherited component of the total inventory of meteoric  $^{10}\text{Be}$  in the profile, and subtract the thickness-weighted average concentration of these two samples from all others, except WA102a and b. Because these two uppermost samples were sourced primarily from airfall tephra, we assume they contained no meteoric  $^{10}\text{Be}$  when deposited.

We use eq. 3 - 1 to calculate a total inventory of meteoric  $^{10}\text{Be}$  ( $N$ ;  $3.02 \pm 0.05 \times 10^{10}$  atoms/cm<sup>2</sup>) deposited and adsorbed since the abandonment of the Waipaoa-1 terrace.

$$N = \Sigma (n_{tot} - n_{inh}) \cdot \rho \cdot l \quad (3 - 1)$$

where,  $n_{tot}$  = the measured concentration of meteoric  $^{10}\text{Be}$  (atoms/g),  $n_{inh}$  = the inherited component of the total concentration ( $3.21 \pm 0.06 \cdot 10^7$  atoms/g),  $\rho$  = the dry density of the depth increment ( $\text{g}/\text{cm}^3$ ), and  $l$  = the increment thickness (cm). The dry density of the overbank silt and clay (WA102c to n) is  $1.68 \pm 0.03 \text{ g}/\text{cm}^3$  based on repeat measurements ( $n=4$ ) of undisturbed samples we collected. We use a literature value for the dry density of tephra ( $1.05 \pm 0.12 \text{ g}/\text{cm}^3$  [Houlbrooke *et al.*, 1997]) for the uppermost tephritic increments (WA102a and b).

We arrive at a geologic delivery rate ( $q$ ; atoms/( $\text{cm}^2 \cdot \text{yr}$ )), corrected for decay and inheritance, for the meteoric  $^{10}\text{Be}$  accumulated within the measured profile ( $N$ ; atoms/ $\text{cm}^2$ ) over the duration of time since the abandonment of the Waipaoa-1 surface ( $t$ ; yrs) and emplacement of the overbank sediment with equation 3 - 2:

$$q = N \cdot \lambda / (1 - e^{-\lambda t}) \quad (3 - 2)$$

We assume  $\lambda = 5.1 \cdot 10^{-7} \text{ yr}^{-1}$ , the decay constant for  $^{10}\text{Be}$  [Nishiizumi *et al.*, 2007]. The calibrated  $1\sigma$  age range of 17,659 to 18,030 cal. yrs translates into a  $1\sigma$  range of decay-corrected deposition rates for meteoric  $^{10}\text{Be}$  of 1.72 to  $1.68 \times 10^6$  atoms/( $\text{cm}^2 \cdot \text{yr}$ ).

Our analysis incorporates all errors associated with AMS measurement, radiocarbon measurement and calibration, and density; however, several possible sources of error are difficult to quantify. If the overbank deposits we sampled were emplaced after the age-constraining basal tephra, the integration time of  $\sim 18$  ka would be an overestimate. If surface erosion over the last 18 ky removed material, the measured  $^{10}\text{Be}$  inventory would be an underestimate. If the radiocarbon age of the basal tephra is younger than the deposit, the period of accumulation we use would be too short.

### 3.8. Discussion

Using precise AMS measurements ( $<2\%$ ,  $1\sigma$ ) of a deep soil profile from a stable depositional surface of constrained age, we provide the first explicit long-term, soil-based calibration of meteoric  $^{10}\text{Be}$  deposition integrated over a geologically relevant time interval. The soil we sampled (Figure 3 - 2; Table 3 – 1 (S1)) contains meteoric  $^{10}\text{Be}$  derived from three distinct sources: 1) meteoric  $^{10}\text{Be}$  inherited prior to the emplacement of the overbank deposits, 2) atmospherically-derived primary meteoric  $^{10}\text{Be}$ , and 3) dust-derived recycled  $^{10}\text{Be}$ . Our approach quantifies and subtracts the inherited component from the total inventory ( $N$ ; eq. 1) allowing us to estimate the temporally averaged meteoric  $^{10}\text{Be}$  delivery rate ( $q$ ; eq. 2) since the exposure we sampled was emplaced. The delivery rate we calculate reflects contributions of both primary and recycled meteoric  $^{10}\text{Be}$ .

Contemporary data suggest that meteoric  $^{10}\text{Be}$  deposition rates in New Zealand correlate well with precipitation (Figure 3 - 2 *inset*) and that the majority of meteoric  $^{10}\text{Be}$  accumulated in the profile we measured is atmospherically-derived (primary). Measurements of meteoric  $^{10}\text{Be}$  in modern precipitation collected over two years at four sites spanning New Zealand show a range in deposition rates from  $1.7$  to  $5.2 \times 10^6$  atoms/( $\text{cm}^2 \cdot \text{yr}$ ), with total flux strongly correlating to annual precipitation [Graham *et al.*, 2003]. When these values are normalized to mean annual rainfall at each site and 700 MV of solar activity [Masarik and Beer, 2009; Usoskin and al, 2005], the between-site variability collapses to  $1.4$  to  $2.1 \times 10^4$  atoms/ $\text{cm}^3$  of rainfall. Based on  $^7\text{Be}$  and dust

concentration measurements, Graham and others [2003] estimate that only about 10% of the contemporary meteoric  $^{10}\text{Be}$  fallout is recycled from dust. If the atmospherically-produced primary component is considered separately, modern meteoric  $^{10}\text{Be}$  deposition rates (Figure 3 - 2 *inset*) in New Zealand range from  $\sim 1.4$  to  $\sim 4.2 \times 10^6$  atoms/( $\text{cm}^2 \cdot \text{yr}$ ).

If these modern  $^{10}\text{Be}$  deposition values represent long-term conditions, and long-term dust flux remained  $\sim 10\%$  of the total meteoric  $^{10}\text{Be}$  deposition, then our measured long-term total meteoric  $^{10}\text{Be}$  deposition rate of  $\sim 1.70 \times 10^6$  atoms/( $\text{cm}^2 \cdot \text{yr}$ ) suggests that precipitation at the Waipaoa site averaged  $\sim 77$  cm/yr. This estimate is  $\sim 30\%$  lower than contemporary measurements [Hessell, 1980], suggesting that precipitation averaged over  $\sim 18$  ky was lower than today. Alternatively, some of the difference may be due to a recent increase in meteoric  $^{10}\text{Be}$  recycled from dust. Contemporary dust is primarily generated by human activities. If the long-term dust flux on the largely unglaciated North Island is negligible and meteoric  $^{10}\text{Be}$  concentrations in contemporary rainfall are otherwise representative of long-term conditions, paleo-precipitation would be  $\sim 91$  cm/year over 18 ky, still about 17% drier than modern climate records indicate. Regional paleoclimate records are consistent with this interpretation of the meteoric  $^{10}\text{Be}$  data, as they suggest that the eastern North Island was substantially drier prior to an ENSO-driven precipitation increase approximately 4 ka [Gomez *et al.*, 2004].

### 3.9. Implications

Our findings demonstrate the feasibility of calibrating long-term meteoric  $^{10}\text{Be}$  accumulation rates using deep, stable, well-dated soil profiles. Such soil-based

calibrations are important because soils constitute the source material for most surface process studies including fluvial sediment analysis [e.g., *Reusser and Bierman, 2010*]. Terrestrial calibration of meteoric  $^{10}\text{Be}$  delivery rates compliments other methods. Polar ice cores reliably record  $^{10}\text{Be}$  fluxes over time at high latitudes [e.g., *Finkel and Nishiizumi, 1997*]; however, these fluxes can differ dramatically from those at lower latitudes because of atmospheric production and mixing processes [e.g., *Heikkilä et al., 2009*]. Deep-sea and most lake sediment records are filtered by drainage basin and biologic processes making delivery rates over time difficult to deconvolve accurately [e.g., *Aldahan, 1999*]. Because deposition rates of meteoric  $^{10}\text{Be}$  to the soil surface change over time and space as rainfall, dust flux, and geomagnetic shielding all vary, performing additional geologic calibrations at a variety of latitudes, in different precipitation regimes, and over different integration times will improve the accuracy and precision of surface process studies using this isotope system.

#### **ACKNOWLEDGMENTS**

We thank B. Gomez and M. Marden for introducing us to the Waipaoa, T. Brown for AMS assistance, and G. Balco and A. Heimsath for helpful reviews. Funded by NSF BCS-0317530 and NSF ARC-0713956.

### 3.10. References cited

- Aldahan, A., et al. (1999), Linking the  $^{10}\text{Be}$  continental record of Lake Baikal to marine and ice archives of the last 50 ka: Implications for the global dust-aerosol input, *Geophysical Research Letters*, 26(18), 2885-2888.
- Baumgartner, S., et al. (1997),  $^{10}\text{Be}$  and Dust, *Nuclear Instruments and Methods in Physics Research B*, 123, 296-301.
- Beer, J. (1994),  $^{10}\text{Be}$  as an indicator of solar variability and climate, in *The solar engine and its influences on terrestrial atmosphere and climate*, edited by D. Nesme-Ribes, pp. 221-233, Springer-Verlag, Berlin.
- Berryman, K. R., et al. (2000), Tectonic and paleoclimatic significance of Quaternary river terraces of the Waipaoa River, east coast, North Island, New Zealand, *New Zealand Journal of Geology and Geophysics*, 43, 229-245.
- Black, R. D. (1980), Upper Cretaceous and Tertiary geology of Mangatu State Forest, Raukumara Peninsula, New Zealand, *New Zealand Journal of Geology and Geophysics*, 23, 293-312.
- Brown, L. J., et al. (1988), Erosion in the eastern United States observed with  $^{10}\text{Be}$ , *Earth Surface Processes and Landforms*, 13, 441-457.

Chmeleff, J., et al. (2010), Determination of the  $^{10}\text{Be}$  half-life by multicollector ICP-MS and liquid scintillation counting, *Nuclear Instruments and Methods in Physics Research B*, 268, 192-199.

Dore, M. H. I. (2005), Climate change and changes in global precipitation patterns: What do we know?, *Environmental International*, 31, 1167-1181.

Eden, D., et al. (2001), Dating the culmination of river aggradation at the end of the last glaciation using distal tephra compositions, eastern North Island, New Zealand, *Geomorphology*, 38(1-2), 133-151.

Egil, M., et al. (2010),  $^{10}\text{Be}$  inventories in alpine soils and their potential for dating land surfaces, *Geomorphology*, 119, 62-73.

Finkel, R., and K. Nishiizumi (1997), Beryllium-10 concentrations in the Greenland Ice Sheet Project 2 ice core from 4-30 ka, *Journal of Geophysical Research*, 102, 26699-26706.

Frank, M., et al. (1997), A 200 kyr record of cosmogenic radionuclide production rate and geomagnetic field intensity from  $^{10}\text{Be}$  in globally stacked deep-sea sediments, *Earth and Planetary Science Letters*, 149, 121-129.

Froggatt, P. C., and D. Lowe (1990), A review of late quaternary silicic and some other tephra formations from New Zealand: their stratigraphy, nomenclature, distribution, volume, and age, *New Zealand Journal of Geology and Geophysics*, 33, 89-109.

Gomez, B., et al. (2004), El Nino-Southern Oscillation signal associated with middle Holocene climate change in intercorrelated terrestrial and marine sediment cores, North Island, New Zealand, *Geology*, 32(8), 653-656.

Graham, I., et al. (2003), Atmospheric deposition of  $^7\text{Be}$  and  $^{10}\text{Be}$  in New Zealand rain (1996-98), *Geochemica et Cosmochemica Acta*, 67(3), 361-373.

Heikkilä, U., et al. (2008), Beryllium-10 and Beryllium-7 in precipitation Dübendorf (440 m) and Jungfraujoch (3580 m), Switzerland (1998-2005), *Journal of Geophysical Research*, 113, D11104.

Heikkilä, U., et al. (2009), Meridional transport and deposition of atmospheric  $^{10}\text{Be}$ , *Atmospheric Chemistry and Physics*, 9, 515-527.

Hessell, J. W. (1980), The climate and weather of the Gisborne region, *New Zealand Meteorological Service, Misc. Publ*, 115, 29 p.

Houlbrooke, D. J., et al. (1997), A study of the effects of bulk density on root and shoot growth of different ryegrass lines, *New Zealand Journal of Agricultural Research*, 40(4), 429-435.

Jungers, M., et al. (2009), Tracing hillslope sediment production and transport with *in situ* and meteoric  $^{10}\text{Be}$ , *Journal of Geophysical Research - Earth Surface*, 114.

Lowe, D. J., et al. (1999), Stratigraphy and chronology of a 15 ka sequence of multi-sourced silicic tephra in a montane peat bog, eastern North Island, New Zealand, *New Zealand Journal of Geology and Geophysics*, 42, 565-579.

Masarik, J., and J. Beer (2009), An updated simulation of particle fluxes and cosmogenic nuclide production in the Earth's atmosphere, *Journal of Geophysical Research*, 114, D11103.

Mazengarb, C., and I. Speden (2000), Geology of the Raukumara Area, Map 6, 1 sheet 1:250,000, 260 pp, Institute of Geological & Nuclear Sciences, Lower Hutt, New Zealand.

Monaghan, M. C., et al. (1986), The global-average production rate of  $^{10}\text{Be}$ , *Earth and Planetary Science Letters*, 76 (1985/86), 279-287.

- Nishiizumi, K., et al. (2007), Absolute calibration of  $^{10}\text{Be}$  AMS standards, *Nuclear Instruments and Methods in Physics Research B*, 258, 403-413.
- Pavich, M., et al. (1984), Beryllium-10 accumulations in a soil chronosequence, *Earth and Planetary Science Letters*, 69, 198-204.
- Pavich, M., et al. (1986),  $^{10}\text{Be}$  distributions in soils from Merced River terraces, California, *Geochemica et Cosmochemica Acta*, 50, 1727-1735.
- Reusser, L. J., et al. (2008), Estimating pre-disturbance rates of sediment generation and erosion with *in situ* and meteoric  $^{10}\text{Be}$ , *Geological Society of America - Abstracts with Programs*, 299-297.
- Reusser, L. J., and P. Bierman (2010), Using meteoric  $^{10}\text{Be}$  to track fluvial sand through the Waipaoa River basin, New Zealand, *Geology*, 38(1), 47-50.
- Stone, J. (1998), A rapid fusion method for separation of beryllium-10 from soils and silicates, *Geochemica et Cosmochemica Acta*, 62(3), 555-561.
- Stuiver, M., and P. J. Reimer (1993), Extended  $^{14}\text{C}$  database and revised CALIB 3.0  $^{14}\text{C}$  age calibration program, *Radiocarbon*, 35, 215-230.

Usoskin, I. G., and e. al (2005), Heliospheric modulation of cosmic rays: monthly reconstruction for 1951-2004, *Journal of Geophysical Research*, 110, A12108.

Valette-Silver, J. N., et al. (1986), Detection of erosion events using  $^{10}\text{Be}$  profiles; example of the impact of agriculture on soil erosion in the Chesapeake Bay area (U.S.A.), *Earth and Planetary Science Letters*, 80(1-2), 82-90.

Walling, D. E., et al. (2003), Using unsupported lead-210 measurements to investigate soil erosion and sediment delivery in a small Zambian catchment, *Geomorphology*, 52, 193-213.

Willenbring, J. K., and F. von Blackenburg (2010), Meteoric cosmogenic Beryllium-10 adsorbed to river sediments and soil: Applications for Earth-surface dynamics, *Earth Science Reviews*, 98, 105-122.

You, C.-F., et al. (1989), The partition of Be between soil and water, *Chemical Geology*, 77(2), 105-118.

Zhou, W., et al. (2007), Disentangling geomagnetic and precipitation signals in a 80-kyr Chinese loess record of  $^{10}\text{Be}$ , *Radiocarbon*, 49(1), 139-160.

### 3.11. Figure captions

FIGURE 3 - 1: Calibration profile located in the middle Waipaoa River basin, New Zealand, North Island.

FIGURE 3 - 2: Meteoric  $^{10}\text{Be}$  concentration results for the depth profile. Letters to the right of each sample are abbreviations (e.g. “a” represents WA102a in Table 3 – 1 (S1)). The inherited concentration is average of samples WA102 l, and n (circled). *Inset* panel shows relationship of long-term meteoric  $^{10}\text{Be}$  delivery rate to contemporary rates measured across the North and South islands of New Zealand [*Graham et al.*, 2003].

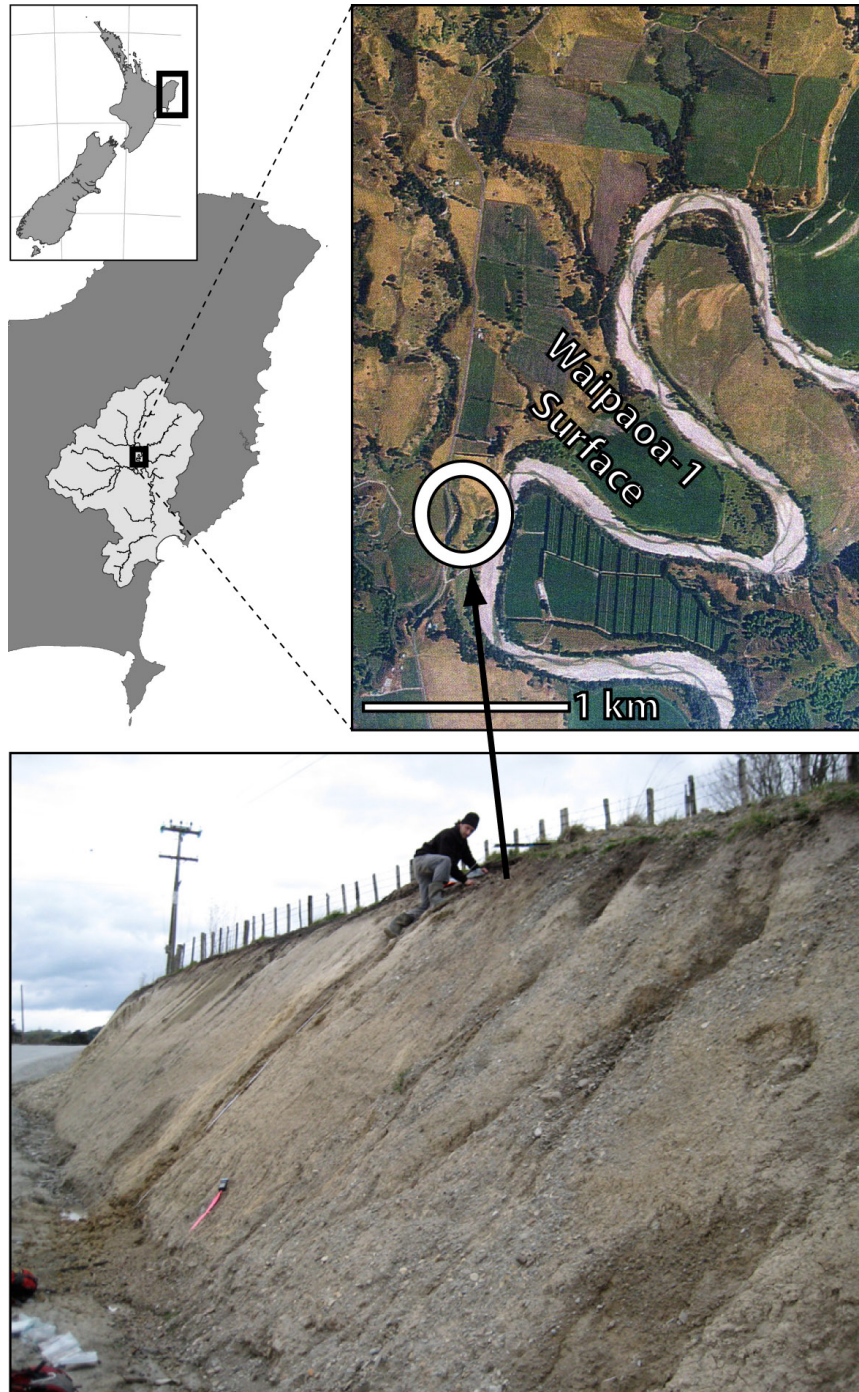


Figure 3 - 1 Calibration profile located in the middle Waipaoa River basin, North Island, New Zealand.

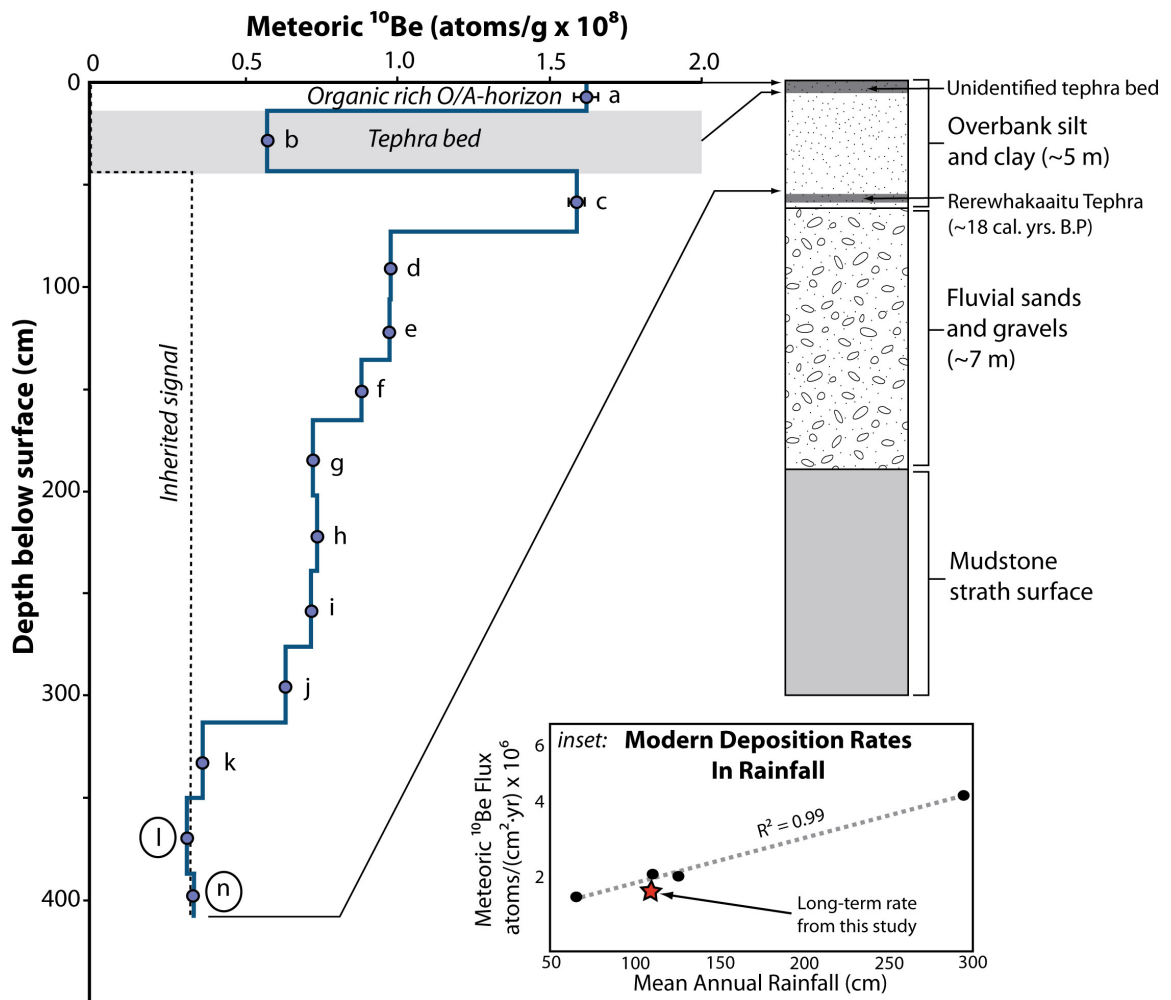


Figure 3 - 2 Meteoric  $^{10}\text{Be}$  concentration results for the depth profile.

### 3.12. Auxiliary Information

Table 3 - 1 (Auxiliary Table 1) Summary information for all sample in the Waipaoa 1 Terrace depth profile published in *Geophysical Research Letters*.

Sample ID	Be Number <sup>a</sup>	Soil Matrix	Increment Thickness (cm)	Measured <sup>10</sup> Be <sup>b</sup> (at/g x 10 <sup>7</sup> )	Inherited <sup>10</sup> Be <sup>c</sup> (at/g x 10 <sup>7</sup> )	Inventory <sup>10</sup> Be <sup>d</sup> (at/g x 10 <sup>7</sup> )	Density (g/cm <sup>3</sup> )	AMS Percent <sup>e</sup>	Density Percent <sup>f</sup>	Inventory <sup>10</sup> Be Flux <sup>g</sup> (at/cm <sup>2</sup> x 10 <sup>9</sup> )
WA102a	BE27032	organic A	14.8	16.27 ± 0.40	0.00 ± 0.00	16.27 ± 0.40	1.05	2.5%	11.7%	2.52 ± 0.30
WA102b	BE27033	tephra	29.6	5.75 ± 0.07	0.00 ± 0.00	5.75 ± 0.07	1.05	1.2%	11.7%	1.78 ± 0.21
WA102c	BE27034	silt and clay	29.6	15.94 ± 0.26	3.21 ± 0.06	12.73 ± 0.26	1.68	2.1%	1.8%	6.32 ± 0.17
WA102d	BE27035	silt and clay	33.3	9.82 ± 0.12	3.21 ± 0.06	6.61 ± 0.14	1.68	2.1%	1.8%	3.69 ± 0.10
WA102e	BE27036	silt and clay	29.6	9.78 ± 0.13	3.21 ± 0.06	6.57 ± 0.15	1.68	2.2%	1.8%	3.26 ± 0.09
WA102f	BE27037	silt and clay	29.6	8.86 ± 0.11	3.21 ± 0.06	5.64 ± 0.13	1.68	2.2%	1.8%	2.80 ± 0.08
WA102g	BE27038	silt and clay	37.0	7.26 ± 0.10	3.21 ± 0.06	4.05 ± 0.12	1.68	2.9%	1.8%	2.51 ± 0.09
WA102h	BE27039	silt and clay	37.0	7.40 ± 0.09	3.21 ± 0.06	4.19 ± 0.11	1.68	2.7%	1.8%	2.60 ± 0.08
WA102i	BE27040	silt and clay	37.0	7.19 ± 0.09	3.21 ± 0.06	3.98 ± 0.11	1.68	2.7%	1.8%	2.47 ± 0.08
WA102j	BE27041	silt and clay	37.0	6.37 ± 0.13	3.21 ± 0.06	3.15 ± 0.15	1.68	4.6%	1.8%	1.96 ± 0.10
WA102k	BE27042	silt and clay	37.0	3.64 ± 0.05	3.21 ± 0.06	0.43 ± 0.08	1.68	18.9%	1.8%	0.27 ± 0.05
WA102l	BE27043	silt and clay	37.0	3.12 ± 0.07	3.21 ± 0.06	0.00 ± 0.00	1.68	na	1.8%	0.00 ± 0.00
WA102n	BE27045	silt and clay	25.9	3.35 ± 0.04	3.21 ± 0.06	0.00 ± 0.00	1.68	na	1.8%	0.00 ± 0.00

a - Be Numbers are unique sample identifiers for every sample measured on the accelerator at the Lawrence Livermore National Laboratory.

b - Actual at/g concentration from accelerator measurement. Errors in nuclide propagated laboratory and measurement uncertainties.

Measured ratios of 10/9 Be normalized to the new 07KNSTD3110 (Nishizumi, et al., 2007).

c - Inheritance concentration for WA102c to k determined through the thickness weighted averaging of WA102l, and n.

d - Inventory concentration is the difference between the measured and inherited concentrations.

Errors are propagated as the square root of the sum of the squared uncertainties attached to the measured and inherited concentrations.

e - Percent uncertainty of the inventory concentration (standard deviation/concentration)

f - Percent uncertainty of density estimates. Refer to text for details

g - Errors are propagated as the square root of the sum of the squared percent uncertainty of concentrations and densities

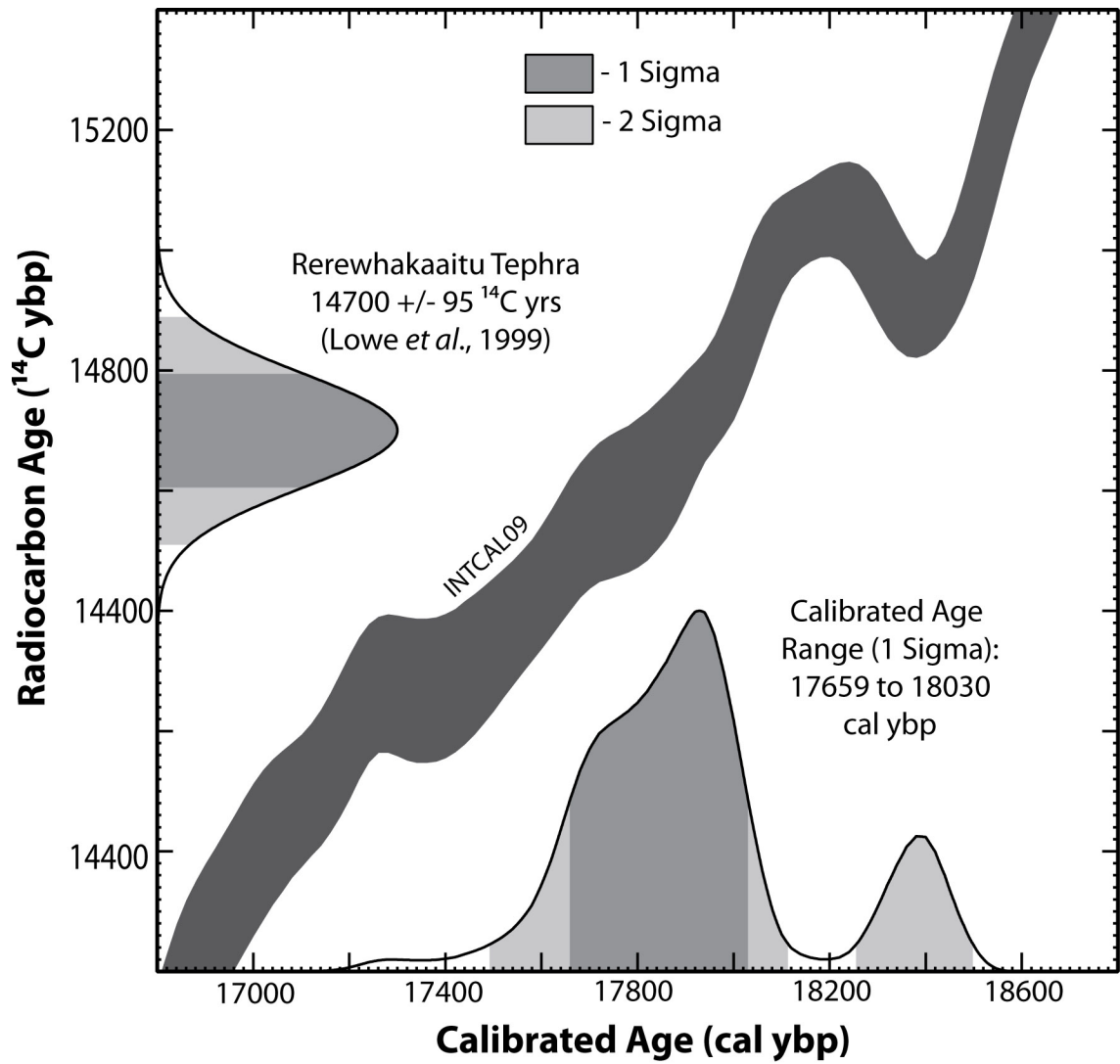


Figure 3 - 3 (Auxiliary Figure 1) Calibrated age for depth profile in the Waipaoa 1 Terrace.

**CHAPTER 4: (FOR SUBMISSION TO *GSA BULLETIN*) USING  $^{10}\text{Be}$  AS A  
TRACER OF LANDSCAPE PROCESSES IN AN EXTREME GEOMORPHIC  
ENVIRONMENT, WAIPAOA RIVER BASIN, NORTH ISLAND, NEW  
ZEALAND**

**Using  $^{10}\text{Be}$  as a tracer of landscape processes in an extreme geomorphic  
environment, Waipaoa River Basin, North Island, New Zealand**

Lucas Reusser<sup>1\*</sup>,

Paul Bierman<sup>1</sup>,

<sup>1</sup> Rubenstein School of Environment and Natural Resources, and Department of Geology,

University of Vermont, Burlington, VT 05405

*\*Corresponding author: [lreusser@uvm.edu](mailto:lreusser@uvm.edu)  
(802) 656-3398 ph. (802) 656-0045 fax.*

#### 4.1. Abstract

Extreme geomorphic environments, including rapidly eroding and uplifting mountain ranges, and landscapes severely disturbed by human activities including deforestation and agriculture, are difficult to study using many isotopic and geochemical techniques because the processes moving mass are non-uniform over time and space. The random nature of geomorphic processes on these landscapes violates the assumptions inherent to interpretive models. In order to understand the utility and limitations of both *in situ* and meteoric  $^{10}\text{Be}$  as a tracer of erosion and sediment movement in a wet, highly disturbed, tectonically active, environment, we measured *in situ* produced  $^{10}\text{Be}$  in 18 samples of river sediment and meteoric  $^{10}\text{Be}$  in 90 samples of river sediment and hillslope materials in the Waipaoa River Basin East Cape region, North Island, New Zealand. We collected samples over a 3 year period (2005 to 2008) and processed them in 3 different laboratories. We find that the concentration of both *in situ* and meteoric  $^{10}\text{Be}$  reproduce well between laboratories but vary significantly ( $2.77 \pm 0.11$  to  $0.11 \pm 0.03 \times 10^4$  at/g for *in situ*  $^{10}\text{Be}$ ;  $5.61 \pm 0.16 \times 10^7$  to  $7.38 \pm 0.90 \times 10^5$  at/g for meteoric  $^{10}\text{Be}$ ) over time and space. Erosion in some regions of the basin is dominated by deep-seated amphitheater gullies that continuously feed prodigious amounts of sediment to tributary and mainstem channels while other parts of the basin are dominated by widespread shallow landsliding triggered during severe cyclonic events. Sediments shed from gully-dominated regions yield exceptionally low and consistent concentrations of meteoric  $^{10}\text{Be}$  (ave. =  $4.30 \times 10^6$  at/g) while concentrations of both *in situ* and meteoric  $^{10}\text{Be}$  from eastern and western tributaries are much higher (ave. =  $2.19 \times 10^7$  at/g) and also highly variable due to the

differing source areas of material entering river channels owing to the variability in precipitation events and landslide initiation through time. Because the vast majority of sediment carried by the mainstem channel originates from the heavily gullied headwater regions of the Waipaoa Basin, concentrations of meteoric  $^{10}\text{Be}$  are exceedingly low in the mainstem channel and only slightly augmented by contributions of sediment from the more stable tributary regions dominated by shallow landsliding. Alternatively concentrations of *in situ*  $^{10}\text{Be}$  down the mainstem channel remain highly variable because the lithologies in which the gully complexes form are nearly devoid of quartz, the mineral phase in which *in situ*  $^{10}\text{Be}$  is isolated. Instead, measurements of *in situ*  $^{10}\text{Be}$  in the mainstem originate in the eastern and western tributary regions. Using this paired isotopic approach allows us to differentiate variability in not just the relative mass of sediment yielded from various regions of the Waipaoa, but also the origin of material carried down the mainstem and eventually offshore into Poverty Bay.

## 4.2. Introduction

The measurement of cosmogenic nuclides in detrital sediment and soil profiles provides information about the rate at which Earth's surface changes over time (Portenga and Bierman, 2011). The accuracy of cosmogenically-derived erosion rates depends on not only the quality of isotopic measurements, which have improved both in precision and detection limit over the past several decades, but on the veracity of assumptions underlying interpretive models used to translate measured isotope concentrations into erosion rates (Brown et al., 1995; Granger et al., 1996; Bierman and Steig, 1996; Neimi

et al., 2005). Such assumptions include not only landscape steady state and the reproducibility of laboratory analyses but also the steadiness of isotope concentrations over time in material transported down river networks and the uniform distribution of quartz in drainage basins.

Few of the assumptions inherent to the successful application of cosmogenic nuclides to measuring erosion rates and tracing sediment sources at a basin scale have been tested explicitly, especially in areas where landscape dynamics suggest that such assumptions may not be valid. Here, we present cosmogenic isotopic data (both *in situ* produced and meteoric  $^{10}\text{Be}$ ) from the Waipaoa River basin on the east coast of New Zealand's North Island, a rapidly and non-uniformly eroding landscape, the result of both natural phenomena and human landuse practices (Figure 4 - 1). This dataset is unlike any other collected because it is from an extreme geomorphic environment where many of the assumptions inherent to commonly used interpretive models are likely not valid. The data set includes numerous temporal and laboratory replicates allowing us to clearly isolate geologic variability and thereby better understand the sediment system from hillslopes down the river network to the ocean margin including the impact of both human activities and extreme precipitation events on erosion and deposition.

In this study, we measured both *in situ*  $^{10}\text{Be}$ , produced by spallation reactions in the mineral quartz and meteoric  $^{10}\text{Be}$  produced in the atmosphere through the spallation of N and O (Lal and Peters, 1967), delivered to the landscape via precipitation and to a lesser extent in the Waipaoa, dust (Graham et al., 2003). Meteoric  $^{10}\text{Be}$  adheres to soil particles on hillslopes of all lithologies (Nyffeler et al., 1984) and eventually makes its

way on these particles into river channels. Because meteoric  $^{10}\text{Be}$  is insensitive to the presence or absence of quartz, it has the potential to provide a more uniform representation of landscapes than *in situ*  $^{10}\text{Be}$  which only represents those regions underlain by quartz-bearing lithologies (Nyffeler, et al., 1984; Monaghan, et al., 1986). In addition, concentrations of meteoric  $^{10}\text{Be}$  measured in terrestrial materials are several orders of magnitude greater than *in situ*  $^{10}\text{Be}$  (Graly, et al., 2010), making measurement of the isotope possible (above AMS detection limits) even in extremely rapidly and disturbed environments such as the Waipaoa River basin.

### **4.3. Geologic and Geographic setting**

The Waipaoa River Basin is located on the east coast of the North Island of New Zealand along an active subduction margin. The basin experiences rapid uplift (Berryman et al., 2000; Mazengarb and Speden, 2000), relatively frequent earthquake activity and volcanic eruptions (Froggatt and Lowe, 1990), and periodic intense cyclonic activity (Hessell, 1980; Hicks et al., 2000). Lithologies within the basin are heavily fractured and faulted, and weakly cemented (Black, 1980; Mazengarb and Speden, 2000). The northern headwaters, where large amphitheater gullies are pervasive, are underlain by an emplaced allochthonous unit of exceptionally weak and crushed calcareous mudstones exceptionally susceptible to erosion (Black, 1980). In contrast, the eastern and western regions of the basin are underlain by more competent interbedded fine sandstone and mudstone units. While these regions are also heavily faulted, they are more resistant to deep mass movements and instead are subject to widespread shallow

landslide during extreme precipitation events. In the eastern and western regions, quartz-bearing lithologies are non-uniformly distributed throughout the basin. Often these erosion-resistant units are found as upturned beds standing above the more easily eroded calcareous mudstones characteristic of the East Cape Region (Mazengarb and Speden, 2000). Many of the headwater river channels contain rounded sandstone boulders eroded from hillslopes upstream throughout the contributing drainage basin. In the Waipaoa basin, these natural conditions, acting in concert with widespread deforestation for agriculture peaking in the 1920's, have resulted in some of the most dramatic erosional features in the world (e.g. Hicks et al., 2000).

#### 4.4. Methods

We conducted three field sessions in New Zealand - May 2004, February and March of 2005, and August of 2008 – allowing us to resample some sites and compile a series of temporal replicate measurements of  $^{10}\text{Be}$  concentration on both tributaries and the mainstem Waipaoa River. At each sample location, we field-sieved several kilograms of fluvial sediment to a grain size fraction of 250 to 850  $\mu\text{m}$ . At the University of Vermont, we tested aliquots of each sample for quartz content to determine which samples contained sufficient quartz to process further for *in situ*  $^{10}\text{Be}$  analysis (cut off, >2% quartz). Because meteoric  $^{10}\text{Be}$  is isolated from bulk samples, we extracted meteoric  $^{10}\text{Be}$  from all samples.

We prepared samples in three separate laboratories (University of Washington, Hebrew University, and the University of Vermont), which provided the opportunity to

test the lab-to-lab reproducibility of our results. Because we prepared meteoric samples in all three labs, we prepared 10 full laboratory-to-laboratory replicates to ensure reproducibility. We prepared all *in situ* samples at the University of Washington Cosmogenic laboratory during which we prepared 5 full laboratory replicates.

Because the lithologies comprising the Waipaoa landscape have little quartz in the grain size (>125  $\mu\text{m}$ ), appropriate for measuring *in situ* produced  $^{10}\text{Be}$ , we mostly measured concentrations of meteoric  $^{10}\text{Be}$  in river sediment and soil samples (n=84). We were able to isolate sufficient amounts of quartz from 18 samples. We use these data to 1) investigate relationships between concentrations of *in situ* vs. meteoric  $^{10}\text{Be}$ , and 2) estimate a background rate of erosion for the Waipaoa Basin.

In order to account for varying production and deposition rates of  $^{10}\text{Be}$ , we normalize *in situ*  $^{10}\text{Be}$  concentrations to the hypsometrically-weighted elevation-latitude-dependent (ELD; (Lal, 1991)) production rate for each basin (Portenga and Bierman, 2011), and similarly normalize meteoric  $^{10}\text{Be}$  concentrations to the elevation-dependent mean annual precipitation (MAP) relationship for the Gisborne area presented in Hessel (1980) for each basin (Graly, et al., 2010).

#### 4.5. Data

##### ***Laboratory replication of in situ and meteoric $^{10}\text{Be}$ samples:***

*In situ*  $^{10}\text{Be}$  laboratory replicate samples (n=5), prepared in the cosmogenic laboratory at the University of Washington, reproduce well (Figure 4 - 2; Table 4 - 1). For three of the replicates (wa02, wa20, and wa24), repeat laboratory preparation and AMS measurements reproduce well (average of  $6.1 \pm 17\%$ ). While a difference of  $\sim 30\%$

for wa54 may seem high, the  $^{10/9}\text{Be}$  isotopic ratios measured were so low as to be at or near the detection limit of the Livermore accelerator. Sample wa44 reproduced poorly, yielding a difference of between replicates of ~14% despite its relatively high concentration of *in situ*  $^{10}\text{Be}$ . We assume this resulted from poor preparation of the sample at some stage in the process; wa44 is from the first batch of samples I ever prepared for *in situ*  $^{10}\text{Be}$  measurement.

With the exception of wa12met (~20% difference), meteoric  $^{10}\text{Be}$  laboratory replicates (n=10) also reproduce well (Figure 4 - 3; Table 4 - 2), with an average percent difference of ~6% (excluding wa12). This reproducibility is encouraging because the laboratory replicates were prepared in three different labs. No two replicate samples were prepared in the same laboratory. All were measured on the AMS at the Livermore National Laboratory and normalized to the 07KNSTD3110 standard (Nishiizumi et al., 2007).

***Temporal variability in  $^{10}\text{Be}$  concentration:***

We temporally replicated *in situ*  $^{10}\text{Be}$  measurements in two basins. Samples wa02 and wa23 were sampled at the outlet of the eastern tributaries and wa12/24 is the downstream-most outlet sample from entire basin (Figures 4 - 1 & 4 - 4; Table 4 - 3). The outlet sample is within the tidal zone of the river and therefore could contain sediment carried upstream from Poverty Bay. Sediment was collected from both sites in May 2004 and again in March 2005. These temporal replicates differ by ~30 and ~40 percent, respectively.

There are meteoric  $^{10}\text{Be}$  temporal replicates at 14 locations within the Waipaoa basin. Each of these replicate locations has meteoric  $^{10}\text{Be}$  data from at least two of four times increments (Figure 4 - 5; Table 4 - 4). Three of these are from each of the field sessions (May 2004; March 2005; August, 2008), and one is from a distinctive overbank flood deposit laid down on July 31<sup>st</sup>, 2008, just prior to our August 2008 field season.

In some regions of the Waipaoa Basin, concentrations of  $^{10}\text{Be}$  are low and steady over time while in other parts of the basin concentrations vary systematically, increasing over time. At the outlets of the prominent eastern (Waihora Basin), and Te Arai tributaries, and at point D along the Waipaoa mainstem (Figures 4 – 5, 4 – 6 & 4 – 7), meteoric  $^{10}\text{Be}$  concentrations consistently increase over three time steps and one flood event. We consider point D, at the Kakanai Bridge, to be the most reliable estimate for the concentration of meteoric  $^{10}\text{Be}$  contained within sediment leaving the Waipaoa system (see Figure 4 - 7 for basin areas); the sample site is in close proximity to the sediment yield gauging station used to estimate contemporary sediment output for the Waipaoa Basin (e.g. Hicks et al., 2000). While concentrations of meteoric  $^{10}\text{Be}$  increase over time for the eastern, and southwestern portions of the basin, concentrations remain essentially constant in the western (Waikohu Basin) and the gullied headwaters (Figure 4 - 5). This is also true for points A, B, & C along the mainstem channel; up to point C, the Waipaoa channel is fed only by gully-prone terrain (Figures 4 – 5, 4 – 6 & 4 – 7). By point D along the Waipaoa channel, sediment from both the eastern and western tributaries have mixed with the low-concentration gully-derived sediment from the northern headwaters. That the Waipaoa mainstem channel (at point D) shows the same

pattern of increasing meteoric  $^{10}\text{Be}$  concentration as in the eastern and southern tributaries over time is strong evidence that meteoric  $^{10}\text{Be}$  can be used as a tracer of sediment sourcing and mixing over space and through time.

Similarly, in the prominent eastern (Waihora Basin) and southwestern (Te Arai Basin) tributaries, as well as at point D along the mainstem channel, the overbank flood deposits have considerably higher concentrations of meteoric  $^{10}\text{Be}$  than the fluvial samples collected in August of 2008 (Figure 4 – 5). This comparison of meteoric  $^{10}\text{Be}$  concentrations measured in sediment carried during baseflow (fluvial samples) vs. that carried during eventflow (flood deposit samples) has several important implications. First, shallow landsliding, with higher concentrations of *in situ*  $^{10}\text{Be}$  than gully-derived sediment, is the dominant erosional style feeding sediment to river channels in some regions of the Waipaoa Basin, but not others. Channels in the northern headwaters for instance are continuously fed deeply sourced sediment containing very low concentration of  $^{10}\text{Be}$ . That samples from the Waipaoa mainstem channel remain constant through time is thus predictable. While concentrations of meteoric  $^{10}\text{Be}$  are higher in sediment from the western tributaries (Waikohu Basin) than from the gullied basins, they show the same consistency in concentration through time, perhaps suggesting a style of sediment sourcing that is insensitive to extreme precipitation events. Second, the increased meteoric  $^{10}\text{Be}$  concentrations measured in flood deposit material relative to active channel sediments suggests that during extreme flow events, the source of sediment changes in the eastern and southwestern prominent tributaries. The higher concentration of meteoric  $^{10}\text{Be}$  in flood deposits could reflect shallower source depths (see depth-

distribution of meteoric  $^{10}\text{Be}$  in Figure 4 – 8) for hillslope materials being fed to tributary channels during high flows following extreme precipitation events. This explanation supports the notion that shallow landslides on agricultural hillslopes increase meteoric  $^{10}\text{Be}$  concentrations in flood deposits, not just in the tributaries, but also in the outlet sample (point D; Figure 4 – 6). This observation suggests that the amount of sediment released during such events is proportionately large enough to be detected even among the presence of large volumes of low-concentration gully-derived sediment that typically overwhelms the Waipaoa system.

***Spatial distribution of in situ and meteoric  $^{10}\text{Be}$  concentrations:***

Concentration of *in situ*  $^{10}\text{Be}$  range from  $2.77 \pm 0.11$  to  $0.11 \pm 0.03 \times 10^4$  at/g for the 18 samples from which we were able to isolate sufficient quartz for AMS measurement (Figure 4 - 9; Table 4 - 5). The lowest concentrations are from the headwater basin draining heavily gullied terrain. The eastern (Waihora) and western (Waikohu) large tributary basins, dominated by periodic shallow landsliding, yield considerably higher concentrations of *in situ*  $^{10}\text{Be}$  presumably because of the longer residence time of near-surface materials and more even sourcing of sediment as opposed to the gullied headwaters. The Te Arai basin sample (wa20) yields the highest *in situ* concentration and was collected from the only tributary basin still remaining under native vegetation, the Waterworks Bush. Mainstem and outlet samples appear to represent a mix of material originating in the heavily gullied headwaters, and the more stable eastern and western tributaries (Figure 4 - 3).

The range of meteoric  $^{10}\text{Be}$  concentrations spans nearly 2 orders of magnitude from  $5.61 \pm 0.16 \times 10^7$  to  $7.38 \pm 0.90 \times 10^5$  at/g for the 87 (77 plus 10 laboratory replicate) river sediment samples we collected from the Waipaoa Basin and basins to the north and south (Figure 4 - 10; Table 4 - 6). The highest concentration is from the Motu River basin located immediately to the north of the Waipaoa, and draining northward into the Bay of Plenty. The lowest concentration was measured at the outlet of the feeder channel draining the Tarndale gully complex in the Te Weraroa basin.

Similar to concentrations of *in situ*  $^{10}\text{Be}$ , the lowest concentrations of meteoric  $^{10}\text{Be}$  originate from the gullied headwaters. Concentrations from the eastern and western tributaries, and the Te Arai basin to the south are typically higher than the headwater samples, and mainstem and outlet samples appear to be dominated by sediment containing little  $^{10}\text{Be}$  and originating from a small percentage of the landscape.

***Hillslope depth-distribution of meteoric  $^{10}\text{Be}$  – the source of river sediment:***

The depth-distribution of meteoric  $^{10}\text{Be}$  concentrations (n=14) measured in samples of material collected from a hillside in the Waimata Basin (Figure 4 - 1) shows the maximum concentration at the surface followed by a sharp decline in concentrations; a pattern typical of quickly eroding land surfaces (e.g. Graly et al., 2010). Six samples collected from a prominent and relatively stable nose on the on the Waimata hillslope to a depth of ~1 m decline steadily from  $\sim 11 \times 10^7$  at/g at the surface to  $\sim 2 \times 10^7$  atoms of  $\times 10^4$  at/g  $\times 10^7$  at/g meteoric  $^{10}\text{Be}$  per gram of material at depth (Figure 4 - 8 upper panel; Reusser, L. and Bierman, P., 2010). This area from which the soil profile was collected

stands above the surrounding hillslope suggesting that this nose is more stable than more rapidly eroding slopes to either side. Lower concentrations of meteoric  $^{10}\text{Be}$  measured in samples of A- and B-horizon soils from these more quickly eroding and less stable parts of the hillslope support the assertion that the profile represents the depth-distribution of meteoric  $^{10}\text{Be}$  in more stable landscape features (Figure 4 - 8 inset boxes in upper panel).

#### 4.6. Discussion

Spatial and temporal variability in both *in situ* and meteoric  $^{10}\text{Be}$  concentrations characterize the most disturbed and geomorphically active areas of the Waipaoa landscape. Laboratory replication, indicates that much of the variability we see in the datasets for both isotopic systems is the result different erosional styles operating in different regions of the Waipaoa basin, and of the stochastic nature of hydrologically-triggered surface processes in this tectonically active and severely disturbed landscape.

Such variability is caused by episodic hydrologic events (cyclones) and tectonically-driven earthquakes which trigger landsliding and both spatially and temporally disjunct sediment delivery to headwater and larger tributary streams. The prevalence of both shallow landslides and deep gullies means that sediment delivered to the river network is derived from a variety of depths ranging from surface wash to several tens of meters below the surface. Further, while the gullied headwaters continually feed the majority of sediment to the mainstem (at a pace that roughly scales with precipitation levels), the more stable eastern and western tributaries only occasionally feed short-lived, large volume pulses of sediment to the mainstem during extreme hydrologic or

earthquake triggered events. Temporal differences in isotope concentrations most likely reflect changing source areas for fluvial sediments over the time interval between sample collection periods whereas spatial differences in concentration represent the relative stability of the landscape both over the long (natural) and short (human-influenced) time scales.

In some cases, long-term patterns of landscape evolution control the concentration of  $^{10}\text{Be}$  in river sediments. For example, upstream of knickpoints in the Waipaoa and adjacent drainage basins, relief is less and the landscape is more subdued. A sample from one of these basins (wa41) has a high concentration of meteoric  $^{10}\text{Be}$ , implying a long residence time for near-surface materials. Being above a knickpoint, and draining somewhat more subdued topography than surrounding areas, this part of the basin remains isolated from many of the natural and anthropogenic drivers of erosion due to its lower slope (e.g. Crosby and Whipple, 2006).

***Comparison of meteoric and in situ  $^{10}\text{Be}$  concentrations:***

There are pronounced differences in the relative concentrations of in situ and meteoric  $^{10}\text{Be}$  measured in the 18 samples in which we have data for both isotope systems (Figure 4 - 11A & B; 15 samples within the Waipaoa Basin; 3 outside the basin). Using both meteoric and in situ measurements made in the same sample, we can differentiate sediment sourced from different parts of the catchment understanding that the *in situ*  $^{10}\text{Be}$  measured in quartz isolated from a bulk sample of river sediment is not necessarily representative of surface process rates throughout the entire watershed.

In the undisturbed Waterworks bush, where vegetation is thick, landslides are rare, and soil creep likely supplies most sediment to the channel, both *in situ* and meteoric  $^{10}\text{Be}$  have relatively high concentrations. In contrast, sediment from the deeply gullied headwaters, sourced from deep gashes into the landscape, has low concentrations of both meteoric and *in situ*  $^{10}\text{Be}$ . In other samples, such as those collected along the mainstem Waipaoa River, the ratio of *in situ*  $^{10}\text{Be}$  to meteoric  $^{10}\text{Be}$  concentration is high (Figure 4 - 11C) suggesting that the quartz within the bulk samples reflects shallower source depths and/or more slowly eroding portions of the basin than the bulk sample. The enhancement of *in situ*  $^{10}\text{Be}$  relative to meteoric  $^{10}\text{Be}$  in the mainstem and outlet samples also indicates that the majority of the sediment carried by the Waipaoa River at these locations comes from deep source depths with very low meteoric  $^{10}\text{Be}$  concentrations, such as the gullied headwaters (refer to Figure 1). The quartz carried by the river today likely comes from outcropping, more resistant sandstone beds. Where large amounts of low-meteoritic  $^{10}\text{Be}$  concentration gully-derived sediment mix with proportionately smaller amounts of sediment from the more stable eastern and western tributaries, containing relatively high concentrations of *in situ*  $^{10}\text{Be}$ , (Figure 4 -12), mainstem channel sediment predominately reflects gullies.

***Regional considerations:***

Concentrations of meteoric  $^{10}\text{Be}$  measured from nearby rivers (Figure 10 lower panels) suggest that most fluvial sediment in the Waimata River basin is sourced from depths equivalent to ~50 cm below more stable land surfaces, represented by the soil

profile data. Concentrations in these fluvial samples ( $\sim 1$  to  $3.5 \text{ at/g} \times 10^7 \text{ at/g}$ ) are similar to those measured in rivers draining the eastern, western and southwestern tributaries in the Waipaoa basin (average =  $2.2 \times 10^7 \text{ at/g}$ ; Figure 4 - 5; Table 4 - 6).

***Background erosion rates in the Waipaoa Basin:***

The interpretation of in situ produced  $^{10}\text{Be}$  concentrations as erosion rates in the Waipaoa Drainage Basin is uncertain because the  $^{10}\text{Be}$  data clearly show temporal changes in isotope concentration and indicate varying sediment sources over time. The cause of such variability likely includes both aerially changing sediment sources and the erosion of sediment from different depths over time. The sometimes substantially different concentrations of  $^{10}\text{Be}$  we measured in sequential samples from the same site may reflect the passage of sediment waves, which originated in discrete events such as landslides, past sampling sites.

Using *in-situ*- $^{10}\text{Be}$ -based erosion rate estimates from the Waihora (eastern; wa02/23ave), the Waihuka (western; wa15), and the Te Arai (southwestern; wa05) tributary outlet samples we generate an area-weighted background erosion rate of  $\sim 250 \text{ m/My}$  (Figure 4 - 13). These basins are most likely to yield a meaningful erosion rate because they are not heavily gullied. Because all of these tributary basins are susceptible to periodic episodes of wide-spread, shallow landsliding during large precipitation events, this estimate may not be fully representative of background erosion rates over millennial time-scales (e.g. Niemi, *et al.*, 2005).

The background erosion rate estimate derived from *in situ*  $^{10}\text{Be}$  (250 m/My) is less than that provided by Kettner, *et al.* (2007), 400 m/My. Interpreting *in situ*  $^{10}\text{Be}$  concentrations has an additional complication –sand size quartz is not uniformly distributed throughout the basin because more indurated sandstone beds generally stand above less-resistant mudstones. If quartz-bearing rocks in the Waipaoa Basin are more erosion-resistant than the surrounding calcareous mudstone typical of the Waipaoa region, *in situ*  $^{10}\text{Be}$  estimates would underestimate regional background rates of erosion. Both estimates of background erosion rates for the Waipaoa Basin are nearly 2 orders of magnitude less than the contemporary erosion rate inferred from sediment loads leaving the catchments (~2.6 km/My; Hicks, 2000), a rate that is reflective of land clearance for agriculture.

#### 4.7. References Cited:

- Balco, G., Stone, J., Lifton, N. A., and Dunai, T. J., 2008, A complete and easily accessible means of calculating surface exposure ages or erosion rates from  $^{10}\text{Be}$  and  $^{26}\text{Al}$  measurements: *Quaternary Geochronology*, v. 3, no. 3, p. 174-195.
- Berryman, K. R., Marden, M., Eden, D., Mazengarb, C., Ota, Y., and Moriya, I., 2000, Tectonic and paleoclimatic significance of Quaternary river terraces of the Waipaoa River, East Coast, North Island, New Zealand, *in* Anonymous, ed., *Proceedings of the 9th Australia New Zealand Geomorphology Group (ANZGG) conference; programme and abstracts*, Publisher Australia New Zealand Geomorphology Group, New Zealand, p. 5.
- Bierman, P., and Steig, E., 1996, Estimating rates of denudation and sediment transport using cosmogenic isotope abundances in sediment: *Earth Surface Processes and Landforms*, v. 21, p. 125-139.
- Black, R. D., 1980, Upper Cretaceous and Tertiary geology of Mangatu State Forest, Raukumara Peninsula, New Zealand: *New Zealand Journal of Geology and Geophysics*, v. 23, p. 293-312.
- Brown, E. T., Stallard, R. F., Larsen, M. C., Bourles, D. L., Raisbeck, G. M., and Yiou, F., 1995, Pre-anthropogenic denudation rates of a perturbed watershed (Cayaguas, Puerto Rico) estimated from in situ-produced  $^{10}\text{Be}$  in river borne quartz: *EOS*, v. 76, no. 46.

- Caine, N., 1980, The rainfall intensity: Duration control of shallow landslides and debris flows: *Geografiska Annaller. Series A, Physical Geography*, v. 62A, no. 1-2, p. 23-27.
- Crosby, B. T., and Whipple, K. X., 2006, Knickpoint migration and distribution within fluvial networks: 236 waterfalls in the Waipaoa River, North Island, New Zealand: *Geomorphology*, v. 82, p. 16-38.
- Eden, D., Palmer, A. N., Cronin, S. J., Marden, M., and Berryman, K. R., 2001, Dating the culmination of river aggradation at the end of the last glaciation using distal tephra compositions, eastern North Island, New Zealand: *Geomorphology*, v. 38, no. 1-2, p. 133-151.
- Elmore, D., and Phillips, F. M., 1987, Accelerator mass spectrometry for measurement of long-lived radioisotopes: *Science*, v. 236, p. 543-550.
- Froggatt, P. C., and Lowe, D., 1990, A review of late quaternary silicic and some other tephra formations from New Zealand: their stratigraphy, nomenclature, distribution, volume, and age: *New Zealand Journal of Geology and Geophysics*, v. 33, p. 89-109.
- Graham, I., Ditchburn, R., and Barry, B., 2003, Atmospheric deposition of  $^7\text{Be}$  and  $^{10}\text{Be}$  in New Zealand rain (1996-98): *Geochemica et Cosmochemica Acta*, v. 67, no. 3, p. 361-373.
- Granger, D. E., Kirchner, J. W., and Finkel, R., 1996, Spatially averaged long-term erosion rates measured from in situ-produced cosmogenic nuclides in alluvial sediments: *Journal of Geology*, v. 104, no. 3, p. 249-257.

- Hessell, J. W., 1980, The climate and weather of the Gisborne region: New Zealand Meteorological Service, Misc. Publ, v. 115, p. 29p.
- Hicks, D. M., Gomez, B., and Trustrum, N. A., 2000, Erosion thresholds and suspended sediment yields, Waipaoa River Basin, New Zealand: Water Resources Research, v. 36, no. 4, p. 1129-1142.
- Kettner, A. J., Gomez, B., and Syvitski, J. P. M., 2007, Modeling suspended sediment discharge from the Waipaoa River system, New Zealand: The last 3000 years: Water Resources Research, v. 43, no. W07411, p. doi: 10.1029/2006WR005570.
- Lal, D., 1991, Cosmic ray labeling of erosion surfaces; *in situ* nuclide production rates and erosion models: Earth and Planetary Science Letters, v. 104, no. 2-4, p. 424-439.
- Lal, D., and Peters, B., 1967, Cosmic ray produced radioactivity on the Earth, *in* Sitte, K., ed., Handbuch der Physik: New York, Springer-Verlag, p. 551-612.
- Mazengarb, C., and Speden, I., 2000, Geology of the Raukumara Area, Map 6: Institute of Geological & Nuclear Sciences, 1 sheet 1:250,000, 260 pp, scale 1:250,000.
- Merchel, S., Arnold, M., Aumaitre, G., Benedetti, L., Boules, D. L., Braucher, R., Alfimov, V., Freeman, S., Steier, P., and Wallner, A., 2008, Toward more precise  $^{10}\text{Be}$  and  $^{36}\text{Cl}$  data from measurements at the 10-14 level: influence of sample preparation: Nuclear Instruments and Methods in Physics Research B, v. 266, p. 4921-4926.

- Monaghan, M. C., Krishnaswami, S., and Turekian, K. K., 1986, The global-average production rate of  $^{10}\text{Be}$ : *Earth and Planetary Science Letters*, v. 76 (1985/86), p. 279-287.
- Niemi, N., Oskin, M., Burbank, D. W., Heimsath, A. M., and Gabet, E., 2005, Effects of bedrock landslides on cosmogenically determined erosion rates: *Earth and Planetary Science Letters*, v. 237, no. 3-4, p. 480-498.
- Nishiizumi, K., Imamura, M., Caffee, M., Southon, J., Finkel, R., and McAninch, J., 2007, Absolute calibration of  $^{10}\text{Be}$  AMS standards: *Nuclear Instruments and Methods in Physics Research B*, v. 258, p. 403-413.
- Nyffeler, U. P., Li, Y.-H., and Santschi, P. H., 1984, A kinetic approach to describe trace-element distribution between particles and solution in natural aquatic systems: *Geochemica et Cosmochemica Acta*, v. 48, p. 1513-1522.
- Reusser, L. J., and Bierman, P., 2010, Using meteoric  $^{10}\text{Be}$  to track fluvial sand through the Waipaoa River basin, New Zealand: *Geology*, v. 38, no. 1, p. 47-50.
- Safran, E. B., Bierman, P., Aalto, R., Dunne, T., and Whipple, K. X., 2005, Erosion rates driven by channel network incision in the Bolivian Andes: *Earth Surface Processes and Landforms*, v. 30, p. 1007-1024.

#### 4.8. Figure Captions:

**Figure 4 - 1:** A. Air photo of the Tarndale Slip. B. Location map of the Waipaoa River Basin. Map shows all data points included in this study. For clarity, sample IDs have been abbreviated (i.e. 10 stands for WA10met in Table DR-1). Temporal replicate ID's are separated with a slash (i.e. 1/21). (X) denotes the location of the soil profile presented in figure 2. C. Photo oriented NW looking up the channel exiting the Tarndale Slip. D. Gully-derived sediments in the mainstem ~2 km downstream from the Tarndale Slip.

**Figure 4 - 2:** Five independently processed and measured *in situ*  $^{10}\text{Be}$  laboratory replicates. All samples prepared in the cosmogenic laboratory at the University of Washington.

**Figure 4 - 3:** Ten independently processed and measured meteoric  $^{10}\text{Be}$  laboratory replicates. Samples were prepared in three separate laboratories at the University of Washington, Hebrew University, and the cosmogenic laboratory at the University of Vermont. A: laboratory replicates within the Waipaoa Basin. B: replicates for large basin to the north and the south of the Waipaoa Basin.

**Figure 4 - 4:** Results for the two pairs of *in situ*  $^{10}\text{Be}$  temporal replicate samples collected for this study. The replicates were collected to investigate the temporal

variability in *in situ*  $^{10}\text{Be}$  concentrations through time. Note the inverse relationship between positive and negative percent differences for pairs plotted as concentrations (A) and inferred background erosion rates (B).

**Figure 4 - 5:** Temporal variability in *in situ*  $^{10}\text{Be}$  concentrations at 14 sample locations, each sampled at least twice. These temporal replicate represent sampling during 3 separate field seasons (May, 2004; March, 2005; August, 2008). There are four separate potential replicates for each locations, three representing collection of active channel sediment during the field season, and one representing collection of a distinctive and recent flood overbank deposit (7/31/2008) identifiable in nearly all regions of the Waipaoa Basin. Refer to figure 6 for location of the 5 separate mainstem channel sampling locations.

**Figure 4 - 6:** Identification of 1) various regions of the basin (Western vs. Eastern) referred to in other figures and text, and 2) locations along the mainstem Waipaoa channel keyed out in figure 7.

**Figure 4 - 7:** Meteoric  $^{10}\text{Be}$  concentration at various locations (see figure 8) for each of the four potential temporal replicates along the Waipaoa mainstem channel as a function of increasing drainage basin area.

**Figure 4 – 8:** Meteoric  $^{10}\text{Be}$  concentrations measured in samples of hillslope materials from a representative hillslope in the Waimata River basin (tributary to the Te Arai basin), as well as fluvial samples from rivers in close proximity to the Waimata hillslope.

**Figure 4 - 9:** All *in situ*  $^{10}\text{Be}$  concentration arranged by region generated in this study. Samples ending in "...ave" are the averaged values from the laboratory replicate presented in Figure 2. A: *in situ*  $^{10}\text{Be}$  concentrations for samples within the Waipaoa Basin. B: *in situ*  $^{10}\text{Be}$  concentrations for samples from large basin to the North and the South of the Waipaoa Basin.

**Figure 4 - 10:** All fluvial meteoric  $^{10}\text{Be}$  concentrations generated in the study arranged by region. A: meteoric  $^{10}\text{Be}$  concentrations for samples within the Waipaoa Basin. B: meteoric  $^{10}\text{Be}$  concentrations for samples from large basins to the north and the south of the Waipaoa Basin.

**Figure 4 - 11:** Results for 18 samples from which both *in situ* and meteoric  $^{10}\text{Be}$  concentrations were measured. *In situ*  $^{10}\text{Be}$  samples reflect only the production and accumulation of the isotope within the crystal lattice of quartz grains, and therefore only reflects quartz bearing lithologies within a drainage basin. Alternatively, meteoric  $^{10}\text{Be}$  concentration represent the amount of the isotope (produced in the atmosphere) adhered to all grains within a sample; these measurements reflect the "bulk sample"

concentrations. Note that the high vs. low relative concentrations of the two forms of  $^{10}\text{Be}$  do not necessarily track from one region to another.

**Figure 4 - 12:** Normalized concentrations of meteoric  $^{10}\text{Be}$  plotted against normalized concentrations of *in situ*  $^{10}\text{Be}$  for all comparison samples within the Waipaoa River basin (n=15). *In situ*  $^{10}\text{Be}$  concentrations were normalized according to their ELD scaling factors to reflect different production rates of the isotope at different elevations and latitudes (Balco et al., 2008; Lal and Peters, 1967). Meteoric  $^{10}\text{Be}$  concentrations were normalized according to the modeled average-basin-elevation-dependent mean annual precipitation (MAP) according to the relationship presented in Hessell (1980) for the North Island, to account for varying delivery rates of the isotope across the basin. Samples from different regions around the basin are noted on the figure.

**Figure 4 - 13:** Compilation of all available erosion rate proxies that have been generated and published. These include sediment yield data compiled and published in Hicks, *et al.* (2000), and modeled estimates of background, post Polynesian arrival, and post European arrival rates of erosion (Kettner et al., 2007). Note that the outlet proxy and outlet *in situ*  $^{10}\text{Be}$  both represent erosion rates for the entire basin that are comparable to one another.

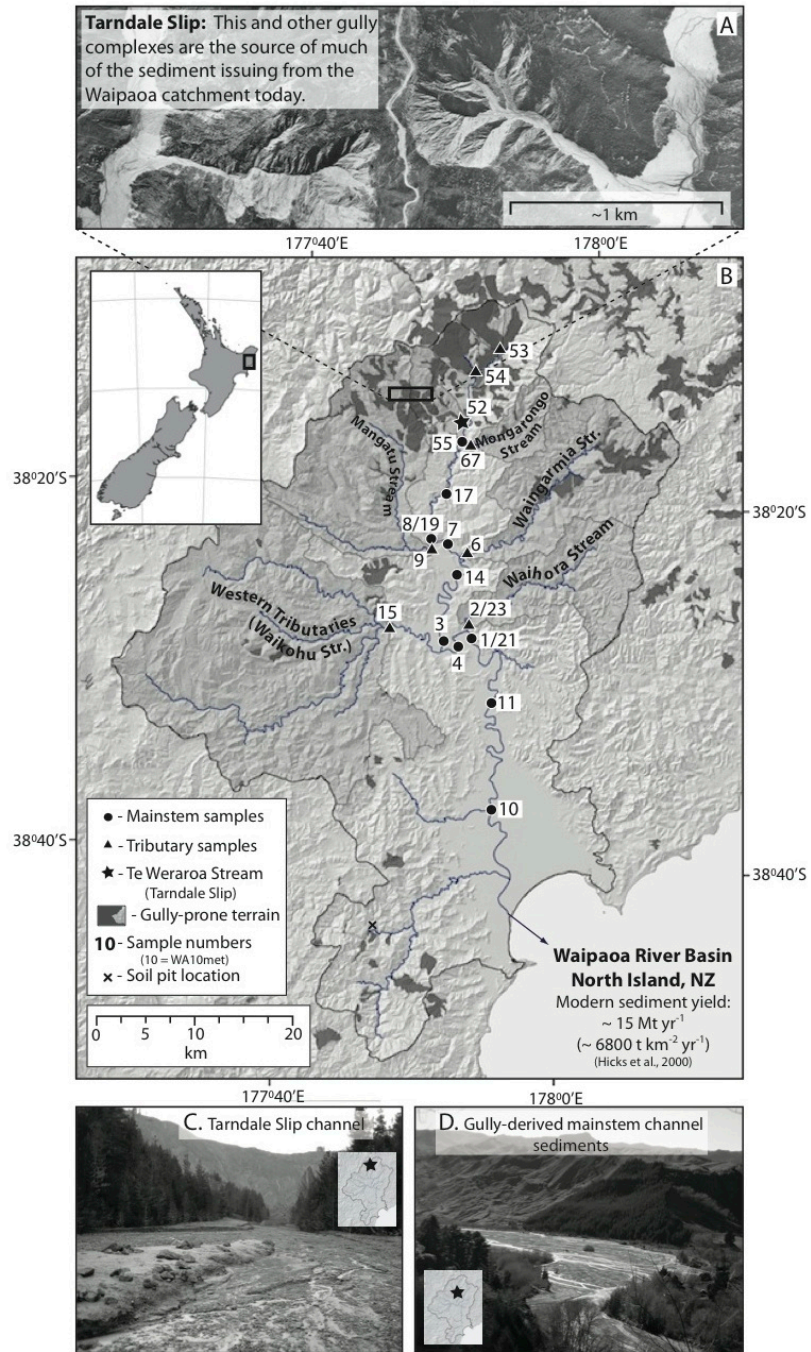


Figure 4 - 1 Location map for the Waipaoa River Basin showing the influence of gullies on channel sediments

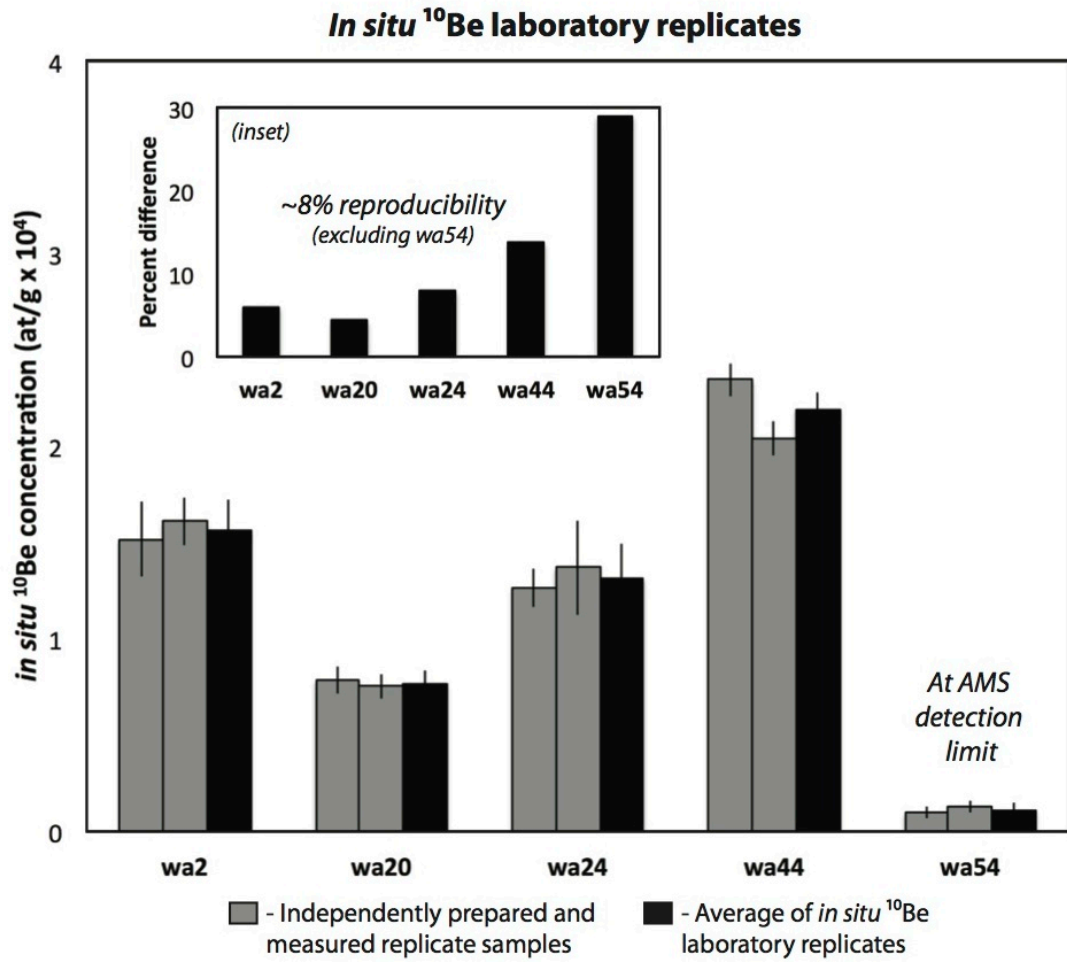


Figure 4 - 2 *In situ* <sup>10</sup>Be laboratory replicates

### Meteoric $^{10}\text{Be}$ laboratory replicates by region

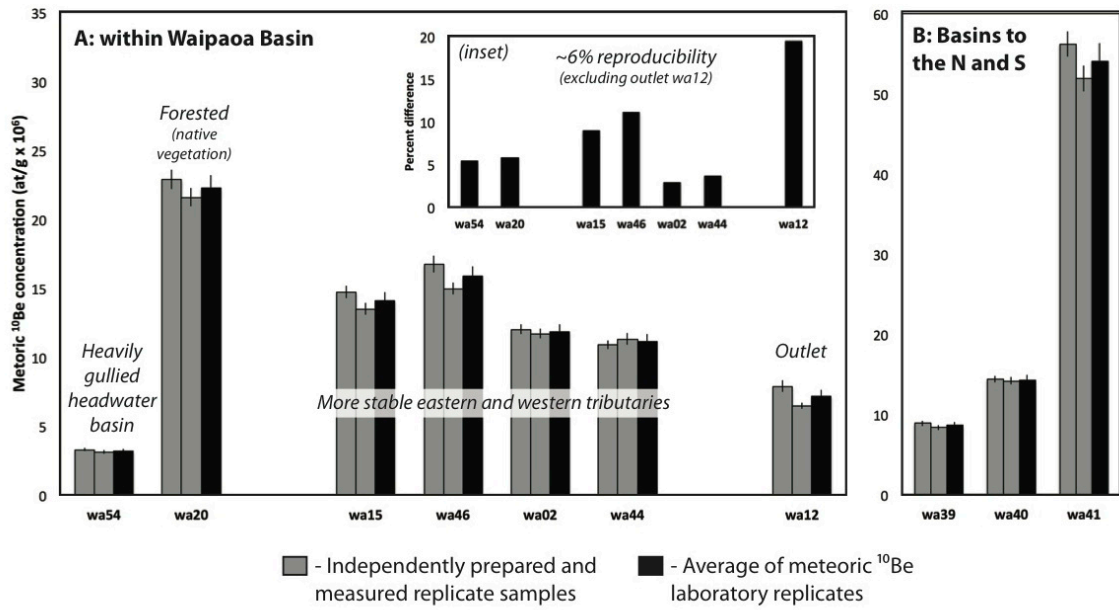


Figure 4 - 3 Meteoric  $^{10}\text{Be}$  laboratory replicates

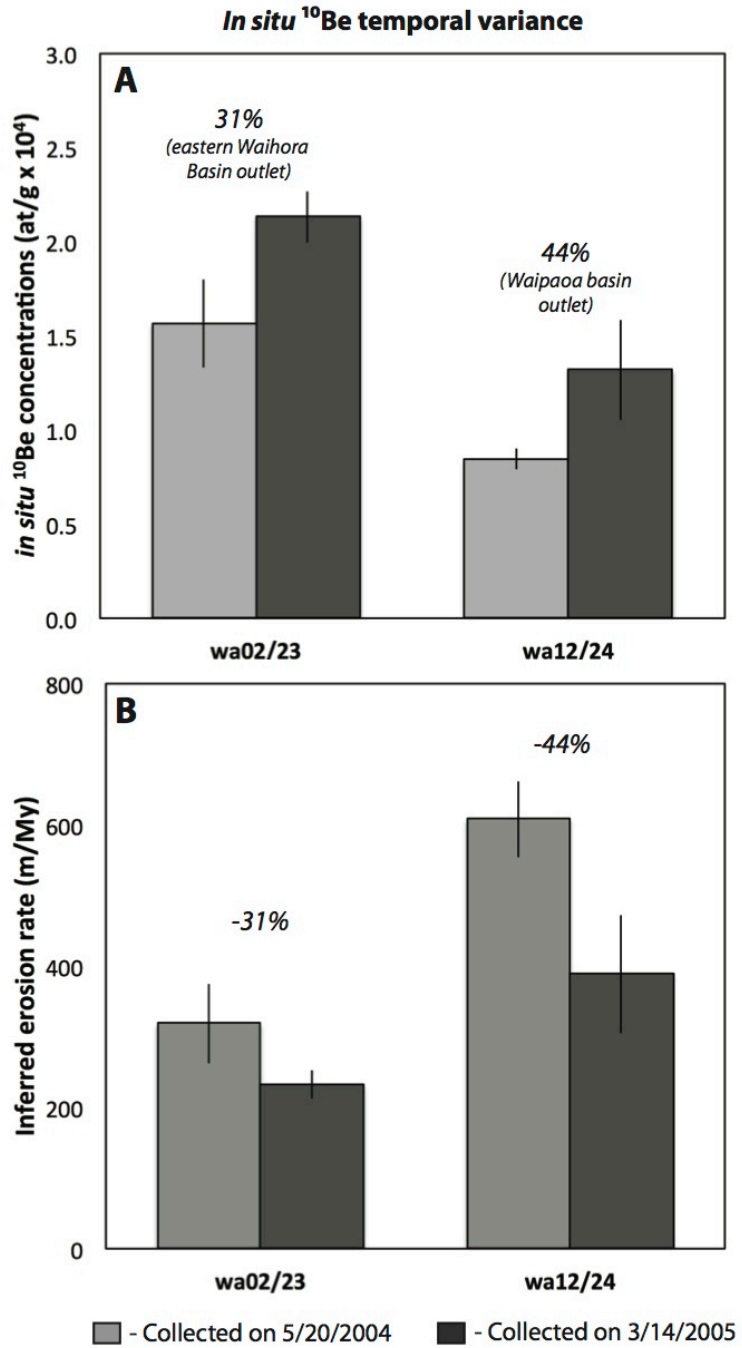


Figure 4 - 4 *In situ* <sup>10</sup>Be temporal variability

### Meteoric <sup>10</sup>Be temporal variance by region

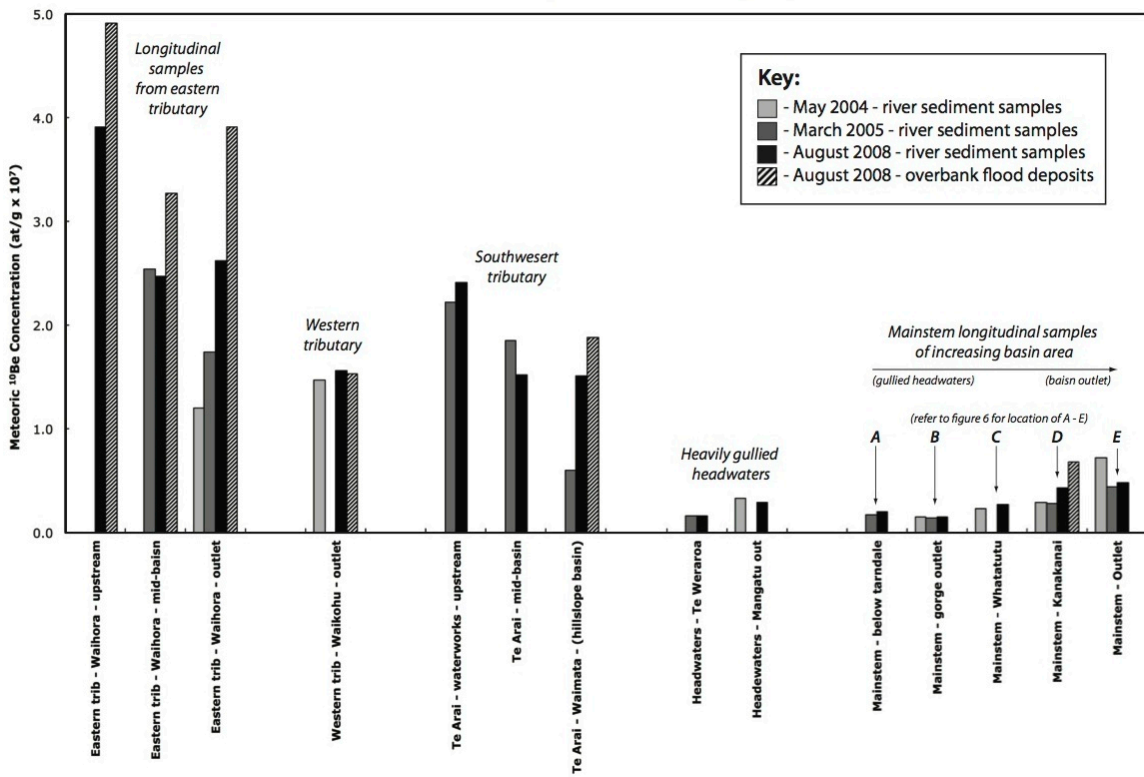


Figure 4 - 5 Meteoric <sup>10</sup>Be temporal variability

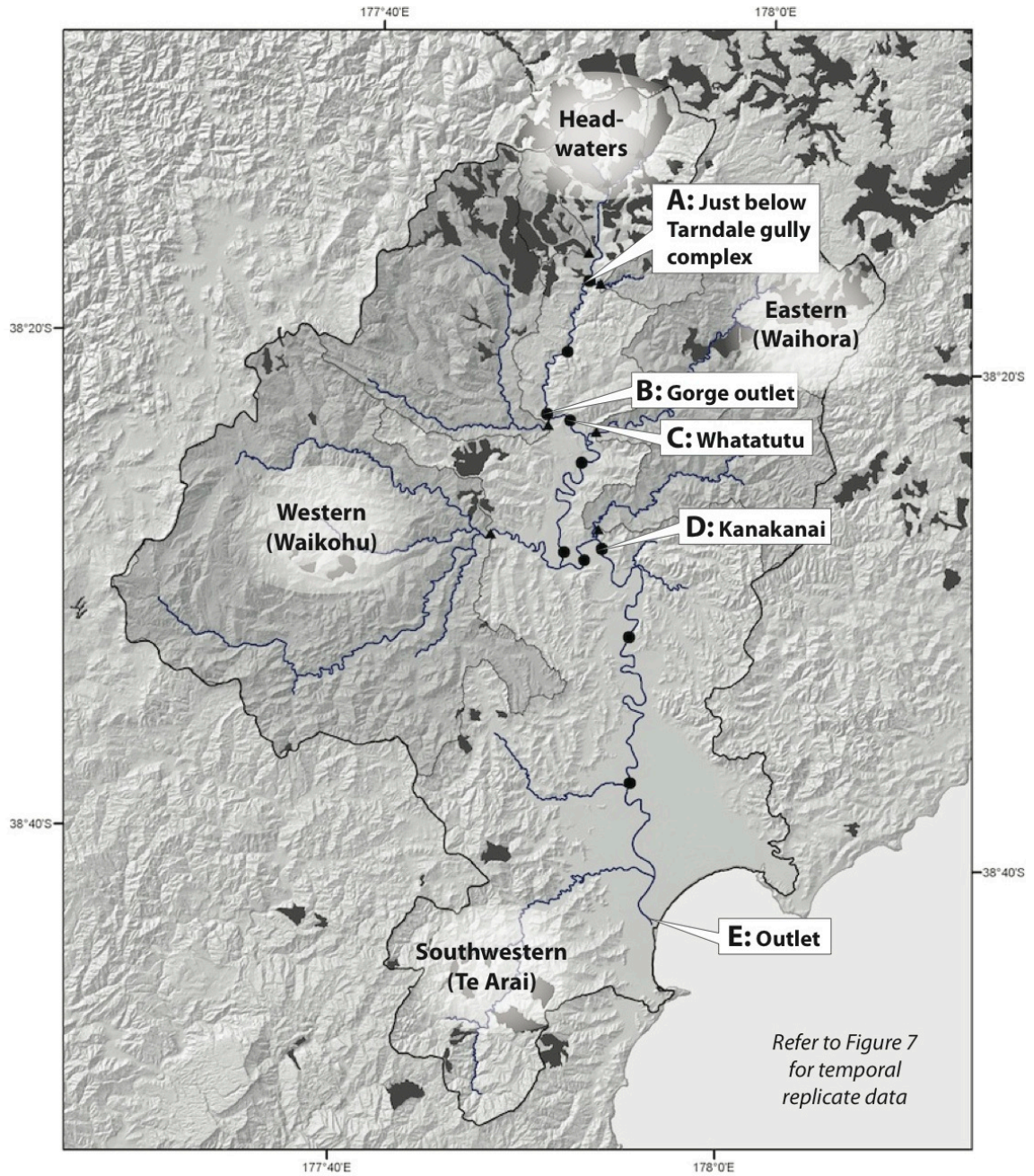


Figure 4 - 6 Map depicting points of interest along the Waipaoa River mainstem from figure 7 and discussed in the text

### Meteoric $^{10}\text{Be}$ temporal variance along mainstem Waipaoa River

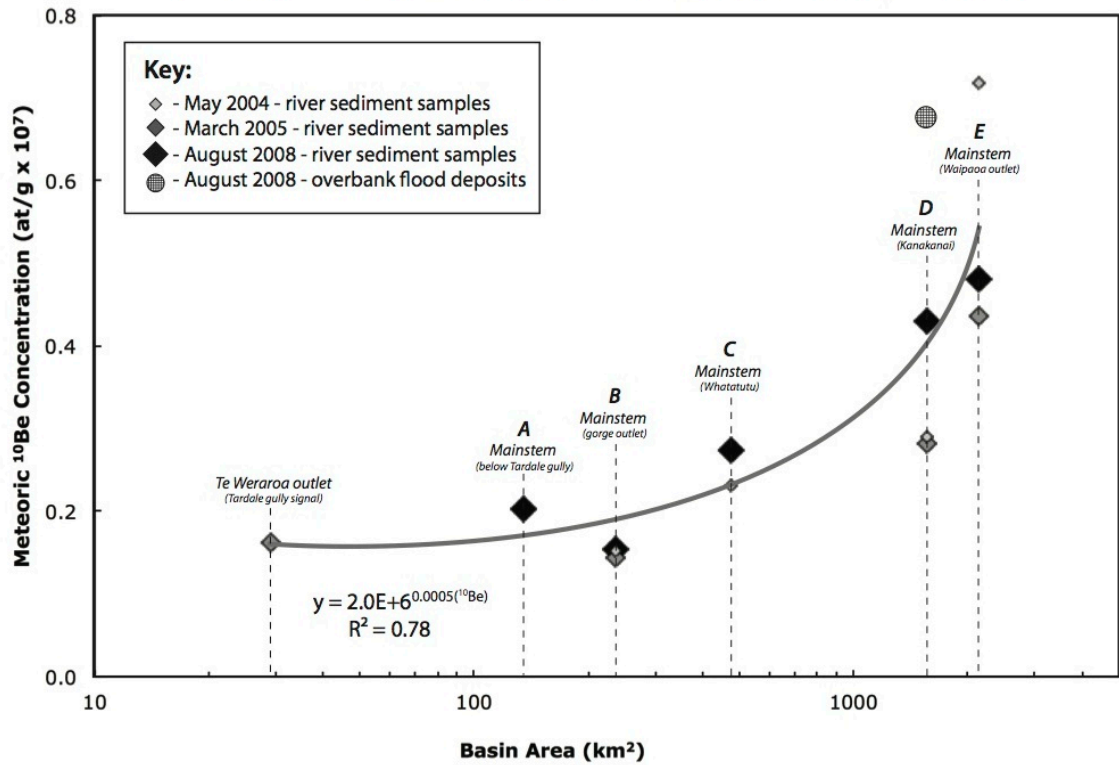


Figure 4 - 7 Temporal variance in meteoric  $^{10}\text{Be}$  concentrations as a function of drainage basin area

# Meteoric $^{10}\text{Be}$ in hillslope materials

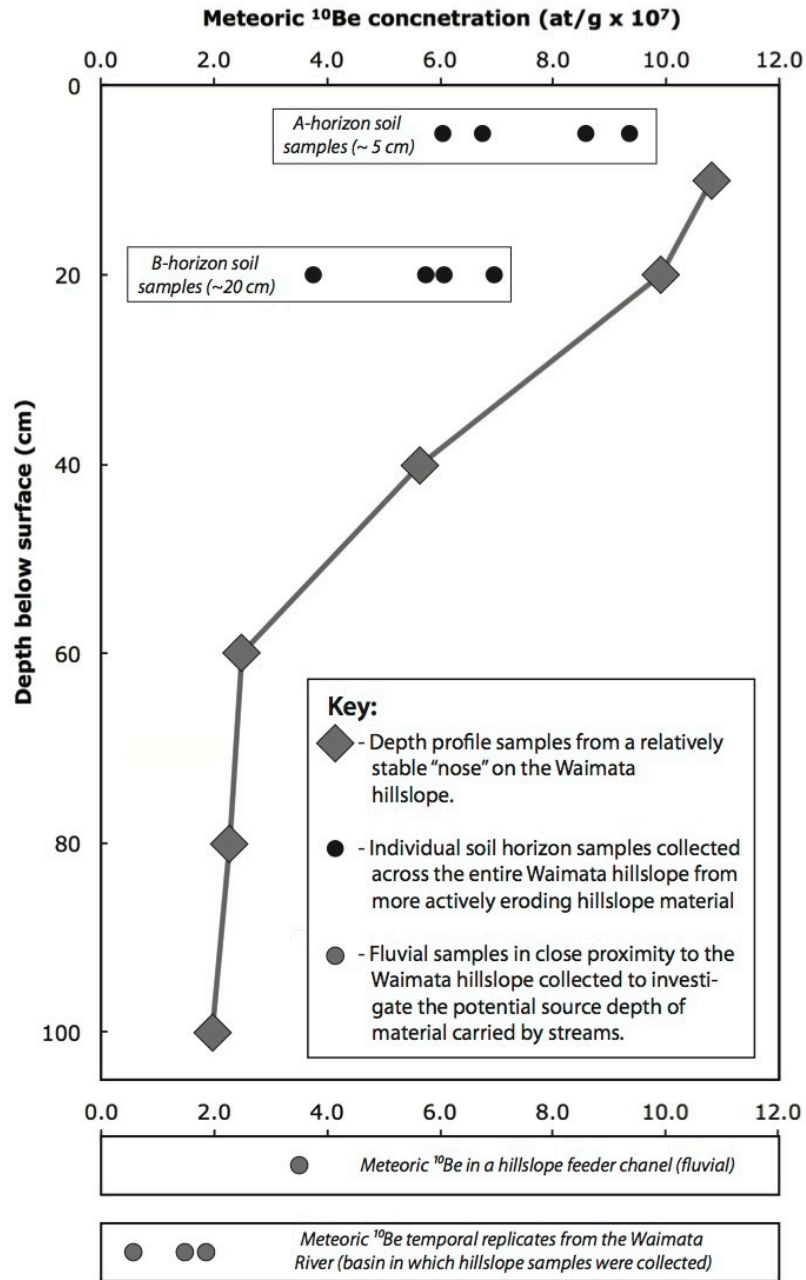


Figure 4 - 8 Depth-distribution of meteoric  $^{10}\text{Be}$  concentrations within soil samples from the Waimata hillslope

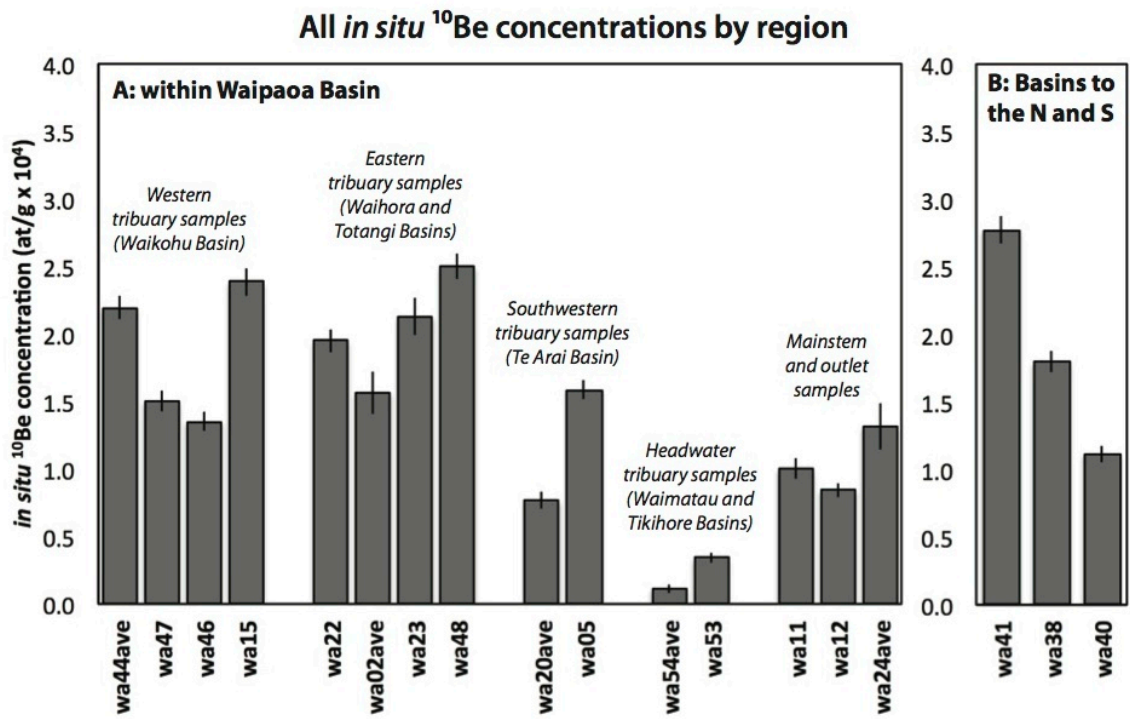


Figure 4 - 9 Distribution of in situ <sup>10</sup>Be across the study area

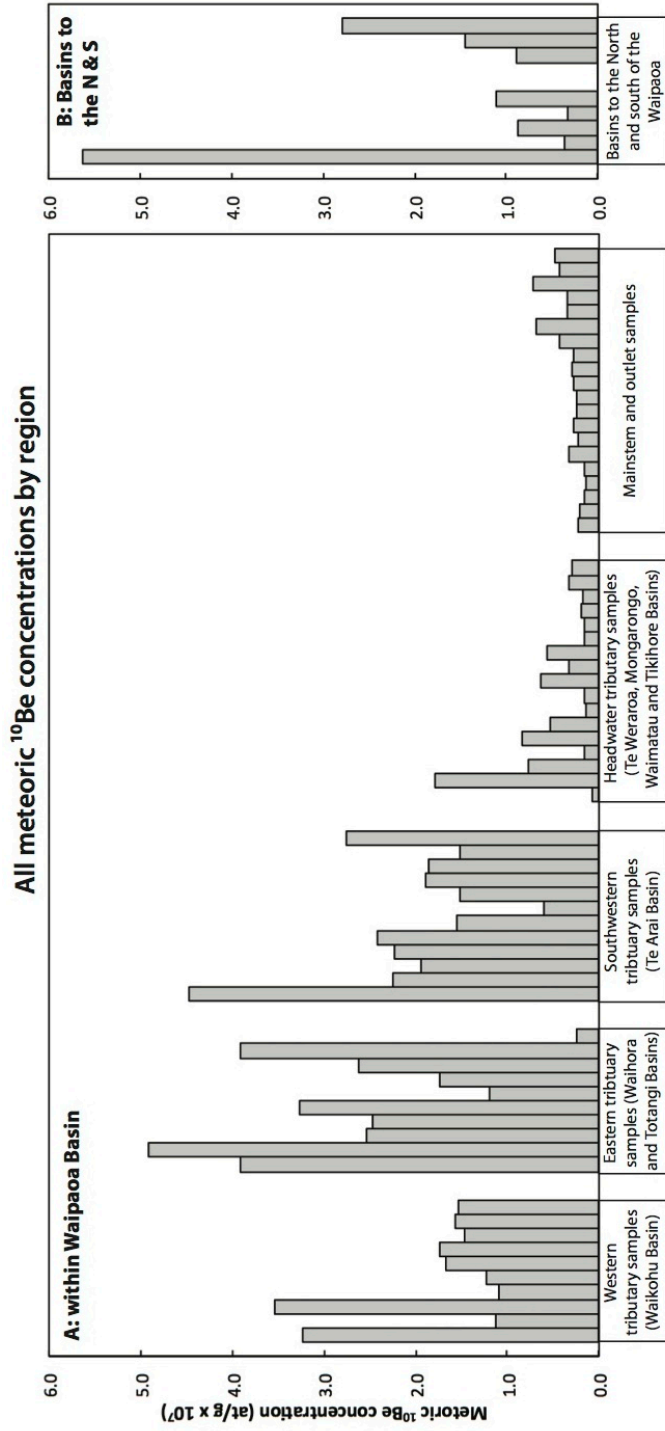


Figure 4 - 10 Distribution of meteoric  $^{10}\text{Be}$  concentration across the landscape.

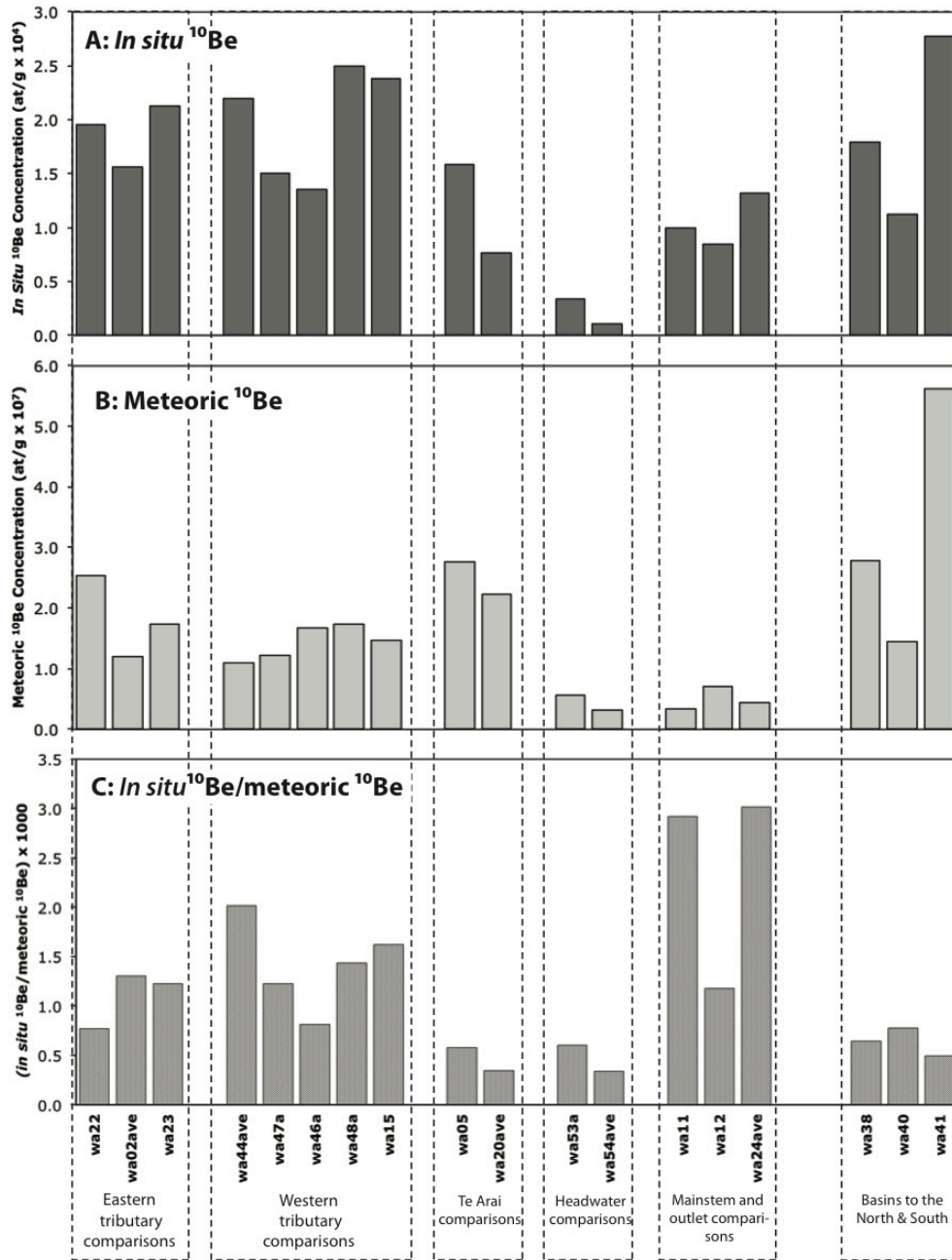


Figure 4 - 11 *In situ* and meteoric <sup>10</sup>Be concentrations from the 18 comparison samples

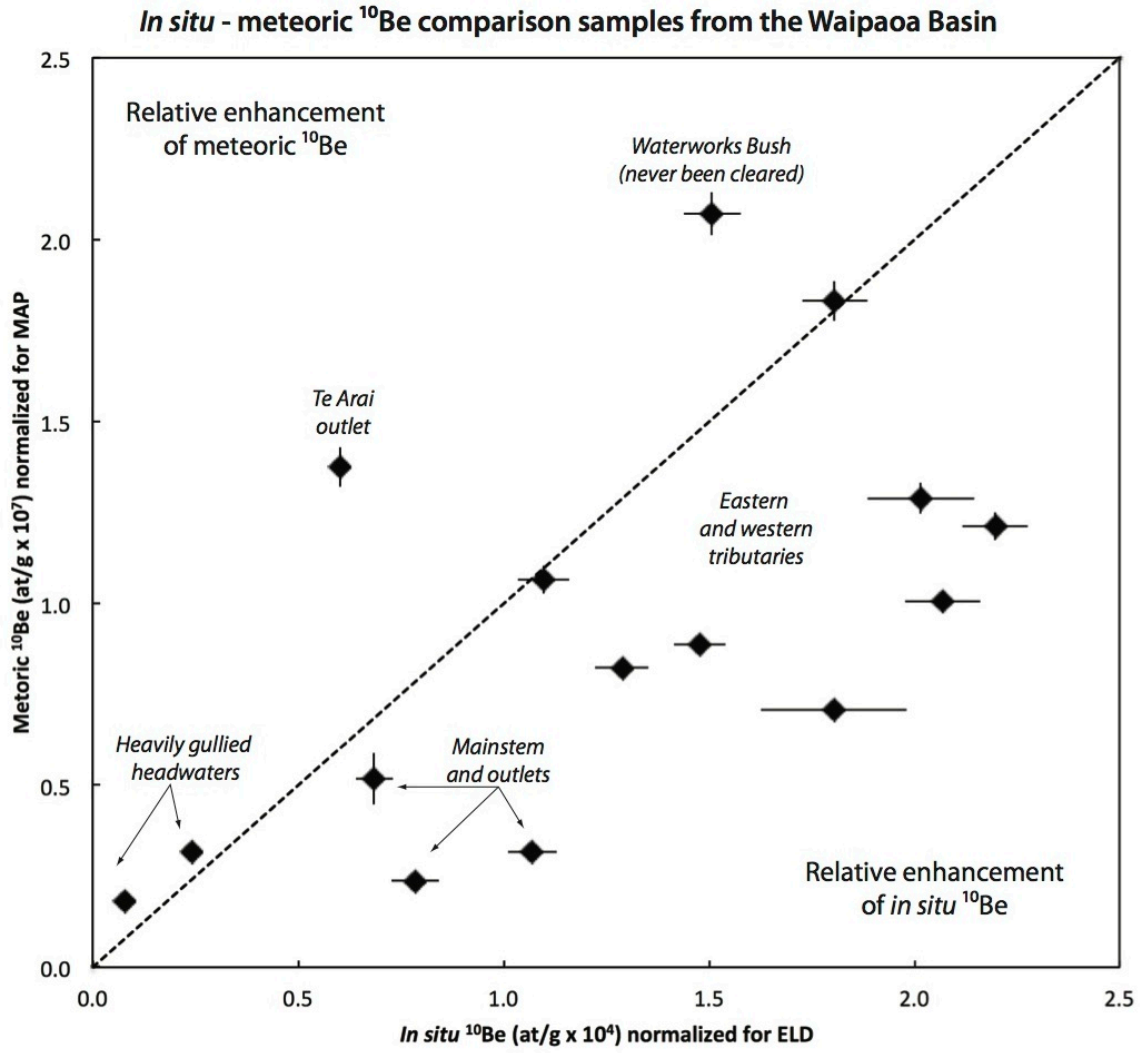


Figure 4 - 12 Normalized concentrations of *in situ* and meteoric <sup>10</sup>Be concentrations

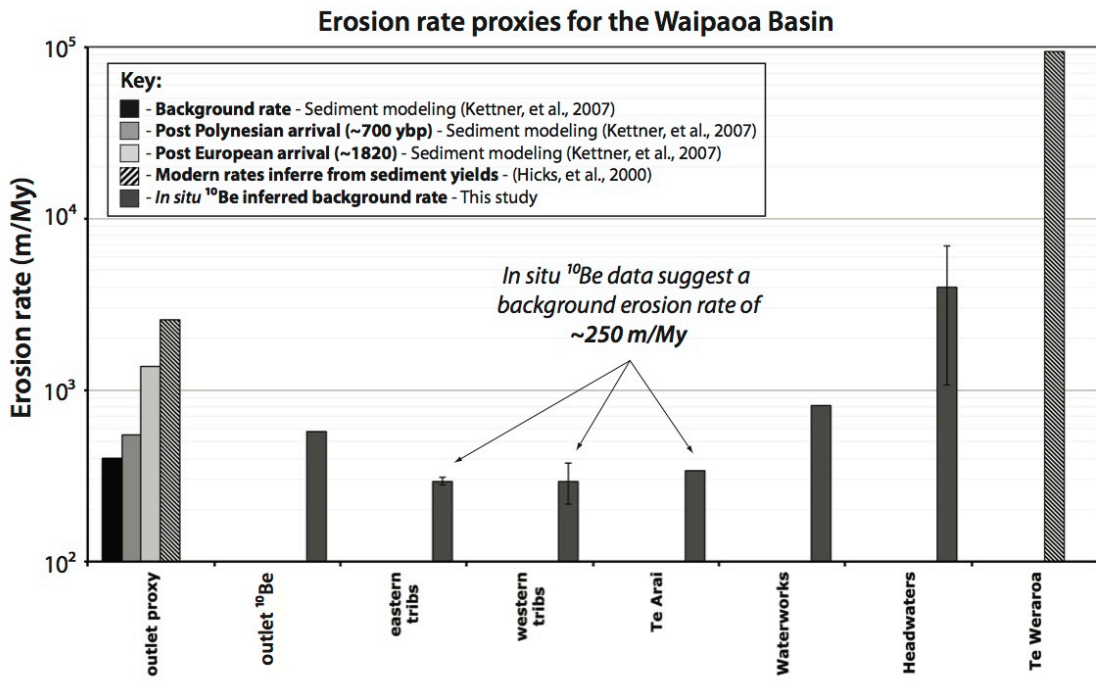


Figure 4 - 13 Estimates of background erosion made with concentrations of *in situ* <sup>10</sup>Be compared to other previously proxy estimates

Table 1: *In situ* <sup>10</sup>Be laboratory/measurement replicate samples from the Waipaoa River Basin, NZ.

Sample ID	Be number	Grain size (µm)	Sample basin	<sup>10</sup> Be extraction lab	Measured at	Measurement date	Measured ratio ( <sup>10</sup> Be/Be × 10 <sup>-12</sup> ; 1σ error)	<i>In situ</i> <sup>10</sup> Be (atoms/g × 10 <sup>-12</sup> ; 1σ error)	AMS % uncertainty	Inferred erosion rate (m/Myr; 1σ error)	<sup>10</sup> Be lab. rep. % difference
wa02	BE24447	850-250	Waihora	Un. of Washington	CAMS - LLNL	10/3/03	1.81 ± 0.23	1.52 ± 0.20	13.0%	328.6 ± 48.0	-
wa02X	BE24926	850-250	Waihora	Un. of Washington	CAMS - LLNL	1/17/04	1.43 ± 0.11	1.61 ± 0.12	7.8%	309.2 ± 30.8	-
wa02ave	-	850-250	Waihora	Un. of Washington	CAMS - LLNL	-	1.62 ± 0.17	1.56 ± 0.16	-	318.9 ± 39.4	6.0%
wa20	BE24578	850-250	Wateworks	Un. of Washington	CAMS - LLNL	11/15/03	0.91 ± 0.08	0.79 ± 0.07	9.3%	729.5 ± 82.5	-
wa20X	BE24928	850-250	Wateworks	Un. of Washington	CAMS - LLNL	1/17/04	0.96 ± 0.08	0.75 ± 0.06	8.3%	762.1 ± 79.9	-
wa20ave	-	850-250	Wateworks	Un. of Washington	CAMS - LLNL	-	0.94 ± 0.08	0.77 ± 0.07	-	745.8 ± 81.2	4.3%
wa24	BE24443	850-250	Waipaoa outlet	Un. of Washington	CAMS - LLNL	10/3/03	1.50 ± 0.11	1.26 ± 0.10	7.9%	404.5 ± 40.6	-
wa24X	BE24927	850-250	Waipaoa outlet	Un. of Washington	CAMS - LLNL	1/17/04	1.63 ± 0.29	1.37 ± 0.24	17.9%	373.4 ± 73.0	-
wa24ave	-	850-250	Waipaoa outlet	Un. of Washington	CAMS - LLNL	-	1.57 ± 0.20	1.32 ± 0.17	-	388.9 ± 56.8	7.9%
wa44	BE24446	850-250	Waihuka	Un. of Washington	CAMS - LLNL	10/3/03	2.78 ± 0.09	2.35 ± 0.09	3.8%	233.0 ± 17.1	-
wa44X	BE24582	850-250	Waihuka	Un. of Washington	CAMS - LLNL	11/15/03	2.41 ± 0.10	2.04 ± 0.09	4.4%	271.1 ± 20.9	-
wa44ave	-	850-250	Waihuka	Un. of Washington	CAMS - LLNL	-	2.60 ± 0.09	2.19 ± 0.09	-	252.1 ± 19.0	13.8%
wa54	BE24454	850-250	Waimatau	Un. of Washington	CAMS - LLNL	10/3/03	0.11 ± 0.04	0.09 ± 0.03	33.4%	6591.6 ± 2509.8	-
wa54X	BE24583	850-250	Waimatau	Un. of Washington	CAMS - LLNL	11/15/03	0.15 ± 0.04	0.13 ± 0.03	25.7%	4915.7 ± 1388.0	-
wa54ave	-	850-250	Waimatau	Un. of Washington	CAMS - LLNL	-	0.13 ± 0.04	0.11 ± 0.03	-	5753.6 ± 1948.9	29.1%

Table 4 - 1 *In situ* <sup>10</sup>Be laboratory replication results

Table 2: Meteoric <sup>10</sup>Be laboratory/measurement replicate samples from the Waipaoa River Basin, NZ.

Sample ID	Be number	Grain size (µm)	Sample basin	<sup>10</sup> Be extraction lab	Measured at	Measurement date	Measured ratio ( <sup>10</sup> Be/ <sup>9</sup> Be × 10 <sup>-13</sup> ; ± error)	Meteoritic <sup>10</sup> Be (atoms/g × 10 <sup>17</sup> ; ± error)	AMS % uncertainty	<sup>10</sup> Be lab. rep. % difference
wa02metuw	BE24455	850-250	Waihora	Un. of Washington	CAMS - LLNL	10/4/07	4.99 ± 0.11	12.00 ± 0.37	3.1%	-
wa02metvt	BE23877	850-250	Waihora	UWM cosmo lab	CAMS - LLNL	7/7/07	4.46 ± 0.10	11.67 ± 0.35	3.0%	-
<b>wa02metave</b>	-	<b>850-250</b>	<b>Waihora</b>	-	-	-	<b>4.72 ± 0.15</b>	<b>11.84 ± 0.51</b>	-	<b>2.8%</b>
wa12metis	BE24693	850-250	Waipaoa outlet	Hebrew Un., Israel	CAMS - LLNL	1/18/08	3.78 ± 0.18	7.88 ± 0.41	5.1%	-
wa12metuw	BE24458	850-250	Waipaoa outlet	Un. of Washington	CAMS - LLNL	10/4/07	2.71 ± 0.08	6.48 ± 0.23	3.6%	-
<b>wa12metave</b>	-	<b>850-250</b>	<b>Waipaoa outlet</b>	-	-	-	<b>3.25 ± 0.20</b>	<b>7.18 ± 0.47</b>	-	<b>19.4%</b>
wa15metuw	BE24459	850-250	Waikohu	Un. of Washington	CAMS - LLNL	10/4/07	6.36 ± 0.15	14.72 ± 0.45	3.0%	-
wa15metvt	BE23881	850-250	Waikohu	UWM cosmo lab	CAMS - LLNL	7/7/07	5.64 ± 0.14	13.47 ± 0.43	3.2%	-
<b>wa15metave</b>	-	<b>850-250</b>	<b>Waikohu</b>	-	-	-	<b>6.00 ± 0.20</b>	<b>14.10 ± 0.62</b>	-	<b>8.9%</b>
wa20metis	BE24698	850-250	Waterworks	Hebrew Un., Israel	CAMS - LLNL	1/18/08	11.21 ± 0.26	22.87 ± 0.71	3.1%	-
wa20metuw	BE24460	850-250	Waterworks	Un. of Washington	CAMS - LLNL	10/4/07	8.93 ± 0.22	21.59 ± 0.68	3.2%	-
<b>wa20metave</b>	-	<b>850-250</b>	<b>Waterworks</b>	-	-	-	<b>10.07 ± 0.34</b>	<b>22.23 ± 0.98</b>	-	<b>5.7%</b>
wa39metuw	BE24465	850-250	Ngaruono	Un. of Washington	CAMS - LLNL	10/4/07	3.88 ± 0.13	8.88 ± 0.34	3.8%	-
wa39metvt	BE23887	850-250	Ngaruono	UWM cosmo lab	CAMS - LLNL	7/7/07	2.83 ± 0.08	8.33 ± 0.28	3.3%	-
<b>wa39metave</b>	-	<b>850-250</b>	<b>Ngaruono</b>	-	-	-	<b>3.36 ± 0.15</b>	<b>8.60 ± 0.44</b>	-	<b>6.4%</b>
wa40metuw	BE24466	850-250	Tutaekuri	Un. of Washington	CAMS - LLNL	10/4/07	6.15 ± 0.14	14.41 ± 0.44	3.1%	-
wa40metvt	BE23888	850-250	Tutaekuri	UWM cosmo lab	CAMS - LLNL	7/7/07	4.66 ± 0.11	14.19 ± 0.45	3.2%	-
<b>wa40metave</b>	-	<b>850-250</b>	<b>Tutaekuri</b>	-	-	-	<b>5.41 ± 0.16</b>	<b>14.30 ± 0.63</b>	-	<b>1.5%</b>
wa41metuw	BE24468	850-250	Motu	Un. of Washington	CAMS - LLNL	10/4/07	23.43 ± 0.46	56.21 ± 1.57	2.8%	-
wa41metvt	BE23889	850-250	Motu	UWM cosmo lab	CAMS - LLNL	7/7/07	17.34 ± 0.42	51.93 ± 1.63	3.1%	-
<b>wa41metave</b>	-	<b>850-250</b>	<b>Motu</b>	-	-	-	<b>20.39 ± 0.62</b>	<b>54.07 ± 2.26</b>	-	<b>7.9%</b>
wa44metuw	BE24469	850-250	Waihuka	Un. of Washington	CAMS - LLNL	10/4/07	4.67 ± 0.11	10.89 ± 0.34	3.1%	-
wa44metvt	BE23890	850-250	Waihuka	UWM cosmo lab	CAMS - LLNL	7/7/07	3.89 ± 0.12	11.30 ± 0.42	3.7%	-
<b>wa44metave</b>	-	<b>850-250</b>	<b>Waihuka</b>	-	-	-	<b>4.28 ± 0.16</b>	<b>11.09 ± 0.54</b>	-	<b>3.7%</b>
wa46metuw	BE24470	850-250	Waikohu	Un. of Washington	CAMS - LLNL	10/4/07	6.99 ± 0.21	16.73 ± 0.59	3.6%	-
wa46metvt	BE23891	850-250	Waikohu	UWM cosmo lab	CAMS - LLNL	7/7/07	6.09 ± 0.14	14.98 ± 0.46	3.1%	-
<b>wa46metave</b>	-	<b>850-250</b>	<b>Waikohu</b>	-	-	-	<b>6.54 ± 0.25</b>	<b>15.65 ± 0.75</b>	-	<b>11.1%</b>
wa54metis	BE24709	850-250	Waimata	Hebrew Un., Israel	CAMS - LLNL	1/18/08	1.62 ± 0.04	3.28 ± 0.10	3.0%	-
wa54metvt	BE23895	850-250	Waimata	UWM cosmo lab	CAMS - LLNL	7/7/07	1.11 ± 0.04	3.11 ± 0.13	4.1%	-
<b>wa54metave</b>	-	<b>850-250</b>	<b>Waimata</b>	-	-	-	<b>1.36 ± 0.05</b>	<b>3.20 ± 0.16</b>	-	<b>5.4%</b>

Table 4 - 2 Meteoric <sup>10</sup>Be laboratory replication results

Table 3: *In situ* <sup>10</sup>Be temporal replicate samples from the Waipaoa River Basin, NZ.

Sample ID	Be number	Collection date	Grain size (µm)	Sample Basin	<sup>10</sup> Be Extraction lab	Measured at	Measurement date	Measured Ratio ( <sup>10</sup> Be/ <sup>9</sup> Be × 10 <sup>-12</sup> ; ± error)	<i>In situ</i> <sup>10</sup> Be (atoms/g × 10 <sup>-12</sup> ; ± error)	AMS % Number	Inferred Erosion Rate (m/ky; ± error)	Temporal % difference
wa25ave	BE2447/926	5/20/04	850-250	Waihora	Un. of Washington	CAMS - LLNL	10/3/07	1.62 ± 0.26	1.56 ± 0.23	14.9%	318.9 ± 57.0	
wa23	BE2442	3/14/05	850-250	Waihora	Un. of Washington	CAMS - LLNL	10/3/07	2.75 ± 0.17	2.13 ± 0.14	6.5%	232.4 ± 20.9	30.7%
wa24ave	BE2443/927	5/20/04	850-250	Waipaoa outlet	Un. of Washington	CAMS - LLNL	10/3/07	1.57 ± 0.31	1.32 ± 0.26	20.1%	388.9 ± 83.6	
wa12	BE2448	3/14/05	850-250	Waipaoa outlet	Un. of Washington	CAMS - LLNL	10/3/07	1.01 ± 0.06	0.85 ± 0.05	6.4%	606.2 ± 54.2	43.6%

Table 4 - 3 *In situ* <sup>10</sup>Be temporal variability results

*Table 4 - 4 is too large to be displayed on  
a single thesis page. A downloadable version  
will be available online at:*

*[http://www.uvm.edu/cosmolab/?Page=pubs\\_papers.html](http://www.uvm.edu/cosmolab/?Page=pubs_papers.html)*

Table 4 - 4 Meteoric  $^{10}\text{Be}$  temporal variability results

*Table 4 - 5 is too large to be displayed on a single thesis page. A downloadable version will be available online at:*

*[http://www.uvm.edu/cosmolab/?Page=pubs\\_papers.html](http://www.uvm.edu/cosmolab/?Page=pubs_papers.html)*

Table 4 - 5 Distribution of *in situ*  $^{10}\text{Be}$  concentrations

*Table 4 - 6 is too large to be displayed on  
a single thesis page. A downloadable version  
will be available online at:*

*[http://www.uvm.edu/cosmolab/?Page=pubs\\_papers.html](http://www.uvm.edu/cosmolab/?Page=pubs_papers.html)*

Table 4 - 6 Distribution of meteoric  $^{10}\text{Be}$  concentrations.

**CHAPTER 5: (FOR SUBMISSION TO *NATURE GEOSCIENCE*) QUANTIFYING  
HUMAN IMPACTS ON RATES OF EROSION AND SEDIMENT TRANSPORT  
AT A LANDSCAPE-SCALE**

**Quantifying human impacts on rates of erosion and  
sediment transport at a landscape-scale**

Lucas Reusser<sup>1\*</sup>,

Paul Bierman<sup>1</sup>,

Dylan Rood<sup>2</sup>

<sup>1</sup> Rubenstein School of Environment and Natural Resources, and Department of Geology,  
University of Vermont, Burlington, VT 05405

<sup>2</sup> AMS Laboratory, Scottish Universities Environmental Research Center, Glasgow, G75,  
0QF, Scotland, UK

*\*Corresponding author: [lreusser@uvm.edu](mailto:lreusser@uvm.edu)  
(802) 656-3398 ph. (802) 656-0045 fax.*

### **5.1. Introductory paragraph**

Establishing background rates of erosion allows the impact of human activities on Earth's surface to be evaluated quantitatively. Here, we present  $^{10}\text{Be}$  estimates of erosion rates from ten large (10,000 to 100,000 km<sup>2</sup>) river basins. These rates are indicative of how the heavily-altered North American passive margin landscape functioned before western settlement. We compare these background rates of erosion to rates of hillslope erosion and sediment yields from the same basins following peak agricultural disturbance during the late 1800's and early 1900's (Trimble, 1974 & 1977). Rates of agriculturally-induced hillslope erosion exceed  $^{10}\text{Be}$ -determined background rates by more than 100-fold. Although sediment yields increased 5 to 10 times above the pre-settlement norms, rivers at the time were transporting only ~6 percent of the eroded material; the bulk of historically-eroded soil remains as legacy sediment stored at the base of hillslopes and along river channels. These findings exemplify the effects that landuse practices have had on natural systems of sediment generation and erosion. Background erosion rates such as these, reflecting the rate at which soil is generated over millennial timescales, inform and enhance landscape management strategies.

### **5.2. Article text**

Quantifying natural, or background rates of landscape erosion is prerequisite to understanding the impact of human activities on natural process rates (National Research Council, 1994). In contrast to these background rates, human activities, such as land-clearance for agriculture, can dramatically elevate the pace at which sediment moves down slopes and into river systems (Hooke, 1994). Traditional approaches used to quantify the mass of sediment moving through fluvial systems, such as contemporary sediment yield data, do not reflect long-term, background rates of erosion (Trimble, 1977). Human-landscape interactions can generate sediment yields and inferred erosion

rates elevated several orders of magnitude over background rates (Meade, 2001). Sediment yield records are often short (years to decades) and thus may miss large volumes of sediment delivered to rivers during high-magnitude, low frequency events (Kirchner, et al., 2001; Wolman and Miller, 1960). Further, if the erosion following human-disturbance outpaces the rate at which streams can transport the material fed to them, sediment yield data represent neither natural erosion nor the maximum degree of upstream erosion. Instead, such streams are transport-limited systems in which sediment yield data represent the maximum carrying capacity of the rivers; much of the eroded material remains trapped on the landscape (Walling, 1983; Wilkinson and McElroy, 2007). Quantitatively determining background rates of erosion remains a difficult but critical task worldwide. Knowing such rates well is prerequisite for making important environmental decisions, such as the regulation of suspended sediment as a pollutant (Whiting, 2006).

Sediment dynamics on the southern Appalachian Piedmont, across the passive, eastern margin of North America, has been studied to understand the erosional consequences of intensive agricultural practices (Trimble, 1977). Contrasting the degree of soil truncation resulting from cotton and tobacco production during peak agricultural use in the early 1900's with the sediment yields recorded on Piedmont-Coastal Plain rivers clearly, established the discordance of hillslope erosion and sediment yields in large, low-gradient river systems<sup>2</sup>. These findings discredited the long-held assumption that the mass of material eroded from hillslopes was in equilibrium with the mass of sediment carried by rivers, an assumption of landscape steady state (Dole and Stabler,

1909; Judson and Ritter, 1964; Menard, 1961). While Trimble's argument was compelling and consistent with those of many others (Meade, 1969; Walling, 1983; Ahnert, 1970), at the time there were no techniques capable of reliably quantifying background rates of erosion. In the absence of this information, there was no reliable way to quantify the degree to which human land-use practices during the peak agricultural period increased erosion above background rates.

Here, we present new *in situ* cosmogenic  $^{10}\text{Be}$  data (n=24) measured in present-day river sediment and use them to infer background drainage basin erosion rates from the same low-gradient southern Appalachian Piedmont catchments studied by Trimble (Trimble, 1977). Concentrations of *in situ*-produced  $^{10}\text{Be}$  measured in fluvial sediments can be used to estimate spatially averaged, millennial-scale rates of sediment production and landscape erosion (Bierman et al., 1996; Brown, 1995; Granger et al., 1996). The concentration of  $^{10}\text{Be}$  is homogenized in the upper ~1 m of Earth's surface as hillslope materials are stirred by bioturbation (Jungers et al., 2009) making erosion rate estimates insensitive to all but the most deeply penetrating forms of mass wasting (Niemi et al., 2005). Thus, in most instances, erosion rates modeled from  $^{10}\text{Be}$  measurements in river sediments still record the isotopic signature of longer-term erosion ( $10^3 - 10^5$  years) and constitute a useful metric for comparison to human-induced rates of erosion (von Blackenburg et al., 2004). Cosmogenic  $^{10}\text{Be}$  data allow us to quantify the erosive effects of human land-use practices in a region with a profound and well documented history of disturbance and compare erosion rates calculated from sediment yields to long-term,

background rates of erosion determined using  $^{10}\text{Be}$  (Trimble, 1977; Meade, 1969; Dole and Stabler, 1909; Costa, 1975; Walter and Merritts, 2008; Wolman, 1967).

The broad low-slope southern Piedmont region of the Appalachian Mountains we studied (Figure 5 - 1), with its subdued topography, humid-temperate climate, and rich soil was subjected to intensive European agricultural practices beginning in the 1700's (Trimble, 1974). The headwaters of the largest catchments (10,000's  $\text{km}^2$ ) draining the Piedmont originate inland in the rugged Blue Ridge province. Prior to settlement, much of the sediment traveling through the Piedmont drainages originated from infrequent but geomorphically significant mass movements in the upstream regions (Neary et al., 1986). Beginning in the 1700's and peaking in the early 1900's, extensive clearance for cotton and tobacco production increased dramatically resulting in widespread erosion of Piedmont hillslopes (average erosion depth of  $\sim 180 \text{ mm}$ )<sup>2</sup> and aggradation of river channels, valley bottoms, and toe slopes (Trimble, 1977; Costa, 1975; Trimble, 1974; Meade and Trimble, 1974; Phillips, 1992; Phillips, 2006) (Figure 5 - 2).

Hillslope erosion and fluvial sediment transport during the time of intensive Piedmont agriculture were largely disconnected. For example, the degree of soil truncation in the ten studied basins (Trimble, 1974 and 1977) suggested an area-weighted erosion rate of  $\sim 950 \text{ m/My}$ . In contrast, the area-weighted sediment-yield-derived erosion rates ( $\sim 53 \text{ m/My}$ ) at the river outlets reflected a sediment delivery ratio (Walling, 1983) of only  $\sim 6$  percent (Figures 5 - 2 and 5 - 3). Much of the hillslope soil eroded during the peak agricultural period is stored as alluvial and colluvial deposits along low-

gradient Piedmont river and valley systems (Trimble, 1977; Walter and Merritts, 2008; Meade and Trimble, 1974).

Background, landscape-scale erosion rates, calculated from the concentration of  $^{10}\text{Be}$  in river sediment, are many times lower than both rates of soil erosion and of sediment transport during peak agriculture. The  $^{10}\text{Be}$  data indicate that during the early 1900's, aerially averaged rates of hillslope erosion ( $\sim 950$  m/My) exceeded  $^{10}\text{Be}$ -derived background erosion rates ( $\sim 9$  m/My) by more than a hundred fold (Figure 5 - 3; Table 5 - 1 (a.k.a. Supplemental Table S1)). Even with an aerially averaged sediment delivery ratio (Walling, 1983) of only  $\sim 6$  percent, streams were yielding nearly 6 times their normal, or "equilibrium" sediment mass due to land clearance (Meade, 1969; Figures 5 - 2 and 5 - 3).

The bulk of the soil (an estimated  $25 \text{ km}^3$ ; Trimble, 1975) went into storage in massive deposits in valley bottoms and toe-slopes (Trimble, 1977; Meade, 1982). Because today, much of the material in these deposits (legacy sediment) is stored away from river channels, it will take time time to ultimately remove the hillslope material off the Piedmont and eventually offshore (Walter and Merritts, 2008; Meade, 1982). As a consequence, the load of sediment carried by these large rivers, and to a lesser degree, tributaries will remain elevated (Meade, 1982; Phillips, 2003; Figure 5 - 2). Further increasing the lag, nearly all Piedmont drainages harbor hydroelectric dams with sediment trap efficiencies of up to 95 percent (Brune, 1953). Thick sediment deposits within the dam reservoirs will remain trapped in all but the largest floods (Trimble, 1977; Meade, 1982). The ultimate removal of stored material originating from the episode of

erosion during peak agriculture will take decades to centuries (Meade, 1982), perhaps longer.

In contrast to the Piedmont-dominated lower-slope outlet samples,  $^{10}\text{Be}$  results indicate that the more rugged Blue Ridge portions of eight of the ten large basins naturally erode faster (8.8 vs. 13.4 m/My respectively; Table 5 – 1 (a.k.a. Supplemental Table S1). Samples collected from mid-way down six of the ten streams (11.0 m/My) suggest that, sediments mix predictably as they travel from Blue Ridge headwater regions to their Piedmont outlets. These findings unequivocally demonstrate the effects that human land-use practices have had on natural systems of sediment generation and erosion along the southern Appalachian Piedmont; a condition that has been studied extensively world wide, yet rarely quantified (Kirchner, et al., 2001; Gomez, et al., 2003; Hicks, et al., 2000; Syvitski et al., 2005).

Due to effective soil conservation measures across the southern Appalachian Piedmont over the last century, sediment yields in many tributary streams have been substantially reduced. For example, deposition of sediment between 1910 and 1934 in the Lloyd Shoals Reservoir, completed in 1910 along a tributary of Georgians Ocmulgee River, suggests a basin-average sediment yield equivalent to  $\sim 73$  m/My of basin-wide erosion (Meade and Trimble, 1974). Between 1967 and 1972, following extensive soil conservation improvements within the watershed, sediment deposition in the reservoir dropped nearly 7 fold to a basin-wide erosion equivalent of  $\sim 10$  m/My, a value which matches well the  $^{10}\text{Be}$  results from this area (9 m/My). These data suggest that soil

conservation practices can reduce sediment yields so that they match well the rate at which the landscape erodes naturally.

Background erosion rates, determined through the measurement of in situ produced  $^{10}\text{Be}$ , provide the context from which to assess nearly all other measures of erosion germane on a human timescale, and thus hold the potential to inform a variety of landscape management strategies. Such isotopic estimates could serve as benchmarks for establishing realistic Total Mean Daily Loads (TMDLs) of not only the mass of sediments carried by streams and/or deposited in water bodies, but also pollutants associated with or adhered to sediment. Because  $^{10}\text{Be}$  integrates over time and space scales appropriate for understanding pre-settlement background rates of erosion, it places human impacts in context making it an important tool for informing landscape management.

### 5.3. Methods

Samples of active channel sediments or recent overbank deposits were collected and field sieved to a grain size fraction of 1000-250  $\mu\text{g}$  for in situ  $^{10}\text{Be}$  analysis. Samples from the outlets of the ten large Piedmont drainages correspond directly to those presented in Trimble (1977). Blue Ridge and mid-basin samples were collected from within a sub-set of the ten large basins (see Supplementary Table S1). All GPS locations were collected with handheld Garmin 12 units. Coordinates are in UTM NAD83 CONUS (see Supplemental Table S1 for UTM zones). All geographic statistics were calculated in ArcGIS<sup>TM</sup> using 1/3 arcsecond ( $\sim 28$  m) digital elevation models downloaded from <http://seamless.usgs.gov>. Quartz was purified using the method of Kohl and Nishiizumi (1992) and Be was extracted using HF dissolution and column chromatography (Corbett, et al., 2011). Isotopic measurements were made on the Livermore National Laboratory

accelerator mass spectrometer. Errors in nuclide concentrations include only ratio measurement uncertainties. Measured ratios of  $^{10}\text{Be}/^9\text{Be}$  were normalized to 07KNSTD3110 standard (Nishiizumi, 2007) with an assumed ratio of  $2850 \times 10^{-15}$ .  $^{10}\text{Be}$  erosion rates were modeled with the CRONUS online calculator (<http://hess.ess.washington.edu/>) using hypsometrically-weighted effective production rates calculated with the method presented in Portenga and Bierman (2011).

#### **5.4. Acknowledgements**

We thank M. Jungers, W. Hackett, and J. Duxbury for field assistance and Livermore National Laboratory for isotope measurements. Support provided by NSF EAR-310208 and DoD DAAD19-03-1-0205.

#### **5.5. Author contributions**

L.J.R. and P.R.B. instigated and directed this research and carried out sample processing. D.R. made AMS measurements. All authors contributed to manuscript preparation.

#### **5.6. References cited**

- Ahnert, F., 1970, Functional relationships between denudation, relief, and uplift in large mid-latitude drainage basins: *American Journal of Science*, v. 268, p. 243-263.
- Bierman, P., Larsen, P., Clapp, E., and Clark, D., 1996, Refining Estimates of  $^{10}\text{Be}$  and  $^{26}\text{Al}$  Production Rates: *Radiocarbon*, v. 38, no. 1, p. 149-173.
- Brown, E. T., Stallard, R. F., Larsen, M. C., Raisbeck, G. M., and Yiou, F., 1995, Denudation rates determined from the accumulation of in situ-produced  $^{10}\text{Be}$  in

- the Luquillo Experimental Forest, Puerto Rico: *Earth and Planetary Science Letters*, v. 129, p. 193-202.
- Brune, G., 1953, Trap efficiencies of reservoirs: *American Geophysical Union Transactions*, v. 34, p. 407-418.
- Corbett, L. B., Young, N. E., Bierman, P., Briner, J. P., Neumann, T. A., Rood, D., and Graly, J., 2011, Paired bedrock and boulder  $^{10}\text{Be}$  concentrations resulting from early Holocene ice retreat near Jakobshavn Isfjord, western Greenland: *Quaternary Science Reviews*, v. 30, p. 1739-1749.
- Costa, J. E., 1975, Effects of agriculture on erosion and sedimentation in the Piedmont province, Maryland: *Geological Society of America Bulletin*, v. 86, p. 1281-1286.
- Dole, R. G., and Stabler, H., 1909, Denudation, *Papers on the Conservation of Water Resources: U.S. Geological Survey Water-Supply Paper 234*, p. 78-93.
- Gomez, B., Banbury, K., Marden, M., Trustrum, N. A., Peacock, D., and Hoskin, P., 2003, Gully erosion and sediment production: Te Weraroa Stream, New Zealand: *Water Resources Research*, v. 39, no. 7, p. ESG 3-1 to ESG 3-7.
- Granger, D. E., Kirchner, J. W., and Finkel, R., 1996, Spatially averaged long-term erosion rates measured from in situ-produced cosmogenic nuclides in alluvial sediments: *Journal of Geology*, v. 104, no. 3, p. 249-257.
- Hicks, D. M., Gomez, B., and Trustrum, N. A., 2000, Erosion thresholds and suspended sediment yields, Waipaoa River Basin, New Zealand: *Water Resources Research*, v. 36, no. 4, p. 1129-1142.

- Hooke, R., 1994, On the efficacy of humans as geomorphic agents: *GSA Today*, v. 4, no. 9, p. 224-225.
- Judson, S., and Ritter, D., 1964, Rates of regional denudation in the United States: *Journal of Geophysical Research*, v. 69, no. 16, p. 3395-3401.
- Jungers, M., Bierman, P., Matmon, A. S., Nichols, K. K., Larsen, J., and Finkel, R., 2009, Tracing hillslope sediment production and transport with *in situ* and meteoric <sup>10</sup>Be: *Journal of Geophysical Research - Earth Surface*, v. 114.
- Kirchner, J. W., Finkel, R., Reibe, C., Granger, D. E., Clayton, J., King, J., and Megahan, W., 2001, Mountain erosion over 10 yr, 10 k.y., and 10 m.y. time scales: *Geology*, v. 29, no. 7, p. 591-594.
- Kohl, C. P., and Nishiizumi, K., 1992, Chemical isolation of quartz for measurement of in-situ-produced cosmogenic nuclides: *Geochimica et Cosmochimica Acta*, v. 56, p. 3583-3587.
- Meade, R. H., 1969, Errors in using modern stream-load data to estimate natural rates of denudation: *Geological Society of America Bulletin*, v. 80, p. 1265-1274.
- , 1982, Sources, sinks and storage of river sediment in the Atlantic drainage of the United States: *Journal of Geology*, v. 90, p. 235-252.
- Meade, R. H., and Trimble, S. W., 1974, Changes in sediment loads in rivers of the Atlantic drainage of the United States since 1900, *Effects of Man on the Interface of the Hydrological Cycle with the Physical Environment*, Volume Hydrol. Pub. 113, *Internat. Assoc. Sci.*, p. 99-104.

- Menard, H. W., 1961, Some rates of regional erosion: *Journal of Geology*, v. 69, p. 154-161.
- National Research Council, 2010, *Landscapes on the edge: New horizons for research on Earth's surface*: The National Academies Press: National Research Council.
- Neary, D. G., Swift, L. W. J., Manning, D., and Burns, R. G., 1986, Debris avalanching in the Southern Appalachians; An influence on forest soil formation: *Soil Science Society of American Journal*, v. 50, p. 465-471.
- Niemi, N., Oskin, M., Burbank, D. W., Heimsath, A. M., and Gabet, E., 2005, Effects of bedrock landslides on cosmogenically determined erosion rates: *Earth and Planetary Science Letters*, v. 237, no. 3-4, p. 480-498.
- Nishiizumi, K., Imamura, M., Caffee, M., Southon, J., Finkel, R., and McAninch, J., 2007, Absolute calibration of  $^{10}\text{Be}$  AMS standards: *Nuclear Instruments and Methods in Physics Research B*, v. 258, p. 403-413.
- Phillips, J. D., 1992, The source of alluvium in large rivers of the lower Coastal Plain of North Carolina: *Catena*, v. 19, p. 59-75.
- , 2003, Alluvial storage and the long-term stability of sediment yields: *Basin Research*, v. 15, p. 153-163.
- , 2006, Residence time of alluvium in an aggrading fluvial system: *Earth Surface Processes and Landforms*, v. 32, p. 307-316.
- Portenga, E. W., and Bierman, P. R., 2011, Understanding Earth's eroding surface with  $^{10}\text{Be}$ : *GSA Today*, v. 21, no. 8, p. doi: 10.1130.

- Syvitski, J. P. M., Vorosmarty, C. J., Kettner, A. J., and Green, P., 2005, Impact of Humans on the flux of Terrestrial Sediment to the Global Coastal Ocean: *Science*, v. 308, p. 376-380.
- Trimble, S. W., 1974, Man-induced soil erosion on the Southern Piedmont 1700-1970: Soil Conservation Society of America, p. 180.
- , 1975, A volumetric estimate of man-induced erosion on the Southern Piedmont, *in* Agr., U. S. D., ed., Volume Present and Prospective Technology for Predicting Sediment Yields and Sources: Fort Worth, p. 142-154.
- , 1977, The fallacy of stream equilibrium in contemporary denudation studies: *American Journal of Science*, v. 277, p. 876-887.
- von Blackenburg, F., Hewawasam, T., and Kubik, P., 2004, Cosmogenic nuclide evidence for low weathering and denudation in the wet, tropical highlands of Sri Lanka: *Journal of Geophysical Research*, v. 109, p. 1-22.
- Walling, D. E., 1983, The sediment delivery problem: *Journal of Hydrology*, v. 65, p. 209-237.
- Walter, R., and Merritts, D. J., 2008, Natural Streams and Legacy of Water-Powered Mills: *Science Magazine*, v. 319, no. 5861, p. 299-304.
- Whiting, P. J., 2006, Estimating TMDL background suspended sediment loading to Great Lake tributaries from existing data: *Journal of American Water Resources Association*, v. 42, no. 3, p. 769-776.
- Wilkinson, B. H., and McElroy, B. J., 2007, The impact of humans on continental erosion and sedimentation: *GSA Bulletin*, v. 119, no. 1.2, p. 140-156.

Wolman, G. M., 1967, A cycle of sedimentation and erosion in urban river channels:  
Geografiska Annaler, v. 49A, p. 385-395.

Wolman, M. G., and Miller, J. P., 1960, Magnitude and frequency of forces in  
geomorphic processes: Journal of Geology, v. 68, no. 1, p. 54-74.

## 5.7. Figure captions

**Figure 5 - 1** - Location map of the Southern Appalachian Piedmont field area along the southeastern passive margin of North America. River basins 1 through 10 are those in Trimble (1977). Blue Ridge (☆), Mid-basin (○), and Outlet (□) denote the locations of *in situ* <sup>10</sup>Be sample sites within each catchment. Modified from Figure 1 in Trimble (1977).

**Figure 5 - 2** – Diagram of different integration times of data presented (A), changing land clearance conditions (B), changing land-cover conditions (C), changing hillslope conditions (D), changing sediment loads carried by streams (E) and storage of legacy sediment in valley bottoms and dam reservoirs (F). Note the horizontal break is long- vs. short-term conditions in panels B to F represented by the separate boxes.

**Figure 5 - 3** – Summary of erosion rates for large-scale catchments presented and discussed in this paper. Refer to figure 1 for the locations. Dark grey (rates of hillslope erosion) and light grey (sediment yield-derived rates of erosion) bars from data presented in Trimble (1977). Black bars represent *in situ* <sup>10</sup>Be background erosion rate estimates.

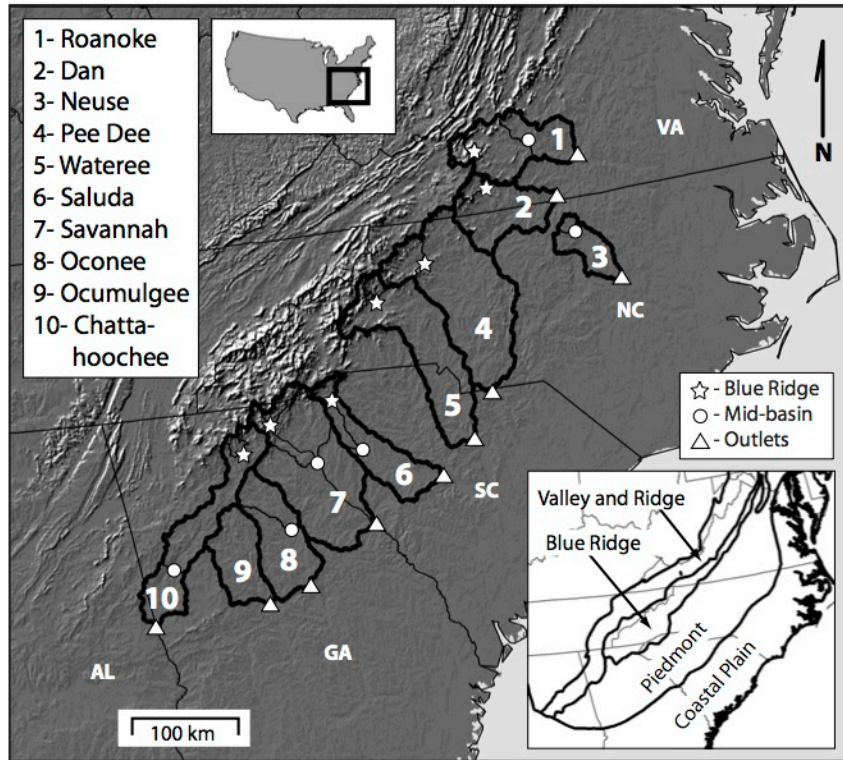


Figure 5 - 1 Location map for the Southern Appalachian Piedmont, USA

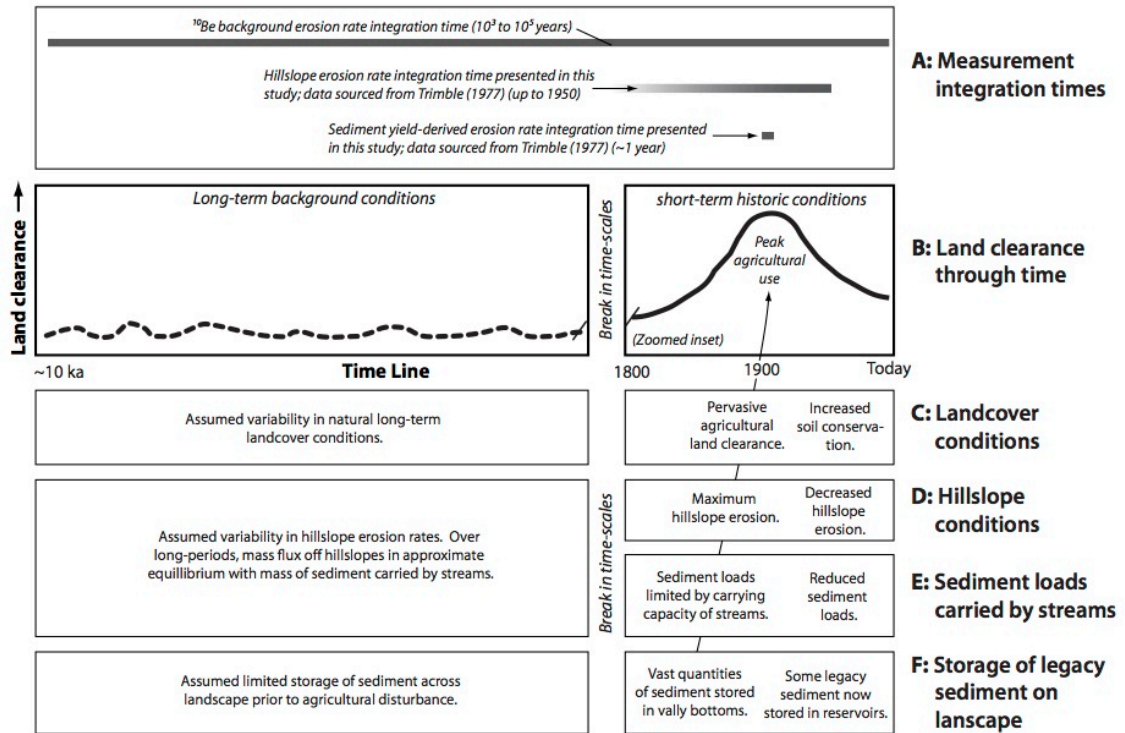


Figure 5 - 2 Conceptual diagram of measurement integration times, land clearance conditions, landcover conditions, hillslope conditions, sediment loads, and sediment storage

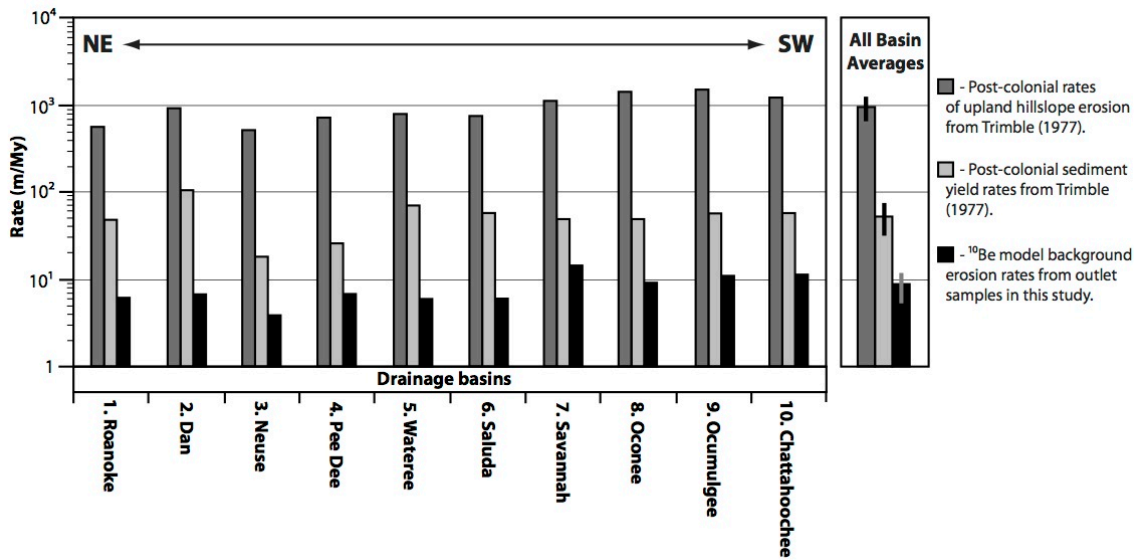


Figure 5 - 3 Compilation of hillslope erosion rates, sediment yield rates, and background <sup>10</sup>Be background erosion rates.

## 5.8. Supplemental information

Table 5 - 1 (Supplemental Table S1) Summary data table for data presented in Nature Geoscience paper.

Table 1: Summary information for large-scale Piedmont catchments

Sample ID	BE Number*	Trimble Basin†	Sample Type§	UTM Zone	Northing#	Eastings#	Area (km <sup>2</sup> )‡	Mean Elevation (m)‡	Mean Slope (degrees)‡	<sup>10</sup> Be (atoms/g x 10 <sup>5</sup> )‡	Model Erosion Rate (m/My)Ω
SAP03	BE27676	Roanoke	Outlet	17	701236	4087858	7676	322	7.9	6.24 ± 0.18	6.17 ± 0.52
SAP04	BE27677	Dan	Outlet	17	670737	4056984	6686	286	6.6	5.50 ± 0.16	6.79 ± 0.57
SAP07	BE27679	Neuse	Outlet	17	734920	3947950	2987	129	3.4	7.74 ± 0.21	3.90 ± 0.35
SAP09	BE27681	Pee Dee	Outlet	17	591286	3882894	16376	280	5.8	5.40 ± 0.14	6.78 ± 0.56
SAP10	BE27682	Waterlee	Outlet	17	527671	3799121	12270	306	6.5	6.10 ± 0.17	5.98 ± 0.50
SAP12	BE27684	Saluda	Outlet	17	482362	3767289	6274	212	3.9	5.55 ± 0.15	6.09 ± 0.51
SAP53	BE28717	Savannah	Outlet	17	388641	3724815	15870	265	5.4	2.72 ± 0.08	14.42 ± 1.11
SAP51	BE28715	Oconee	Outlet	17	294420	3667665	7549	200	3.7	3.78 ± 0.10	9.34 ± 0.73
SAP50	BE27895	Ocmulgee	Outlet	17	245302	3656461	5438	231	3.8	3.35 ± 0.10	10.98 ± 0.87
SAP66	BE27901	Chattahoochee	Outlet	16	669074	3643249	8900	332	5.7	3.48 ± 0.14	11.38 ± 0.96
SAP39	BE27887	Roanoke	Mid-Basin	17	651634	4107904	4613	387	9.6	6.35 ± 0.18	6.36 ± 0.54
SAP05	BE27678	Neuse	Mid-Basin	17	689752	4011251	366	183	2.9	9.79 ± 0.25	3.11 ± 0.28
SAP13	BE28703	Saluda	Mid-Basin	17	387503	3806254	1495	348	7.2	3.65 ± 0.09	11.01 ± 0.85
SAP17	BE27736	Savannah	Mid-Basin	17	332802	3802906	5426	421	9.1	2.81 ± 0.08	15.62 ± 1.19
SAP52	BE28716	Oconee	Mid-Basin	17	287577	3733626	2438	248	4.2	4.83 ± 0.12	7.31 ± 0.59
SAP69	BE28724	Chattahoochee	Mid-Basin	16	695086	3706075	6247	368	6.3	3.29 ± 0.08	12.44 ± 0.95
SAP41	BE27888	Roanoke	Blue Ridge	17	571636	4121141	666	631	15.0	5.39 ± 0.14	9.19 ± 0.75
SAP45	BE27892	Dan	Blue Ridge	17	588442	4071770	561	475	13.5	3.78 ± 0.10	12.09 ± 0.95
SAP32	BE27883	Pee Dee	Blue Ridge	17	499518	4006148	1941	510	13.2	4.34 ± 0.14	10.45 ± 0.85
SAP27	BE27743	Waterlee	Blue Ridge	17	435721	3965723	527	628	16.8	2.12 ± 0.06	24.89 ± 1.86
SAP26	BE27742	Saluda	Blue Ridge	17	360778	3867333	666	457	11.7	2.50 ± 0.07	18.15 ± 1.38
SAP22	BE28705	Savannah	Blue Ridge	17	280243	3848234	468	755	16.3	3.34 ± 0.08	16.01 ± 1.23
SAP56	BE28718	Chattahoochee	Blue Ridge	17	230245	3824544	390	557	12.0	4.71 ± 0.11	9.50 ± 0.75
SAP60	BE28721	Chattahoochee	Blue Ridge	17	246607	3847401	50	819	19.7	3.25 ± 0.08	17.16 ± 1.32

\* BE Number denotes the sample identification tag logged during measurement at the Lawrence Livermore National Laboratory.

† Trimble Basin designates which of the 10 large-scale Piedmont catchments each sample was collected from.

‡ Outlet samples were collected at approximately the Piedmont-Coastal Plain transition. Blue Ridge samples were collected from the higher slope upstream portions of catchments. Mid-Basin samples were collected approximately mid-way down the trunk streams draining each catchment. Refer to figure 1 for visual locations.

# All GPS locations provided in UTM NAD83 CONUS. Note the change in zone for the southwesternmost basin.

‡ All geographic statistics were calculated in ArcGIS® using 1/3 arcsecond (~28m) digital elevation models downloaded from <http://seamless.usgs.gov>.

‡ Errors in nuclide concentrations include propagated laboratory and measurement uncertainties. Measured ratios of <sup>10</sup>Be normalized to the new 07KNS1D3110 standard (Nishizumi, et al., 2007).

Ω Erosion rates modeled with the CRONUS online calculator (<http://hess.ess.washington.edu/>) using hypsometrically weighted effective ELDs for each basin.

**CHAPTER 6: (FOR SUBMISSION TO *JOURNAL OF GEOPHYSICAL RESEARCH: EARTH SURFACE*) ROBUSTLY CHARACTERIZING LANDSCAPE-SCALE EROSION WITH *IN SITU* <sup>10</sup>BE**

**Robustly characterizing landscape-scale erosion with *in situ* produced <sup>10</sup>Be**

Lucas Reusser<sup>1\*</sup>,

Paul Bierman<sup>1</sup>,

Donna Rizzo<sup>2</sup>

Dylan Rood<sup>3</sup>

<sup>1</sup> Rubenstein School of Environment and Natural Resources, and Department of Geology,  
University of Vermont, Burlington, VT 05405

<sup>2</sup> School of Civil and Environmental Engineering, University of Vermont,  
Burlington, VT 05405

<sup>3</sup> AMS Laboratory, Scottish Universities Environmental Research Center, Glasgow, G75,  
0QF, Scotland, UK

*\*Corresponding author: [lreusser@uvm.edu](mailto:lreusser@uvm.edu)  
(802) 656-3398 ph. (802) 656-0045 fax.*

## 6.1. Abstract

The concentration of *in situ*  $^{10}\text{Be}$ , measured in samples of fluvial sediment collected from river sub-basins, has been used extensively to estimate long-term rates of landscape erosion. Because cosmogenic isotopic analyses are both expensive and time consuming, most studies make inferences based on a small number of samples. Previous research shows that basin scale erosion rates are typically correlated to basin average slope; yet, basin hypsometry varies widely suggesting that statistically representative sampling designs need to consider the probability distribution of sub-basin slopes in order to generate aerially-weighted average erosion rates that are representative of the basin as a whole.

Here, we present a large data set ( $n=66$ ), collected using a new, GIS-based experimental design based on the cumulative probability density function of sub-basin average slopes across the southern Appalachian Piedmont, eastern North America. A predictive model, trained on erosion rates measured in 37 sub-basins ( $\sim 20 \text{ km}^2$ ) selected to represent the distribution of average basin slopes across the entire Piedmont, is capable of predicting erosion rates ( $R^2 = 0.88$ ) for drainage basins of any size across the southern Appalachian Piedmont. We find that on average, the southern Piedmont is eroding at  $\sim 9 \text{ m/My}$  and that hydroelectric and flood control dams, which impede the downstream flow of sediment, can affect erosion rates calculated from concentrations of  $^{10}\text{Be}$ ; a complexity so far unaddressed in  $^{10}\text{Be}$ -based erosion rate studies.

## 6.2. Introduction

Since the mid 1990s, concentrations of *in situ* produced  $^{10}\text{Be}$  measured in samples of fluvial sediment have been used to estimate spatially and temporally averaged rates of natural sediment generation and erosion at the scale of individual drainage basin [Bierman and Steig, 1996; Brown *et al.*, 1995; Darryl E. Granger *et al.*, 1996]. To date, more than 1200 such measurements have been made [D. E. Granger *et al.*, 2013; Portenga and Bierman, 2011]. Because the method is both expensive and time consuming, most studies rely on a limited number of  $^{10}\text{Be}$  measurements made in sub-basins and averaged, often using aerial weighting, to generate a landscape-scale average erosion rate. Such averaging will only generate meaningful data if the sample dataset is statistically representative of the population of sub-basins comprising the landscape as a whole [Sullivan, 2007; Sullivan *et al.*, 2006].

In many studies [e.g. Cox *et al.*, 2009; Darryl E. Granger *et al.*, 1996; Matmon *et al.*, 2003a; Riebe *et al.*, 2000] as well as a global compilation of >1200 measurements of  $^{10}\text{Be}$  in fluvial sediment, the best predictor of basin-scale erosion rate is average drainage basin slope or other similar metrics including relief. Such a relationship makes sense, as slope is positively related both to diffusive and advective sediment flux. However, the dependence of erosion rate on average basin slope means that if the sub-population of basins from which samples were collected does not have the same distribution of average basin slopes as the entire landscape, the results, such as the landscape average erosion

rate will not be representative and could over or underestimate the actual landscape erosion rate.

Here, we present a new dataset consisting of  $^{10}\text{Be}$ -based drainage basin erosion rates ( $n=66$ ) from the southern Appalachian Piedmont along the North American passive margin (Figure 6 – 1). We specifically designed a sampling strategy so that the resulting dataset is statistically representative of the entire landscape. To do this, we used GIS to identify and then sample 37 headwater basins ( $\sim 20 \text{ km}^2$ ) reflecting the distribution of average basin slopes across the entire study area. We use these data to train models capable of predicting rates of erosion for larger drainage basins that lack  $^{10}\text{Be}$  data, and in doing so, investigate, along major river systems, the influence of dams and the reservoirs they impound, on  $^{10}\text{Be}$  erosion rate estimates.

### 6.3. Background

Accurately inferring spatially and temporally averaged erosion rates from measured concentrations of *in situ*  $^{10}\text{Be}$  measured in samples of fluvial sediment depends on the veracity of several assumptions. Foremost is the assumption that the sediment collected at a point along a channel network has been sourced evenly from all parts of the drainage basin upstream of the sample location [Bierman and Steig, 1996; Brown *et al.*, 1995; Gosse and Phillips, 2001; Darryl E. Granger *et al.*, 1996; Darryl E. Granger *et al.*, 2013], and that quartz, the mineral phase from which  $^{10}\text{Be}$  is isolated, is evenly distributed across the basin [Safran *et al.*, 2005]. In most  $^{10}\text{Be}$  erosion rate studies, sand-sized material is analyzed and assumed to be isotopically representative of material

fluxing through the system. Samples of rivers sediment are considered to be representative of background, temporally-integrated erosion rates, because in most environments the upper meter or so of hillslope materials moving into river channels are mixed through physical and biological stirring [e.g. *Jungers et al.*, 2009]. This assumption is valid in all but the most extreme environments where deeply-penetrating erosional features feed material with substantially lower  $^{10}\text{Be}$  concentrations to river channels [e.g. *Niemi et al.*, 2005; *Reusser and Bierman*, 2010] causing erosion rates to be overestimated.

Dams, and the reservoirs they impound, can impede the movement of sediment through river networks, potentially affecting the concentration of  $^{10}\text{Be}$  measured in samples collected downstream of such channel obstructions. Because dams have been built along most large rivers around the globe, their effect needs to be considered when interpreting denudation rates from  $^{10}\text{Be}$  concentrations. Although human activities have increased the load of sediment transported by rivers worldwide [*Wilkinson and McElroy*, 2007], the construction of artificial reservoirs has reduced the amount of sediment that reaches the world's coasts [*Syvitski et al.*, 2005]. The pertinent question is whether sediment sampled downstream of a dam is locally derived or whether it is representative of sediment issuing from the drainage basin upstream.

## 6.4 Methods

We employed a multi-tiered sampling strategy allowing us to investigate the variability in erosion rate at different and spatial scales. Our experimental design

explicitly addresses the relationship between basin average slope and erosion rate, as well as the potential pitfalls of interpreting  $^{10}\text{Be}$  concentrations in river sediments collected along rivers with large, sediment-retaining dams.

To characterize the cumulative probability density function that describes the population of average basin slopes in the southern Atlantic Piedmont, we subdivided each of the 10 large basins into small hydrologic units (average basin area  $\sim 20 \text{ km}^2$ ), resulting in 5104 unique sub-basins ( $\sim 20 \text{ km}^2$ ). We did this using publicly available data, including HUC maps (<http://water.usgs.gov/GIS/huc.html>) and one arc-second DEMs (<http://seamless.usgs.gov>) and various hydrology tools in ESRI ArcGIS™. We selected  $\sim 10$  small basins from each of four of the 10 large basins (Roanoke, Pee Dee, Savannah, and Chattahoochee; 3053 potential sample sites; Figures 6 - 2 & 6 - 3) as potential sample sites. We chose these four basins because they represent the greatest north-south spatial variability along the southern Piedmont and because they all tap the higher-slope Blue Ridge province to the northwest of the Piedmont. We chose each of the 10 slope divisions to reflect the distribution of average basin slopes present in the 3053 sub-basins comprising the four large basins (Figure 6 - 3). Because the majority of the study area lies in the subdued Piedmont, we evenly spaced seven of the slope divisions between zero and  $12^\circ$ . The long tail of the frequency distribution with much higher slopes (up to  $25^\circ$ ) reflects the steeper Blue Ridge. To capture this natural landscape variability in slopes, we spaced the last three slope divisions evenly between 12 and  $25^\circ$  (Figure 6 - 3). For  $\sim 20 \text{ km}^2$  basins, basin average basin slope ranges from 1.9 to 25.7 degrees in the study area.

We collected samples in December 2006 and June 2008. At each sample site, we collected and field sieved samples of active channel sediment or recent overbank deposits to a grain size fraction of 1000-250  $\mu\text{g}$  for *in situ*  $^{10}\text{Be}$  analysis. We successfully retrieved sediment samples from large basins (n=24), dam-pair sites (n=4), and a temporal replicate site (n=1), as well 37 smaller basin, for a total of 66  $^{10}\text{Be}$  samples and analyses.

At the largest spatial scale ( $10^4 \text{ km}^2$ ), we sampled the outlets of the 10 large drainage basins, in most cases, close to the Piedmont/Coastal Plain transition (Figure 1). These are the same basins studied by Trimble (1977) allowing us to compare  $^{10}\text{Be}$  data with prior estimates of soil erosion, sediment yield, and dam trap efficiency. We also collected samples upstream from the outlets at the Blue Ridge/Piedmont transition (n=8; areas  $10^2$  to  $10^3 \text{ km}^2$ ) to investigate the influence of the higher basin-average slopes characteristic of the Blue Ridge headwaters of most of the 10 basins (Figure 6 - 1 & 6 - 2C) and we sampled mid-way down several of the trunk streams (n=6; areas  $10^2$  to  $10^3 \text{ km}^2$ ) to determine if sediments mix predictably as they travel from the rugged Blue Ridge onto the more topographically subdued Piedmont (Figure 6 - 1, 6 - 2B & 2C).

At four locations within the study area, we collected samples both below hydroelectric dams and upstream of their associated reservoirs to investigate the influence of dams along rivers on the concentration of *in situ*  $^{10}\text{Be}$  measured in river sediment. We refer to these samples as “dam pairs.” Two of dam pair samples are located at the outlets of the Pee Dee River (SAP08 downstream; SAP09 upstream) and Chattahoochee River (SAP64 downstream; SAP66 upstream). One of the pairs is located

mid-basin along the Neuse River (SAP06 downstream; SAP05 upstream), while the other is located in the Blue Ridge/Piedmont transition along the Savannah River (SAP19 downstream; SAP22 upstream; Figure 6 - 1).

To test the temporal reproducibility of our  $^{10}\text{Be}$  results, we resampled a site mid-way down the Savannah River approximately 1.5 years after the initial sampling (initial sampling 12/5/2006 SAP17; resampled 6/11/2008 as SAP55). This site is located in close proximity (<0.5 km) to the downstream face of the Hartwell dam, approximately half way between the headwaters and Piedmont outlet of the Savannah River (Figure 6 - 1; Table 6 – 1 (a.k.a. Supplemental Table S1).

We prepared all samples at the University of Vermont using standard laboratory methods for the purification of quartz [Kohl and Nishiizumi, 1992] and the extraction of  $^{10}\text{Be}$  [Corbett *et al.*, 2011]. We measured  $^{10}\text{Be}/^9\text{Be}$  ratios measured at the Center for Accelerator Mass Spectrometry at the Lawrence Livermore National Laboratory. All measured isotopic ratios were blank corrected, and then normalized to the 07KNSTD3110 standard with a reported  $^{10}\text{Be}/^9\text{Be}$  ratio of  $2850 \times 10^{-15}$  [Nishiizumi *et al.*, 2007].

To calculate in situ  $^{10}\text{Be}$  background erosion rates, we used the CRONUS online calculator [Balco *et al.*, 2008] (<http://hess.ess.washington.edu>). Hypsometrically-weighted effective elevations, average latitudes, and average longitudes were generated for each sample site using the method presented in Portenga and Bierman [2011] and fed into the CRONUS calculator enabling us to calculate drainage basin-scale  $^{10}\text{Be}$  erosion rates.

### ***Modeling***

Using erosion rate data from the 37 small-basin samples, selected for their average basin slopes, we developed and tested several models to predict erosion rates in unsampled drainage basins along the southern Piedmont. Initially, we regressed the measured  $^{10}\text{Be}$  erosion rates against respective average basin slopes. Then, we used this bivariate regression model to predict background erosion rates for each of the unique small sub-basins ( $n=5104$ ;  $\sim 20 \text{ km}^2$  each) across the entire study region ( $\sim 95,000 \text{ km}^2$ ); these predicted rates are referred to as  $E_{ps}$  in the following sections.

To determine if a more complex statistical method would better predict erosion rates than the simple bivariate slope model, we employed a number of other statistical techniques in JMP™ using a variety of summary statistics generated with ArcGIS™ for the same 37 slope-test samples. The variables included for each sample included: average basin elevation (m), basin relief (m), standard deviation of elevation (m), average basin slope (m), standard deviation of slope (m), basin area ( $\text{km}^2$ ), mean annual temperature ( $^{\circ}\text{C}$ ), mean annual precipitation (mm), physiographic province, and underlying lithology. We initially generated a multivariate correlation matrix to eliminate the possibility of including any autocorrelated variables into a multiple regression model. Further, we generated Principal Components from all variables listed above for the 37 slope samples to determine if these could be used more effectively in a multiple regression model to predict erosion rates.

Finally, we compiled a database containing topographically-derived and meteorological summary statistics, as well as the  $E_{ps}$  predicted erosion rates for each of the 5104 sub-basins contained within the 10 large-scale Piedmont drainages. We used this database to probe the similarities and difference of erosion rates predicted for small-scale basins across the entire Piedmont region.

One of the goals of producing the database was to facilitate the prediction of erosion rates for much larger-scale basins in order to predict background erosion rates in the absence of  $^{10}\text{Be}$  data. To this effect, we imported the database into ArcGIS™, and selected the sub-set of small basins falling with each of the large-scale outlet as well as the mid, and Blue Ridge sub-basins (n=28). We then predicted erosion rates for each of the 28 large basins with  $E_{ps}$  using two different approaches. First, we calculated the area-weighted average erosion rates of all sub-basin  $E_{ps}$  predictions contained within each large basin. We call these values the “aggregated”  $E_{ps}$  predicted erosion rates. Second, we use predict erosion rates for each large basin based on the summary statistics representing each entire basin (not the area-weighted sub-basins). We refer to these values the “whole-basin”  $E_{ps}$  predicted erosion rates.

## 6.5. Results

Concentrations of  $^{10}\text{Be}$  in the 66 samples presented in this study range from 1.44 to  $14.2 \times 10^5$  at/g, yielding CRONUS-modeled background erosion rates ( $E$ ) ranging from 1.95 to 50.5 m/My, in agreement with previously published drainage-basin scale  $^{10}\text{Be}$  erosion rates for the southern Appalachian Mountains [*Duxbury, 2009; Matmon et*

*al.*, 2003a; *Matmon et al.*, 2003b; *Portenga and Bierman*, 2011; *Sullivan*, 2007; *Trodick*, 2011].

The ten large basins (2,987 to 17,715 km<sup>2</sup>) are eroding slowly. <sup>10</sup>Be erosion rates for samples collected at the outlets of the ten large basins range from ~14 to ~4 m/My with an area weighted averaged rate of 8.8 ± 3.3 m/My (Table 6 – 1 (a.k.a. Supplemental Table S1)). In general, <sup>10</sup>Be data suggest that regions from the Savannah basin and south erode naturally approximately twice as fast (12.2 ± 2.1 m/My) as basins to the north (6.3 ± 1.1 m/My). Erosion rates in the higher-slope Blue Ridge range from ~25 to ~9 m/My with an area weighted average of 13.7 ± 4.9 m/My, while rates from mid-basin samples fall between the two with an area weighted average of 11.0 ± 3.7 m/My.

Smaller basins (~1 to 50 km<sup>2</sup>), collected for our slope test, are also eroding slowly at rates between 2 and 50 m/My and indicate that average basin slope is positively related to <sup>10</sup>Be background erosion rate. The linear bi-variate mean slope-erosion rate relationship for all individual 37 slope samples (R<sup>2</sup> = 0.57, p<0.0001) yields the following model expression:

$$E_{ps} = 0.98 \times (S_m) + 1.05 \quad (eq.1)$$

When the 37 samples are binned into ten discrete slope divisions (Figure 6 - 3), the resulting linear slope-erosion rate relationship (R<sup>2</sup>=0.88; p<0.0001) is robust (Figure 6 - 4; Table 6 – 2 (a.k.a. Supplemental Table S2)).

Results from our multivariate correlation matrix indicate that the only non-autocorrelated variables are mean basin slope and latitude (at the centroid of each basin). This is logical as slope is a proxy for nearly every other morphometric variable entered

into the multivariate analysis. Latitude appear to be uncorrelated as the Appalachian Mountain Chain runs nearly 45° NE to SW and  $^{10}\text{Be}$  production rates and erosion rate calculation vary as a function of latitude. When latitude is included to produce a multiple regression model, very little to no predictive capability is gained ( $R^2 = 0.57$ ,  $p < 0.0001$ ). Similarly, a multiple regression model generated with first 5 Principal Components yields a maximum adjusted  $R^2$  of 0.46 ( $p < 0.0001$ ). This analysis indicates that we gain little from employing more complex statistics and we therefore use the much stronger slope-only based predictive model from the 10 binned slope divisions (*eq. 2*).

When we use our database to predict aggregated  $E_{ps}$  rates for each of the ten large-scale outlet basins, we find that these predictions are, on average, ~25 percent lower than the area-weighted average  $^{10}\text{Be}$  rate we measured ( $^{10}\text{Be} = 8.75 \pm 3.25$ ;  $E_{ps} = 6.46 \pm 1.21$ ). The difference between predicted erosion rates and  $^{10}\text{Be}$  erosion rates become more pronounced when plotted against one another (Figure 6 - 5A);  $^{10}\text{Be}$  appears to overestimate rates of erosion relative to the predictions made with the aggregated  $E_{ps}$  model. Predicted aggregated  $E_{ps}$  erosion rates track well with the average values of  $elev_m$ ,  $rel$ ,  $S_m$ ,  $MAP$ , and  $MAT$  used to generate the multiple regression model (Figure 6 - 6A & B). The simple slope model ( $E_{ps}$ ) yields nearly identical results using either the aggregated or whole-basin approaches ( $R^2=0.99$ ,  $p < 0.0001$ ; Figure 6 - 7A).

Results from our four dam-pairs indicate that in most instances, dams influence calculated  $^{10}\text{Be}$  erosion rates.  $^{10}\text{Be}$  erosion rates for two dam-pairs, collected near dams at the outlets of the Pee Dee and Chattahoochee Rivers (Figure 6 - 1), yield erosion rates that are between ~55 and 60 percent greater downstream than upstream counterparts

( $17.6 \pm 1.3$  vs.  $11.4 \pm 0.9$  m/My, and  $10.9 \pm 0.9$  vs.  $6.8 \pm 0.6$  m/My respectively; Figure 6 - 6A; Table 6 – 1 (a.k.a Supplemental Table S1). The downstream/upstream difference is even greater (nearly 2-fold) for the dam-pair collected approximately mid-way down the Neuse River ( $6.0 \pm 0.5$  vs.  $3.1 \pm 0.3$  m/My). Alternatively, in the much higher slope Blue Ridge, where the basins are substantially smaller than at the outlets, a dam-pair along the Savannah River suggests that differences in erosion rates (~11 percent) are within the uncertainty of  $^{10}\text{Be}$  measurement and modeling ( $14.2 \pm 1.2$  vs.  $16.0 \pm 1.2$  m/My). Overall, we consider the samples collected upstream of dams as more reliable measures of background erosion and, where possible, use their values in calculations of average  $^{10}\text{Be}$  erosion rates.

Results from temporal replication of a sampling site along the Savannah River (SAP17,  $15.6 \pm 1.2$  m/My; SAP55,  $13.4 \pm 1.0$  m/My) suggest a temporal variance of ~14% in  $^{10}\text{Be}$  concentration and resulting erosion rate estimates. Because the temporal replication site is located just downstream of a hydroelectric dam, we consider this percentage to be an upper limit on temporal variability.

## 6.6. Discussion

Using a sampling plan that represents well the distribution of average drainage basin slopes, a clear control on erosion rates in eastern North American [*Portenga and Bierman, 2011*], we determined that the Piedmont physiographic province erodes at a rate of ~9 m/My over millennial time scales. This value is somewhat lower than previously reported  $^{10}\text{Be}$  erosion rates in other parts of the Appalachians, such as the Great Smoky

Mountains, ( $27 \pm 4$  m/My; [Matmon *et al.*, 2003a; Matmon *et al.*, 2003b]), or along the Blue Ridge Escarpment ( $\sim 7$  to 38 m/My; [Sullivan, 2007]), or in Shenandoah National Park, VA ( $12 \pm 5$  m/My m/My; [Duxbury, 2009]); however, these three studies were conducted in rugged parts of the Blue Ridge Province with much higher average basin slopes. The topographically subdued southern Piedmont, with its rolling topography, erodes on average more slowly.

Evidence from dam pairs and modeling results from our slope-test sampling, illuminate some of the complexities and potential shortcoming associated with sampling large basins in  $^{10}\text{Be}$  erosion rate studies. Of particular interest to this study is the presence of numerous hydroelectric dams constructed along the big rivers of the southern Piedmont due to the relatively steep breaks in slope at both the Blue Ridge/Piedmont and Piedmont/Coastal Plain transitions. Although  $^{10}\text{Be}$  has been used to generate erosion rates for large river systems elsewhere around the globe previously [e.g. Schaller *et al.*, 2001], the influence of dams on the concentrations of  $^{10}\text{Be}$  measured in fluvial sediment, and in turn the calculated erosion rates, has never been addressed explicitly.

Large dams with high trap efficiencies [Brune, 1953] by design impede the flow of water and thus sediment; in turn, interpretations of  $^{10}\text{Be}$  concentration measured in sediment below such obstructions as basin-scale erosion rates is uncertain because the origin of the downstream material is uncertain. Although sediment deposited in reservoirs can become remobilized and be transported over dams during extreme flood events [Meade, 1982], it is not possible to determine if this were the case for a particular sample. More likely, a sample collected directly downstream of a dam is either locally

sourced from eroding bank material or saprolite of unknown depth, is reworked alluvium pre-dating the dam, or is a mix of local and upstream material. Only pre-dam alluvium will provide information about the long-term erosion rate upstream of the dam.

When samples collected from downstream of the dams are interpreted as erosion rates under the assumption that the sediment was sourced evenly from the entire upstream basin, they appear to significantly overestimate background of erosion rates relative to their upstream counterparts (see Results section; Table 6 – 1 (a.k.a Supplemental Table S1). The two outlet dam-pairs from the Pee Dee and Chattahoochee Rivers (Figure 6 - 1) differ by ~60 and ~54 percent respectively (Figure 6 - 6A), while the mid-basin dam pair differs by ~93 percent. If we assume instead that the material we sampled for the 2 outlet and 1 mid basin pairs originated from local sources below the dams (surface wash only), and apply the corresponding local elevations as opposed to the hypsometrically weighted elevations for the entire basins, we reduce the differences in upstream vs. downstream erosion rates from an average of ~69 percent for the three sets to ~35 percent (Table 6 – 1 (a.k.a. Supplemental Table S1)). Because less than half of the difference between upstream and downstream erosion rates is explained by considering local sourcing alone, the samples we collected below the dams probably originated locally, but from depth beneath the surface (eroding bluff for instance; Figure 6 - 8). The implication is clear; samples collected downstream of dams are potentially erroneous indicators of background erosion rates for regions upstream. For instance, we collected the outlet sample for the Savannah River immediately downstream of the Thurmond Lake Dam (Figure 6 - 8). Its deviation from surrounding outlet samples (Figure 6 - 6) resembles that

of the downstream outlet samples for the Pee Dee and Chattahoochee Rivers. Similarly, samples for the outlets of the Oconee and Ocumulgee basins to the south were collected in close proximity to the downstream faces of dams (Figure 6). In the southern Piedmont, the absolute differences in erosion rates are relatively small (e.g. 3 vs. 6 m/My), but the relative difference, 50% is large.

Simple models, along with data from a representative sample of smaller basins, can be used to predict the erosion rate of large basins. Scaling up the  $E_{ps}$  model using the aggregate approach provides reasonable prediction of average erosion rates for the 10 large outlet basins ( $^{10}\text{Be} = 8.8 \pm 3.3$ ;  $E_{ps} = 6.5 \pm 1.2$ ;  $E_{pm} = 6.8 \pm 1.3$  m/My). However, when examined individually from north to south, comparisons between  $^{10}\text{Be}$  erosion rates and predicted rates vary considerably from basin to basin (Figure 6 - 6A). Most notably,  $^{10}\text{Be}$  and predicted rates agree far better in the six northern basins (Roanoke to the Saluda Rivers) than in the southernmost basins (Savannah to the Chattahoochee Rivers; Figures 6 - 1 & 6 - 6A). There are two possible explanations for this latitudinal difference along the southern Piedmont; first, that there are fundamental difference in either the geology or land-use history between the northern and southern basins, and second, that dams have had more of an effect on the concentration of  $^{10}\text{Be}$  we measured in samples collected from the southern rivers. Although there does not appear to be pronounced differences in either the geology or land-use history between the northern and southern basins [e.g. *Meade and Trimble, 1974; Trimble, 1977*] access to the river channels for the four southern basins limited sampling to sites in close proximity to dams (from several km's downstream to immediately below dams). The southernmost basin (Chattahoochee

River) is one of our dam pair tests and shows an ~54 percent increase in  $^{10}\text{Be}$  erosion rates between the downstream sample (SAP64,  $17.6 \pm 1.3$  m/My) and the upstream sample (SAP66,  $11.4 \pm 0.9$  m/My; Figure 6 - 6A). We therefore attribute at least the majority of the discrepancy between the higher  $^{10}\text{Be}$  erosion rates and the lower  $E_{ps}$  aggregated predicted rates for these basins to the sourcing of sampled material caused by the presence dams.

The slope-based predicted model we generated from the 37 small basins (10's of  $\text{m}^2$ ) offers us a potentially better method of estimating erosion rates for larger basins because the small basins headwater are less susceptible the presence of dams along larger channels. When we compare aggregated  $E_{ps}$  predicted values (the erosion rate calculated from the spatial of average rate predicted for all sub-basins contained within a larger basin) to whole-basin  $E_{ps}$  predicted values (the erosion rate predicted from the average basin slope of the entire large basin), we find that the  $E_{ps}$  predictive model is fully scalable making it a very flexible model for predicting background rates of erosion (Figure 6 – 7A). Average basin slope is dimensionless and thus largely insensitive to spatial scaling. Site-specific models such as this could be used to quickly estimate a background erosion rate for any size basin once the region has been characterized. These estimates could prove useful for informing land management strategies.

In summary, although the linear regression model for predicting erosion rate from average basin slope ( $E_{ps}$ ) is simple, after more than two decades of drainage basin-scale  $^{10}\text{Be}$  erosion rate studies conducted around the globe, average basin slope consistently proves to be a reliable predictor of erosion rate both at study site scale [Matmon *et al.*,

2003a; Matmon *et al.*, 2003b; Sullivan, 2007] and when considered globally [Portenga and Bierman, 2011]. Our results suggest that this model ( $E_{ps}$ ; eq. 2) is fully scalable, and therefore theoretically capable of predicting a background drainage basin-scale erosion rate at any point along a river network across the entire southern Appalachian Piedmont.

## 6.7. Conclusions

At large spatial scales, the 10 large, Piedmont dominated, low-gradient outlet basins suggest that the region as a whole naturally erodes more slowly ( $\sim 9$  m/My) than the steeper headwater Blue Ridge basins ( $\sim 14$  m/My). Samples collected mid-way down several of the outlets basins have erosion rates intermediate between the outlet and Blue Ridge rates ( $\sim 11$  m/My) indicating that material from the Blue Ridge is mixing with material sourced from the lower-slope Piedmont as it travels downstream. The dam pair tests indicate that, especially at large-scales, samples collected downstream of dams are not reliable indicators of basin-scale erosion rates; rather, material downstream of large dams appears to be locally sourced. These findings suggest that perhaps the best indication of the background exposure history of hillslope materials from regions that have experienced periods of intensive agricultural land use may be found in the sediment trapped in the dam reservoirs themselves. Finally, a simple model ( $E_{ps}$ ), considering only basin-average slope, is capable of predicting erosion rates at any point along the Southern Piedmont for basins of any size.

## 6.8. References cited

Balco, G., J. Stone, N. A. Lifton, and T. J. Dunai (2008), A complete and easily accessible means of calculating surface exposure ages or erosion rates from  $^{10}\text{Be}$  and  $^{26}\text{Al}$  measurements, *Quaternary Geochronology*, 3(3), 174-195.

Bierman, P., and E. Steig (1996), Estimating rates of denudation and sediment transport using cosmogenic isotope abundances in sediment, *Earth Surface Processes and Landforms*, 21, 125-139.

Brown, E. T., R. F. Stallard, M. C. Larsen, G. M. Raisbeck, and F. Yiou (1995), Denudation rates determined from the accumulation of in situ-produced  $^{10}\text{Be}$  in the Luquillo Experimental Forest, Puerto Rico, *Earth and Planetary Science Letters*, 129, 193-202.

Brune, G. (1953), Trap efficiencies of reservoirs, *American Geophysical Union Transactions*, 34, 407-418.

Corbett, L. B., N. E. Young, P. Bierman, J. P. Briner, T. A. Neumann, D. Rood, and J. Graly (2011), Paired bedrock and boulder  $^{10}\text{Be}$  concentrations resulting from early Holocene ice retreat near Jakobshavn Isfjord, western Greenland, *Quaternary Science Reviews*, 30, 1739-1749.

Cox, R., P. Bierman, and M. Jungers (2009), Erosion rates and sediment sources in Madagascar inferred from  $^{10}\text{Be}$  analysis of lavaka, slope, and river sediment, *Journal of Geology*, 117, 363-376.

Duxbury, J. (2009), Erosion rates in and around Shenandoah National Park, VA determined using analysis of cosmogenic  $^{10}\text{Be}$ , 123 pp, University of Vermont, Burlington, VT.

Gosse, J., and F. M. Phillips (2001), Terrestrial *in situ* cosmogenic nuclides: theory and applicaiton, *Quaternary Science Reviews*, 20, 1475-1560.

Granger, D. E., J. W. Kirchner, and R. Finkel (1996), Spatially averaged long-term erosion rates measured from *in situ*-produced cosmogenic nuclides in alluvial sediments, *Journal of Geology*, 104(3), 249-257.

Granger, D. E., L. A. Lifton, and J. K. Willenbring (2013), A cosmic trip: 25 years of cosmogenic nuclides in geology, *GSA Bulletin*, doi: 10.1130/B30774.30771.

Jungers, M., P. Bierman, A. S. Matmon, K. K. Nichols, J. Larsen, and R. Finkel (2009), Tracing hillslope sediment production and transport with *in situ* and meteoric  $^{10}\text{Be}$ , *Journal of Geophysical Research - Earth Surface*, 114.

Kohl, C. P., and K. Nishiizumi (1992), Chemical isolation of quartz for measurement of in-situ-produced cosmogenic nuclides, *Geochimica et Cosmochimica Acta*, 56, 3583-3587.

Matmon, A., P. Bierman, J. Larsen, S. Southworth, M. Pavich, and M. Caffee (2003a), Temporally and Spatially Uniform Rates of Erosion in the Southern Appalachian Great Smokey Mountains, *Geology*, 31(2), 155-158.

Matmon, A., P. R. Bierman, J. Larsen, S. Southworth, M. Pavich, R. Finkel, and M. Caffee (2003b), Erosion of an ancient mountain range, the Great Smoky Mountains, North Carolina and Tennessee, *American Journal of Science*, 303(10), 972-973.

Meade, R. H. (1982), Sources, sinks and storage of river sediment in the Atlantic drainage of the United States, *Journal of Geology*, 90, 235-252.

Meade, R. H., and S. W. Trimble (1974), Changes in sediment loads in rivers of the Atlantic drainage of the United States since 1900, in *Effects of Man on the Interface of the Hydrological Cycle with the Physical Environment*, edited, pp. 99-104, Internat. Assoc. Sci.

Niemi, N., M. Oskin, D. W. Burbank, A. M. Heimsath, and E. Gabet (2005), Effects of bedrock landslides on cosmogenically determined erosion rates, *Earth and Planetary Science Letters*, 237(3-4), 480-498.

Nishiizumi, K., M. Imamura, M. Caffee, J. Southon, R. Finkel, and J. McAninch (2007), Absolute calibration of  $^{10}\text{Be}$  AMS standards, *Nuclear Instruments and Methods in Physics Research B*, 258, 403-413.

Portenga, E. W., and P. R. Bierman (2011), Understanding Earth's eroding surface with  $^{10}\text{Be}$ , *GSA Today*, 21(8), doi: 10.1130.

Reusser, L. J., and P. Bierman (2010), Using meteoric  $^{10}\text{Be}$  to track fluvial sand through the Waipaoa River basin, New Zealand, *Geology*, 38(1), 47-50.

Riebe, C. S., J. W. Kirchner, D. E. Granger, and R. C. Finkel (2000), Erosional equilibrium and disequilibrium in the Sierra Nevada, inferred from cosmogenic  $^{26}\text{Al}$  and  $^{10}\text{Be}$  in alluvial sediment, *Geology*, 28(9), 803-806.

Safran, E. B., P. Bierman, R. Aalto, T. Dunne, and K. X. Whipple (2005), Erosion rates driven by channel network incision in the Bolivian Andes, *Earth Surface Processes and Landforms*, 30, 1007-1024.

Schaller, M., F. v. Blanckenburg, N. Hovius, and P. Kubik (2001), Large-scale erosion rates from in situ-produced cosmogenic nuclides in European river sediments, *Earth and Planetary Science Letters*, 188, 441-458.

Sullivan, C. (2007),  $^{10}\text{Be}$  erosion rates and landscape evolution of the Blue Ridge Escarpment, southern Appalachian Mountains, 66 pp, University of Vermont, Burlington, VT.

Sullivan, C., P. Bierman, M. Pavich, J. Larsen, and R. Finkel (2006), Cosmogenically derived erosion rates for the Blue Ridge Escarpment, southern Appalachian Mountains, *Geological Society of America - Abstracts with Programs*, 38(7), 279.

Syvitski, J. P. M., C. J. Vorosmarty, A. J. Kettner, and P. Green (2005), Impact of Humans on the flux of Terrestrial Sediment to the Global Coastal Ocean, *Science*, 308, 376-380.

Trimble, S. W. (1977), The fallacy of stream equilibrium in contemporary denudation studies, *American Journal of Science*, 277, 876-887.

Trodick (2011), in situ and meteoric  $^{10}\text{Be}$  concentration of fluvial sediment collected from the Potomac River Basin, 203 pp, University of Vermont, Burlington, VT.

Wilkinson, B. H., and B. J. McElroy (2007), The impact of humans on continental erosion and sedimentation, *GSA Bulletin*, 119(1.2), 140-156.

### **6.9. Acknowledgments**

We thank M. Jungers, W. Hacket, and J. Duxbury for assistance in the field, D. Rood for all AMS measurements, and G. Balco for assistance preparing our data for use with the CRONUS calculator to generate basin-scale erosion rates. Support provided by NSF EAR-310208 and DoD DAAD19-03-1-0205.

## 6.10. Figure captions

**Figure 6 - 1** – Location map of the southern Appalachian Piedmont field area along the southeastern seaboard of the North America. River basins 1 through 10 are those in Trimble (1977). Blue Ridge (☆), Mid-basin (○), and Outlet (Δ) denote the locations of *in situ* <sup>10</sup>Be sample sites within each catchment. Modified from Figure 1 in Trimble (1977).

**Figure 6 - 2** – A: location map of the four large basins used for determining the distribution of various landscape characteristics for small basins (~10 km<sup>2</sup>) such as average basin slope, basin relief, and average basin elevation . B, C: graphics depicting the small sub-basins within the Pee Dee Basin mapped by average basin elevation and average basin slope respectively.

**Figure 6 - 3** –Frequency distribution (bars) and cumulative probability density function (PDF; solid line) of the average basin slopes for 3053 sub-basins within the four basins shown in figure 2. The skewed distribution of average basin slopes reflects the relative proportion of higher slope Blue Ridge sub-basins (tail) and lower slope Piedmont (majority of sub-basins). Diamonds represent the 10 slope divisions for which samples were collected. The seven lower slope divisions incorporate mostly Piedmont sub-basins; the three highest slope divisions incorporate mostly Blue Ridge sub-basins representing the higher slope tail of the distribution.

**Figure 6 - 4** – Average basin slope and erosion rates are well correlated for 37 small sub-basins. The samples were selected based on the slope division show in Figure 6 - 3.

**Figure 6 - 5** – Aggregated  $E_{ps}$  predicted erosion rates for all outlet, mid, and Blue Ridge large-scale basin samples vs. measured  $^{10}\text{Be}$  erosion rates. The poor relationships reflect the multiple uncertainties associated with calculating background  $^{10}\text{Be}$  erosion rates for large-scale ( $\sim 10^4 \text{ km}^2$ ) drainage basins. The apparent overestimation of erosion rates with  $^{10}\text{Be}$  likely reflects the influence of dams; the samples we collected downstream of dams probably contain at least some low-concentration, locally sourced material that biases our  $^{10}\text{Be}$  erosion rates.

**Figure 6 - 6** – Compilation figure showing, basin by basin, all data relevant for interpreting the  $^{10}\text{Be}$  background erosion rates measure in this study as well as the erosion rates predicted with the slope-based ( $E_{ps}$ ) using the aggregated approach. A: larger diamonds are  $^{10}\text{Be}$  erosion rates; smaller circles are erosion rates predicted with the slope-based model ( $E_{ps}$ ). Both upstream and downstream  $^{10}\text{Be}$  erosion rates and predicted erosion rates are shown for the Pee Dee and Chattahoochee River dam-pairs. B: basin-by-basin average values of several morphometric and climatologic variables. Note that all erosion rates for the six northern basins (Roanoke to the Saluda Rivers) track well with the model parameters in the lower panel, while  $^{10}\text{Be}$  erosion rates for the four basins to the south deviate substantially from the modeled rates due the proximity of the sample sites to dam locations.

**Figure 6 - 7** – Relationship between erosion rates predicted with the simple slope ( $E_{ps}$ ) model for all outlet, mid-basin, and Blue Ridge samples using both the aggregated and whole-basin approaches. The 1 to 1 relationship indicates that average basin slope alone can be used to predict erosion rates for drainage basins independent of spatial scale.

**Figure 6 - 8** – Field photos from sample site SAP53 collected just downstream of the Thurmond Lake Dam at the Piedmont/Coastal Plain transition along the Savannah River. In the lower photo, note the eroding bluff in the background. The material we collected most likely originated from a range of depths from this bluff, and not from sediment sourced upstream of the dam. These photos correspond to the  $^{10}\text{Be}$  erosion rate for the Savannah River in Figure 6 - 6A that deviates substantially from the predicted erosion rates, further suggesting that this sample is not representative of the erosional history of the landscape upstream.

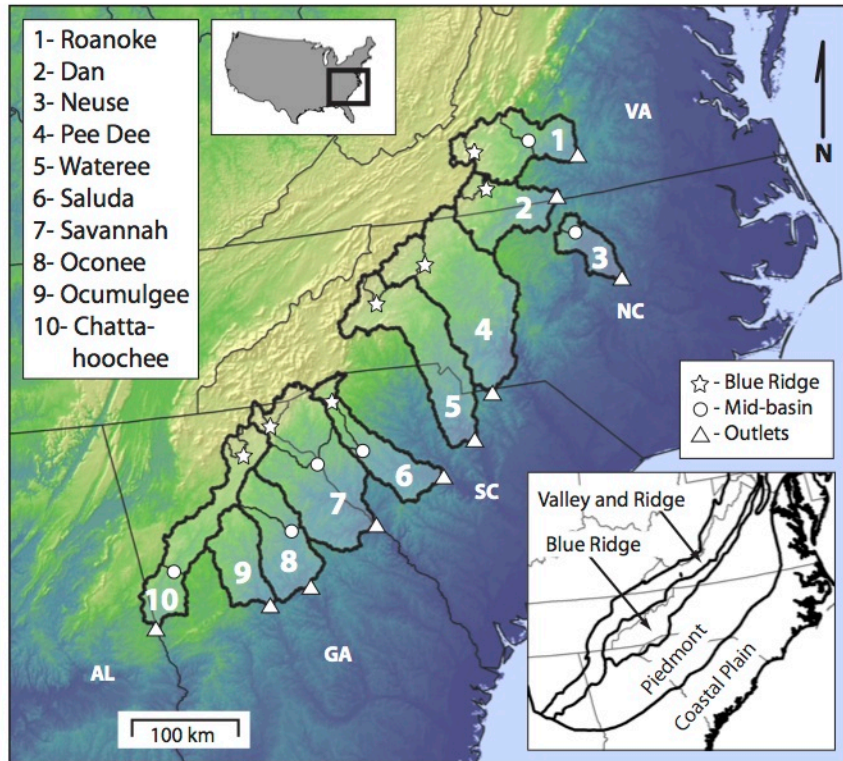


Figure 6 - 1 Location map for the southern Appalachian Piedmont draining the North American Atlantic Passive Margin

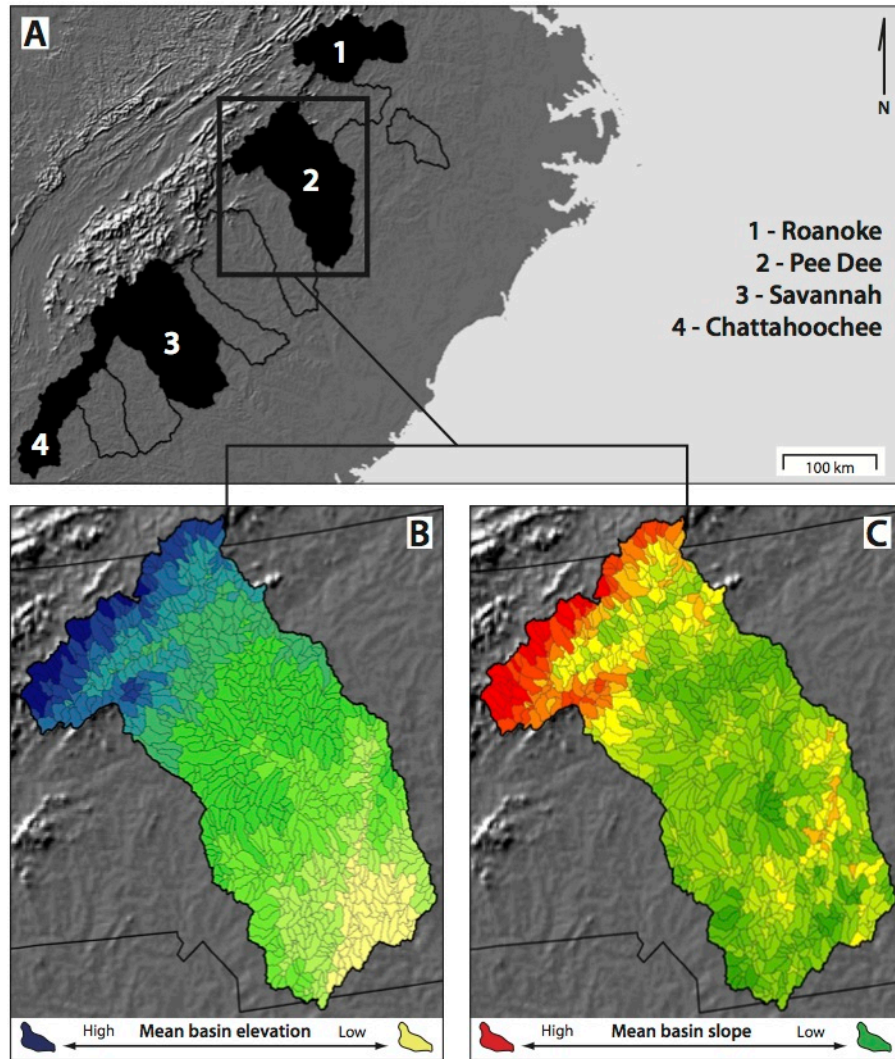


Figure 6 - 2 The four basins out of ten Piedmont drainages summarized and used to generate the slope-test

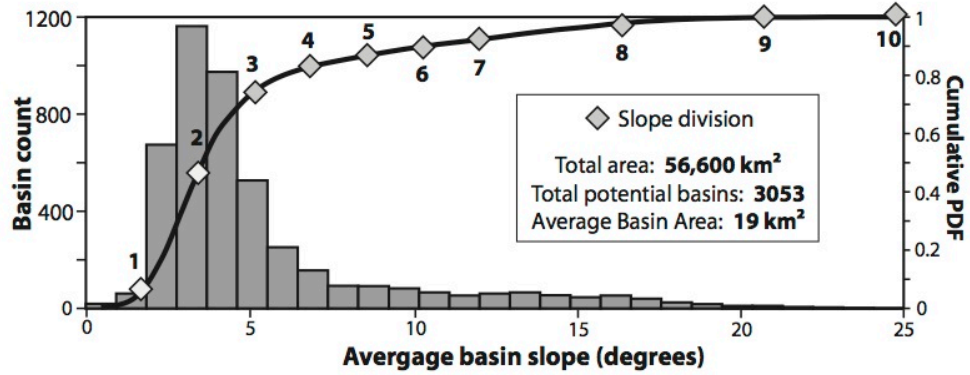


Figure 6 - 3 Frequency distribution of average basin slopes for all sub-basin with the four large basins in Figure 2 used to select the 40 slope-test samples

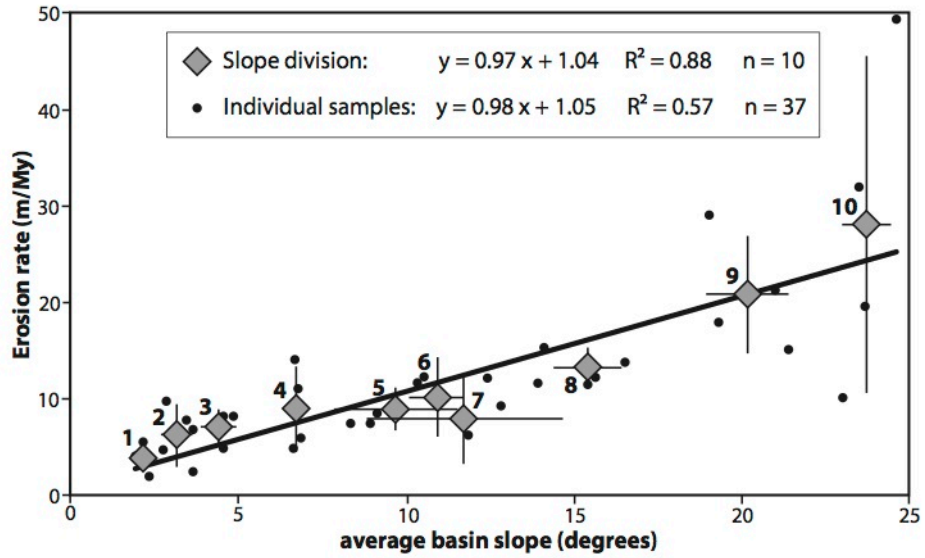


Figure 6 - 4 Results from the small-basin slope test. The average basin slope vs. erosion rate relationship is used to predict rates in basin without  $^{10}\text{Be}$  data.

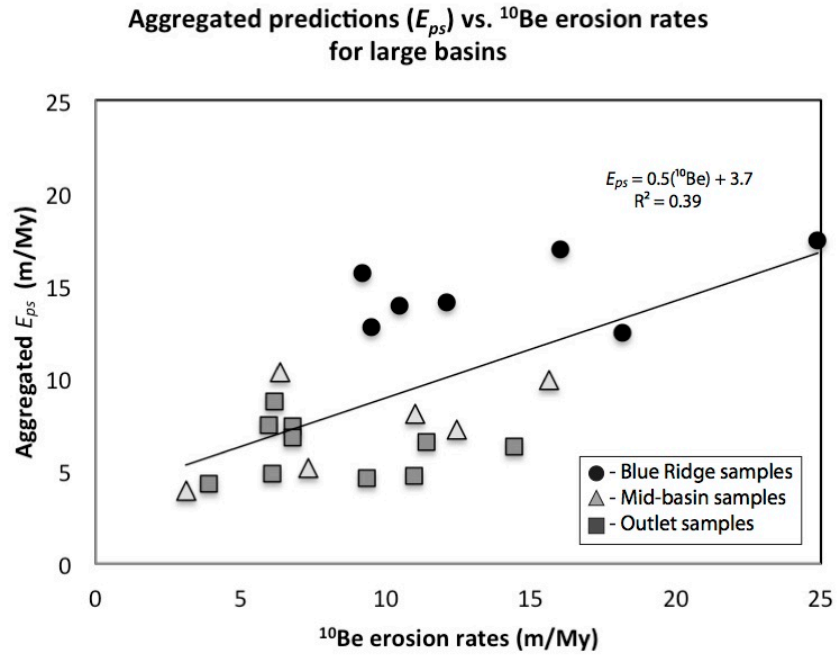


Figure 6 - 5 Relationships between our measured  $^{10}\text{Be}$  erosion rates, and the aggregated  $E_{ps}$  predicted erosion rates for large basins.

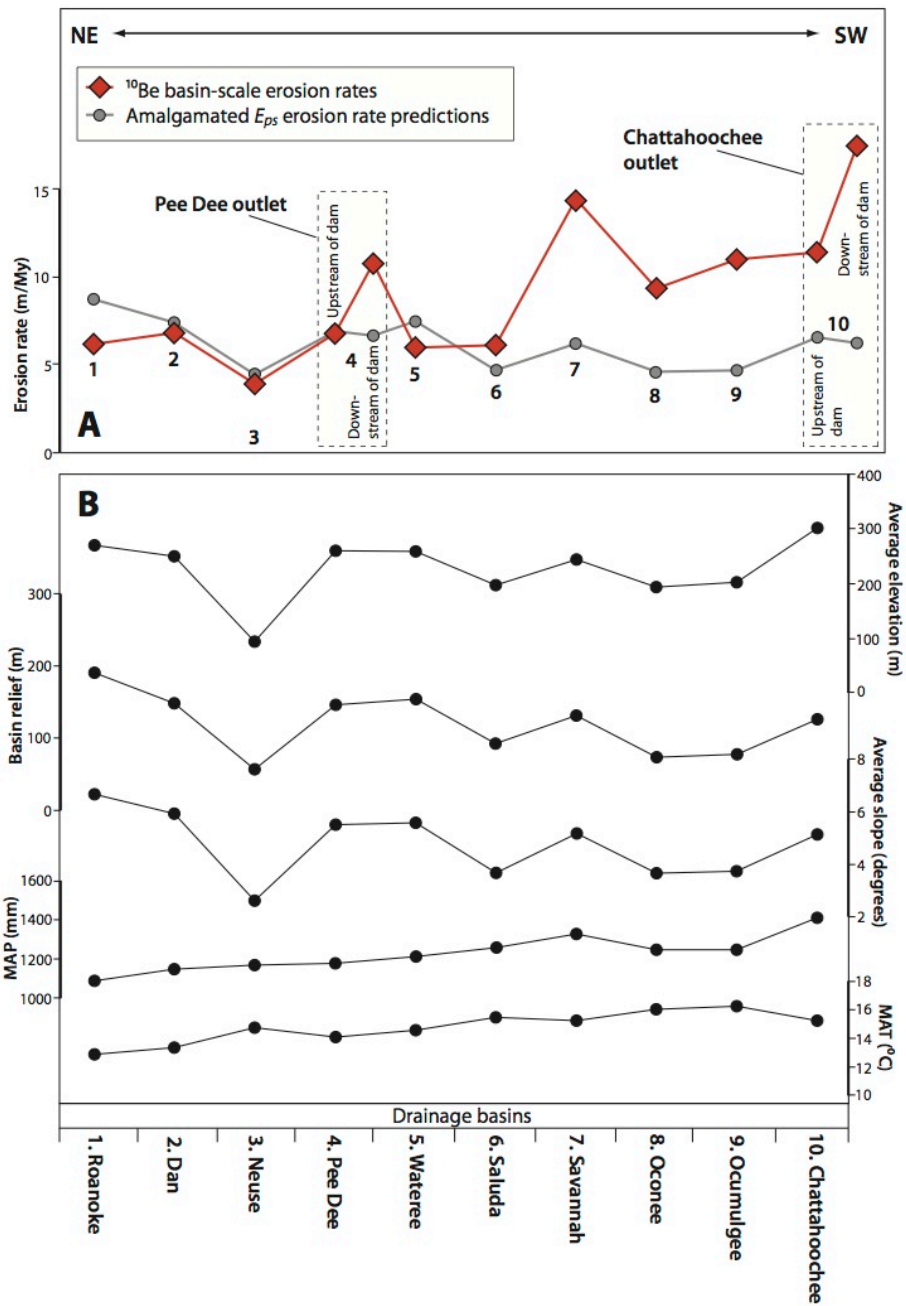


Figure 6 - 6 A: compilation of  $^{10}\text{Be}$  erosion rates and  $E_{ps}$  predicted erosion rates for all large-scale outlet basins, and B: basin-by-basin average values several morphometric and meteorological variables.

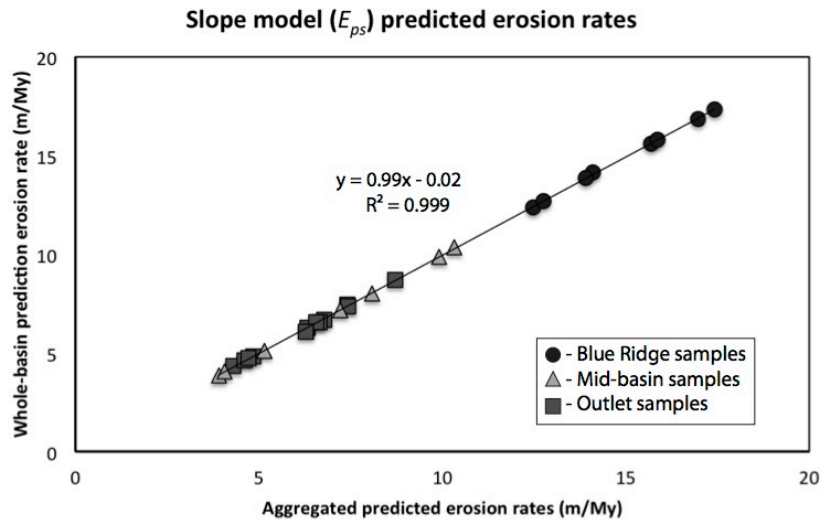


Figure 6 - 7 Effects of spatial scaling on  $E_{ps}$  predicted erosion rate using the amalgamated approach vs. the whole-basin approach.

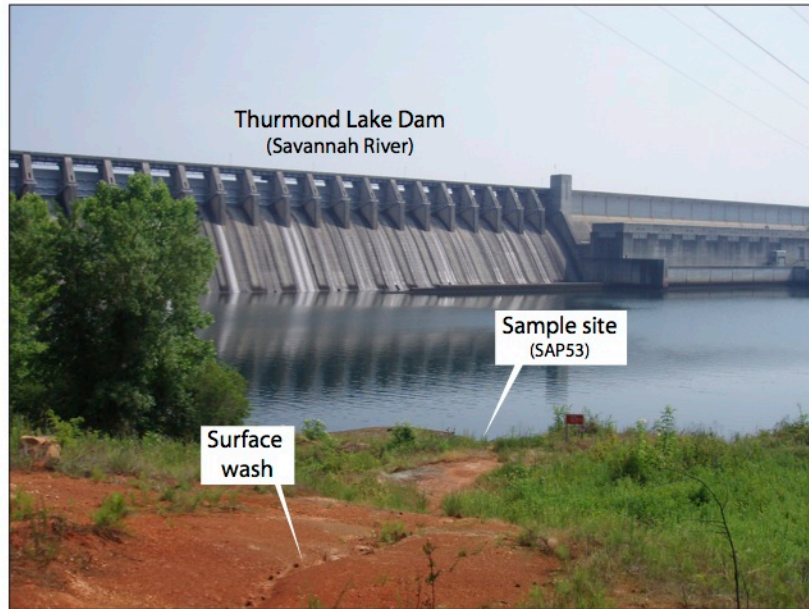


Figure 6 - 8 Example of sample site located below a large hydroelectric dam along the Savannah River showing the eroding bluff in the background.

Table 6 - 1 (Supplemental Table S1) Summary information for all large-scale basins from the southern Appalachian Piedmont.

Sample ID	BE Number*	Basin†	Sample Type§	UTM Zone	Northing#	Eastings#	Area (km²)‡	Mean Elevation (m)‡	Mean Slope (degrees)‡	<sup>10</sup> Be (atoms/g x 10 <sup>15</sup> )‡	Model Erosion Rate (m/My)Ω
SAP03	BE27676	Roanoke	Outlet	17	701236	4087858	7676	322	7.9	6.24 ± 0.18	6.17 ± 0.52
SAP04	BE27677	Dan	Outlet	17	670737	4056984	6686	286	6.6	5.50 ± 0.16	6.79 ± 0.57
SAP07	BE27679	Neuse	Outlet	17	734920	3947950	2987	129	3.4	7.74 ± 0.21	3.90 ± 0.35
SAP09	BE27681	Pee Dec	Outlet	17	591286	3882894	16376	280	3.8	5.40 ± 0.14	6.78 ± 0.56
SAP10	BE27682	Waterce	Outlet	17	527671	3799121	12270	306	6.0	6.10 ± 0.17	5.98 ± 0.50
SAP12	BE27684	Saluda	Outlet	17	482362	3767289	6274	212	3.9	5.55 ± 0.15	6.09 ± 0.51
SAP53	BE28717	Savannah	Outlet	17	388641	3724815	15870	265	5.4	2.72 ± 0.08	14.42 ± 1.11
SAP51	BE28715	Oconee	Outlet	17	294420	3667665	7549	200	3.7	3.78 ± 0.10	9.34 ± 0.73
SAP50	BE27895	Ocmulgee	Outlet	17	245302	3656461	5438	231	3.8	3.35 ± 0.10	10.98 ± 0.87
SAP66	BE27901	Chattahoochee	Outlet	16	669074	3643249	8900	332	5.7	3.48 ± 0.14	11.38 ± 0.96
SAP39	BE27887	Roanoke	Mid-Basin	17	651634	4107904	4613	387	9.6	6.35 ± 0.18	6.36 ± 0.54
SAP05	BE27678	Neuse	Mid-Basin	17	689752	4011251	366	183	2.9	9.79 ± 0.25	3.11 ± 0.28
SAP13	BE28703	Saluda	Mid-Basin	17	387503	3806254	1495	348	7.2	3.65 ± 0.09	11.01 ± 0.85
SAP17	BE27736	Savannah	Mid-Basin	17	332802	3802906	5426	421	9.1	2.81 ± 0.08	15.62 ± 1.19
SAP52	BE28716	Oconee	Mid-Basin	17	287577	3733626	2438	248	4.2	4.83 ± 0.12	7.31 ± 0.59
SAP69	BE28724	Chattahoochee	Mid-Basin	16	695086	3706075	6247	368	6.3	3.29 ± 0.08	12.44 ± 0.95
SAP41	BE27888	Roanoke	Blue Ridge	17	571636	4121141	666	631	15.0	5.39 ± 0.14	9.19 ± 0.75
SAP45	BE27892	Dan	Blue Ridge	17	588442	4071770	561	475	13.5	3.78 ± 0.10	12.09 ± 0.95
SAP32	BE27883	Pee Dec	Blue Ridge	17	499518	4006148	1941	510	13.2	4.34 ± 0.14	10.45 ± 0.85
SAP27	BE27743	Waterce	Blue Ridge	17	435721	3965723	527	628	16.8	2.12 ± 0.06	24.89 ± 1.86
SAP26	BE27742	Saluda	Blue Ridge	17	360778	3867333	666	457	11.7	2.50 ± 0.07	18.15 ± 1.38
SAP22	BE28705	Savannah	Blue Ridge	17	280243	3848234	468	755	16.3	3.34 ± 0.08	16.01 ± 1.23
SAP56	BE28718	Chattahoochee	Blue Ridge	17	230245	3824544	390	557	12.0	4.71 ± 0.11	9.50 ± 0.75
SAP60	BE28721	Chattahoochee	Blue Ridge	17	246607	3847401	50	819	19.7	3.25 ± 0.08	17.16 ± 1.32

\* BE Number denotes the sample identification tag logged during measurement at the Lawrence Livermore National Laboratory.

† Trimble Basin designates which of the 10 large-scale Piedmont catchments each sample was collected from.

§ Outlet samples were collected at approximately the Piedmont-Coastal Plain transition. Blue Ridge samples were collected from the higher slope upstream portions of catchments. Mid-Basin samples were collected approximately mid-way down the trunk streams draining each catchment. Refer to figure 1 for visual locations.

# All GPS locations provided in UTM NAD83 CONUS. Note the change in zone for the southwesternmost basin.

‡ All geographic statistics were calculated in ArcGIS® using 1/3 arcsecond (~28m) digital elevation models downloaded from <http://seamless.usgs.gov>.

Ω Errors in nuclide concentrations include propagated laboratory and measurement uncertainties. Measured ratios of <sup>10</sup>Be normalized to the 07KNSSTD3110 standard with reported <sup>10</sup>Be/<sup>9</sup>Be ratio of 2.859 x 10<sup>-15</sup> (Nishizumi, et al., 2007).

Ω Erosion rates modeled with the CRONUS online calculator (<http://hess.ess.washington.edu>) using hypsometrically weighted effective ELDs for each basin.

Table 6 - 2 (Supplemental Table S2) Summary information for all 37 small-scale slope-test samples.

Table 2: Summary information for small-scale slope division samples

Sample ID	BE Number*	Triamble Basin†	Slope Division‡	UTM Zone	Northing#	Eastings#	Province°	Area (km²)	Mean Elevation (m)‡	Basin Relief (m)‡	Mean Slope (degrees)‡	Mean Annual Precipitation (mm)‡	Mean Annual Temperature (°C)‡	<sup>10</sup> Be (atoms/g x 10 <sup>15</sup> )‡	Model Erosion Rate (m/My)‡
SAP14	BE27734	Savannah	Slope 1	17	358450	3775505	Piedmont	10.0	147	66	1.9	1193	16.0	7.56 ± 0.22	3.98 ± 0.35
SAP28	BE27886	Pee Dee	Slope 1	17	569918	3938304	Piedmont	12.1	199	73	2.3	1151	15.0	14.16 ± 0.33	1.95 ± 0.19
SAP65	BE27900	Chattahoochee	Slope 1	16	702000	3653993	Piedmont	6.2	257	46	2.1	1343	13.0	6.18 ± 0.16	5.56 ± 0.47
SAP02a	BE27675	Roanoke	Slope 2	17	701820	4106283	Piedmont	9.4	160	70	3.4	1095	16.0	4.54 ± 0.15	7.76 ± 0.65
SAP16	BE28704	Savannah	Slope 2	17	331585	3788593	Piedmont	50.1	215	109	2.7	1277	15.1	6.86 ± 0.17	4.74 ± 0.4
SAP37	BE28709	Pee Dee	Slope 2	17	574613	3952647	Piedmont	6.6	243	110	3.6	1150	14.5	12.13 ± 0.28	2.47 ± 0.23
SAP67	BE27902	Chattahoochee	Slope 2	16	699265	3673650	Piedmont	9.1	251	51	2.8	1343	16.0	3.77 ± 0.11	9.77 ± 0.77
SAP01	BE27674	Roanoke	Slope 3	17	691367	4099259	Piedmont	6.8	152	84	4.5	1094	13.0	4.30 ± 0.18	8.19 ± 0.72
SAP15	BE27753	Savannah	Slope 3	17	352900	3765579	Piedmont	7.6	153	76	4.5	1197	16.0	6.38 ± 0.17	4.89 ± 0.42
SAP36	BE27885	Pee Dee	Slope 3	17	553624	3954130	Piedmont	6.4	229	263	4.3	1132	14.0	4.42 ± 0.12	8.13 ± 0.65
SAP68	BE28723	Chattahoochee	Slope 3	16	687113	3676524	Piedmont	22.5	232	270	3.6	1354	16.0	5.13 ± 0.15	6.78 ± 0.56
SAP18	BE27737	Savannah	Slope 4	17	278407	3813393	Piedmont	7.1	254	155	6.7	1423	15.0	2.74 ± 0.08	14.02 ± 1.07
SAP35	BE28708	Pee Dee	Slope 4	17	507157	3980209	Piedmont	7.9	353	494	6.8	1229	13.0	6.38 ± 0.16	5.91 ± 0.49
SAP40	BE28710	Roanoke	Slope 4	17	630642	4091612	Piedmont	12.0	268	297	6.6	1107	12.9	7.40 ± 0.22	4.79 ± 0.42
SAP63	BE27899	Chattahoochee	Slope 4	16	738179	3789130	Piedmont	7.7	364	273	6.7	1463	14.0	3.64 ± 0.10	11.01 ± 0.87
SAP21	BE27740	Savannah	Slope 5	17	280116	3843499	Blue Ridge	8.6	564	359	9.1	1708	12.9	5.23 ± 0.14	8.48 ± 0.69
SAP34	BE28707	Pee Dee	Slope 5	17	517414	4003551	Piedmont	8.8	392	217	8.3	1221	12.9	5.28 ± 0.13	7.44 ± 0.6
SAP49	BE27894	Roanoke	Slope 5	17	611418	4124415	Blue Ridge	13.2	322	279	8.9	1066	12.8	3.78 ± 0.11	12.18 ± 0.96
SAP58	BE27897	Chattahoochee	Slope 5	17	248317	3836400	Piedmont	5.1	560	494	12.4	1673	12.9	3.93 ± 0.13	11.62 ± 0.94
SAP20	BE27759	Savannah	Slope 6	17	278342	3842337	Piedmont	13.3	556	410	10.3	1712	12.8	3.60 ± 0.11	12.21 ± 0.97
SAP33	BE27759	Savannah	Slope 6	17	514252	4026920	Blue Ridge	14.5	438	350	10.5	1189	12.0	6.81 ± 0.17	6.3 ± 0.52
SAP46	BE28712	Roanoke	Slope 6	17	604699	4136157	Blue Ridge	9.5	476	771	11.8	1207	11.7	4.82 ± 0.13	9.25 ± 0.75
SAP31	BE27882	Pee Dee	Slope 7	17	491103	4024602	Blue Ridge	5.8	505	719	12.8	1058	11.8	12.61 ± 0.29	2.78 ± 0.26
SAP44	BE27890	Roanoke	Slope 7	17	600214	4113989	Blue Ridge	7.8	476	771	11.8	1207	11.7	4.82 ± 0.13	9.25 ± 0.75
SAP62	BE27741	Chattahoochee	Slope 7	17	243314	3835541	Blue Ridge	7.8	370	556	8.4	1069	13.0	12.61 ± 0.29	2.78 ± 0.26
SAP29	BE27880	Savannah	Slope 8	17	281314	3860444	Blue Ridge	1.5	657	275	14.1	1762	13.0	3.25 ± 0.09	15.35 ± 1.19
SAP47	BE27880	Pee Dee	Slope 8	17	465837	4004282	Blue Ridge	8.2	585	393	16.5	1295	12.2	3.97 ± 0.10	11.55 ± 0.9
SAP57	BE28719	Roanoke	Slope 8	17	603231	4119416	Blue Ridge	11.6	408	435	15.6	1083	12.2	3.61 ± 0.10	12.18 ± 0.96
SAP24	BE27706	Chattahoochee	Slope 8	17	233326	3837563	Blue Ridge	7.2	567	523	15.4	1640	12.9	3.25 ± 0.09	13.76 ± 1.08
SAP28	BE27706	Savannah	Slope 9	17	267417	3868289	Blue Ridge	17.8	1012	913	21.0	1921	10.3	3.01 ± 0.09	21.26 ± 1.68
SAP43	BE27744	Pee Dee	Slope 9	17	451617	3993805	Blue Ridge	6.7	606	345	19.0	1312	12.0	1.79 ± 0.05	29.07 ± 2.16
SAP61	BE28711	Roanoke	Slope 9	17	559371	4106240	Blue Ridge	5.7	653	363	21.4	1043	11.0	3.45 ± 0.09	15.16 ± 1.17
SAP25	BE28706	Chattahoochee	Slope 9	17	244406	3844786	Blue Ridge	7.3	832	506	19.3	1789	11.3	3.14 ± 0.08	17.89 ± 1.38
SAP30	BE27881	Savannah	Slope 10	17	266494	3874369	Blue Ridge	23.3	1146	927	24.7	1928	10.0	1.44 ± 0.04	50.49 ± 3.78
SAP42	BE27889	Pee Dee	Slope 10	17	486696	4025782	Blue Ridge	21.6	778	709	23.5	1282	10.4	1.84 ± 0.06	32.01 ± 2.43
SAP59	BE28720	Roanoke	Slope 10	17	568451	4114934	Blue Ridge	7.4	627	1072	23.0	1043	11.0	4.88 ± 0.15	10.21 ± 0.84
SAP59	BE28720	Chattahoochee	Slope 10	17	249358	3851716	Blue Ridge	4.6	884	617	23.7	1823	11.1	2.98 ± 0.09	19.66 ± 1.54

\* BE Number denotes the sample identification tag logged during measurement at the Lawrence Livermore National Laboratory.  
† Triamble Basin designates which of the 4 large-scale drainages each small-scale basin sample was collected from.  
‡ Small-scale (~10 km<sup>2</sup>) slope sample basins selected to represent the range of slopes across the Blue Ridge and Piedmont physiographic provinces. Basins from slope divisions 1 through 10 reflect average basin slopes of approximately 2, 3, 4, 5, 6.5, 10, 11, 12, 15, 20, 24 degrees respectively.  
# All GPS locations provided in UTM NAD83 CONUS. Note the change in zone for the southwestmost basin.  
° Province designates whether each of the slope sample basin falls into the higher-slope Blue Ridge or lower-slope Piedmont physiographic province.  
Y All geographic statistics were calculated in ArcGIS® using 1/3 arcsecond (~28m) digital elevation models downloaded from <http://seamless.usgs.gov>.  
φ Mean annual precipitation and temperature data (1 km resolution) from Hijmans, et al., 2005.  
‡ Errors in nuclide concentrations include propagated laboratory and measurement uncertainties. Measured ratios of <sup>10</sup>Be normalized to 07KNSTD3110 standard with reported <sup>10</sup>Be/<sup>9</sup>Be ratio of 2859 x 10<sup>-15</sup> (Nishizumi, et al., 2007).  
& Erosion rates modeled with the CRONUS online calculator (<http://hess.ess.washington.edu/>) using hypsometrically weighted effective ELDs for each basin. Errors are 1 sigma standard deviations.

## CHAPTER 7: CONCLUSIONS AND FUTURE RESEARCH

### 7.1. Summary of findings

Using concentrations of both meteoric  $^{10}\text{Be}$  (produced in the atmosphere and adhered to sediment grains) and *in situ*  $^{10}\text{Be}$  (produced within the mineral lattice of quartz), measured in samples of fluvial sediment collected from river networks draining the tectonically active east coast of New Zealand's North Island, and the southern Appalachian Piedmont draining the North American Atlantic Passive Margin, I have quantified the impacts of human landuse practices on background rates of erosion and the sourcing of sediment carried by these river systems today. While these two study areas represent vastly different geologic, tectonic, and climatic conditions,  $^{10}\text{Be}$  results demonstrate that both landscapes experienced pronounced and pervasive erosional impacts from the clearance of land for agriculture over the past several centuries. During the period of intensive agriculture, the concepts of soil conservation and landscape management did not yet exist. As a result, across both landscapes, the effects of intensive episodes of human landuse in the past are still evident today. Large volumes of legacy sediment stored on the landscapes will take centuries or more for rivers to transport to the sea, and thus must be factored into contemporary land management recommendation and policies.

Several of the most important findings from this research regarding the influence human landuse practices can have on background rates of erosion are as follow:

For the Waipaoa River Basin draining the east coast of New Zealand's North Island:

- I find that concentrations of meteoric  $^{10}\text{Be}$  measured in samples of fluvial sediment can reliably be used to illuminate the contemporary sourcing, movement, and mixing of sediment in a disturbed and rapidly eroding environment across which sediment is non-uniformly sourced from different parts of the landscape.
- Further, I developed a simple mixing model and find that the heavily gullied headwater region of the Waipaoa catchment issues sediment at a rate  $\sim 20$  times that of the more stable eastern and western regions of the basin. In the Waipaoa Basin, the uneven sourcing of sediment is evident to even the casual observer. As such, our study constitutes a proof of concept, and indicates that meteoric  $^{10}\text{Be}$  can be used to estimate the relative contribution of sediment originating from different tributary regions. It therefore is of utility for assessing the relative contributions of sediment from different parts of other landscapes where non-uniform sediment sourcing is not visible to the naked eye.
- We calculate the first robust site-specific long-term accumulation rate of meteoric  $^{10}\text{Be}$  in soil for the Waipaoa region. We use samples collected from the vertical face of a fluvial terrace of known age ( $\sim 18$  ka) to characterize the depth-distribution of meteoric  $^{10}\text{Be}$  and calculate an accumulation rate of  $\sim 1.7 \times 10^6$  at/( $\text{cm}^2 \cdot \text{yr}$ ).

- Using a limited number of *in situ*  $^{10}\text{Be}$  samples, we estimate a background erosion rate for the Waipaoa landscape of  $\sim 300$  m/My, more than 10 times less than the modern rate of sediment yield  $\sim 3$  km/My inferred from contemporary data. Even though our background estimate is uncertain, it emphasizes that modern sediment yield data do not reflect longer-term rates of landscape denudation; the rate of 3 km/My is unsustainable.
- Data presented in chapter 4 have several importation implications. In rapidly eroding environments, measurements of  $^{10}\text{Be}$  may not be interpretable as any meaningful measure of surface process rates. However, even in one of the most rapidly eroding and stochastic natural environments, through repeated sampling, patterns and changes in concentration do emerge through time. This perhaps constitutes the next step for  $^{10}\text{Be}$  in such environments. That is, rather than cosmogenic isotopes being used to quantify process rates, they instead be used to detect temporal changes in isotope concentrations and thus track changing source areas of sediment fluxing through fluvial system as a function of climatic and hydrologic events and conditions.

For the southern Appalachian Piedmont draining the North American Atlantic passive margin:

- Our *in situ*  $^{10}\text{Be}$  results suggest that, on average, the subdued southern Piedmont naturally erodes at a rate of  $\sim 9$  m/My over millennial time scales.

The higher slopes of the Blue Ridge province naturally erode more quickly (~14 m/My).

- When compared to data presented in Trimble (1977), my *in situ*  $^{10}\text{Be}$  results suggest that rates of hillslope erosion outpaced rates of long-term background erosion by more than 100-fold at the time of peak agricultural disturbance in the early 1900's.
- Long-term background  $^{10}\text{Be}$  rates indicate that at the time of peak agricultural disturbance, large rivers draining the Piedmont were incapable of transporting the vast quantities of sediment fed to them from the rapidly eroding hillslopes. This finding further supports the notion that because the majority of the sediment eroded during the agricultural period is stored on the landscape even today, sediment loads carried by large rivers draining the southern Piedmont will likely remain elevated above their pre-disturbance levels for the foreseeable future.
- We provide quantitative evidence that dams along the rivers draining the southern Piedmont substantially affect the concentrations of *in situ*  $^{10}\text{Be}$  measured in samples collected downstream of them. When modeled as erosion rates, the samples collected downstream of dams consistent yield higher erosion rates relative to their upstream counterparts. Because the dams impede the flow of sediment, the material sampled downstream is most likely sourced locally from bank material or saprolite representing a range of depths below the landscape surface. As a result, these downstream samples are not

representative of the long-term erosion of upstream drainage basins. This is an issue that has never been addressed explicitly in *in situ*  $^{10}\text{Be}$  background erosion rate studies.

- Because sampling strategies were carefully designed to be statistically robust,  $^{10}\text{Be}$  results accurately characterize background erosion rates at the landscape-scale. As a result, I generate dependable predictive models of background erosion. The  $E_{ps}$  model, being fully scalable, is capable of predicting a background erosion rate at any point along a river network across the entire southern Piedmont without  $^{10}\text{Be}$  data. These models could prove valuable for establishing TMDL values for sediment loads and pollutant associated with sediment transported by rivers.

## 7.2. Suggestion for future research

Because I returned to the Waipaoa River Basins on three separate occasions over the course of my dissertation work, I have a series of temporal replicates that is more comprehensive than for virtually any other region characterized with either meteoric or *in situ*  $^{10}\text{Be}$ . To more robustly investigate the spatial and temporal variability in concentration of meteoric  $^{10}\text{Be}$  from river sediment, a possible future research project could entail establishing a set of “reference” collection points along tributary streams that represent different erosional styles, as well as at several points along the mainstem channel to investigate how sediments from different regions mix. Sediment samples could then be collected on an annual basis to investigate the year-to-year differences in

$^{10}\text{Be}$  to discern the sourcing and mixing sediment through time. In addition, sediment samples could be collected to represent a range flow conditions (particularly extreme flows vs. baseflow) to hopefully determine the precipitation levels required to trigger shallow landslides. Gullies in the northern headwaters continually supply large volumes of deeply sourced sediment containing low concentrations of  $^{10}\text{Be}$  that overwhelm the sediment carried down the mainstem channel of the Waipaoa River. Conversely, erosion in the more stable eastern and western region of the basin is dominated by hydrologically triggered shallow landsliding. Sampling across the flow frequency distribution could establish at what point (at what precipitation and antecedent landscape conditions) these regions begin feeding appreciable amount of sediment to the mainstem channel.

To better constrain the variability in long-term accumulation rates of meteoric  $^{10}\text{Be}$ , similar studies such as the one I conducted in the Waipaoa, could be done elsewhere around the globe.

The predictive erosion models I generated for the southern Appalachian Piedmont can be tested. A simple and quick way of testing their applicability would be to return to the Lloyd Shoals Reservoir (Meade and Trimble, 1974) where the effects of careful soil conservation and reforestation efforts have already been quantified. Results from this work demonstrate that stabilizing hillslopes in this small basin reduced the sediment loads by nearly 7-fold inferring a modern rate of  $\sim 10$  m/My, in good agreement with our  $^{10}\text{Be}$  rate of  $\sim 9$  m/My across the entire Piedmont suggesting that the conservation efforts in this watershed were effective. The average basin slope of the contributing area above the reservoir could be generated relatively easily with hydrology modeling tools in

ArcGIS™ and the DEM of the area, and the slope-based predictive model could be applied to predict a background erosion rates. There is no concrete rational to expect the long-term predicted <sup>10</sup>Be model-based background rate to match exactly the short-term sediment yield inferred erosion rate for a rehabilitated basin, but the comparison would be informative none the less.

Because our data suggest that sediment samples collected immediately downstream of large dams may reflect the dosing history of locally sourced material as opposed the entire contributing upstream drainage basin, researchers should instead look to the where the eroded material is current stored; look to sediments deposited in the reservoirs. These sediments presumably record a stratigraphic history of upstream erosion and deposition within the dam reservoir (with the oldest sediment at the bottom of the stack and the youngest at the top); drilling a sediment core into these sediments could yield the best estimate of the exposure history and background erosion rate of the entire upstream landscape. The most appropriate location for such a core will probably need to be carefully chosen to optimize for the best-preserved sediment package of a coarse enough grain size to survive the sample processing before <sup>10</sup>Be measurement. Unfortunately, because most of these large dams contain <100 years of accumulated sediment, quantifying changes in exposure history through time (from the bottom to the top of the core) most likely will not be possible and the best approach would be to aggregate the entire core into one representative average sample for <sup>10</sup>Be measurement.

Over longer time frames, depositional terraces standing above the modern river channels could be used to detect changes in the exposure history and background erosion

rates for these large Piedmont streams. In conjunction with *in situ*  $^{10}\text{Be}$  measurements (providing approximates for background erosion through time), measurements of  $^{14}\text{C}$  within organic material or OSL dosing of nearby sediments could help constrain the terraces ages provided that they are older enough that the modern channel (typically at least several hundred years).

Finally, employing carefully planned sampling strategies designed to be representative of the distribution of landscape characteristics, such as I have done for the southern Piedmont, in other regions around the world is the next step to take. The southern Piedmont constitutes a relatively stable and predictable landscape. Future efforts should ideally utilize similar strategies in more extreme and unpredictable environments to establish the boundaries of this approach.

## COMPREHENSIVE BIBLIOGRAPHY

- Ahnert, F., 1970, Functional relationships between denudation, relief, and uplift in large mid-latitude drainage basins: *American Journal of Science*, v. 268, p. 243-263.
- Allsop, F., 1973, *The Story of Mangatu: the forest which healed the land*, Wellington, New Zealand, New Zealand Forest Service, 99 p.:
- Balco, G., Stone, J., Lifton, N. A., and Dunai, T. J., 2008, A complete and easily accessible means of calculating surface exposure ages or erosion rates from  $^{10}\text{Be}$  and  $^{26}\text{Al}$  measurements: *Quaternary Geochronology*, v. 3, no. 3, p. 174-195.
- Berryman, K. R., Marden, M., Eden, D., Mazengarb, C., Ota, Y., and Moriya, I., 2000, Tectonic and paleoclimatic significance of Quaternary river terraces of the Waipaoa River, East Coast, North Island, New Zealand, *in* Anonymous, ed., *Proceedings of the 9th Australia New Zealand Geomorphology Group (ANZGG) conference; programme and abstracts*, Publisher Australia New Zealand Geomorphology Group, New Zealand, p. 5.
- Bierman, P., Larsen, P., Clapp, E., and Clark, D., 1996, Refining Estimates of  $^{10}\text{Be}$  and  $^{26}\text{Al}$  Production Rates: *Radiocarbon*, v. 38, no. 1, p. 149-173.
- Bierman, P., and Steig, E., 1996, Estimating rates of denudation and sediment transport using cosmogenic isotope abundances in sediment: *Earth Surface Processes and Landforms*, v. 21, p. 125-139.
- Black, R. D., 1980, Upper Cretaceous and Tertiary geology of Mangatu State Forest, Raukumara Peninsula, New Zealand: *New Zealand Journal of Geology and Geophysics*, v. 23, p. 293-312.
- Brown, E. T., Stallard, R. F., Larsen, M. C., Bourles, D. L., Raisbeck, G. M., and Yiou, F., 1995a, Pre-anthropogenic denudation rates of a perturbed watershed (Cayaguas, Puerto Rica) estimated from in situ-produced  $^{10}\text{Be}$  in river borne quartz: *EOS*, v. 76, no. 46.
- Brown, E. T., Stallard, R. F., Larsen, M. C., Raisbeck, G. M., and Yiou, F., 1995b, Denudation rates determined from the accumulation of in situ-produced  $^{10}\text{Be}$  in

- the Luquillo Experimental Forest, Puerto Rico: *Earth and Planetary Science Letters*, v. 129, p. 193-202.
- Brown, L. J., Pavich, M., Hickman, R. E., Klein, J., and Middleton, R., 1988, Erosion in the eastern United States observed with  $^{10}\text{Be}$ : *Earth Surface Processes and Landforms*, v. 13, p. 441-457.
- Brune, G., 1953, Trap efficiencies of reservoirs: *American Geophysical Union Transactions*, v. 34, p. 407-418.
- Caine, N., 1980, The rainfall intensity: Duration control of shallow landslides and debris flows: *Geografiska Annaler. Series A, Physical Geography*, v. 62A, no. 1-2, p. 23-27.
- Clapp, E. M., Bierman, P. R., Schick, A. P., Lekack, J., Enzel, Y., and Caffee, M., 2000, Sediment yield exceeds sediment production in arid region drainage basins: *Geology*, v. 28, no. 11, p. 995-998.
- Corbett, L. B., Young, N. E., Bierman, P., Briner, J. P., Neumann, T. A., Rood, D., and Graly, J., 2011, Paired bedrock and boulder  $^{10}\text{Be}$  concentrations resulting from early Holocene ice retreat near Jakobshavn Isfjord, western Greenland: *Quaternary Science Reviews*, v. 30, p. 1739-1749.
- Costa, J. E., 1975, Effects of agriculture on erosion and sedimentation in the Piedmont province, Maryland: *Geological Society of America Bulletin*, v. 86, p. 1281-1286.
- Cox, R., Bierman, P., and Jungers, M., 2009a, Erosion rates and sediment sources in Madagascar inferred from  $^{10}\text{Be}$  analysis of lavaka, slope, and river sediment: *Journal of Geology*, v. 117, p. 363-376.
- Cox, R., Bierman, P., Jungers, M., and Rakotondrazafy, A. F. M., 2009b, Erosion rates and sediment sources in Madagascar inferred from  $^{10}\text{Be}$  analysis of lavaka, slope, and river sediment: *Journal of Geology*, v. 117, no. 4, p. doi: 10.1086/598945.
- Crosby, B. T., and Whipple, K. X., 2006, Knickpoint migration and distribution within fluvial networks: 236 waterfalls in the Waipaoa River, North Island, New Zealand: *Geomorphology*, v. 82, p. 16-38.
- Davis, W. M., 1889, The rivers and valleys of pennsylvania: *National Geographic Magazine*, v. 1, no. 3, p. 183-253.

- Dole, R. G., and Stabler, H., 1909, Denudation, Papers on the Conservation of Water Resources: U.S. Geological Survey Water-Supply Paper 234, p. 78-93.
- Duxbury, J., 2009, Erosion rates in and around Shenandoah National Park, VA determined using analysis of cosmogenic  $^{10}\text{Be}$  [Masters of Science: University of Vermont, 123 p.
- Eden, D., Palmer, A. N., Cronin, S. J., Marden, M., and Berryman, K. R., 2001, Dating the culmination of river aggradation at the end of the last glaciation using distal tephra compositions, eastern North Island, New Zealand: *Geomorphology*, v. 38, no. 1-2, p. 133-151.
- Elmore, D., and Phillips, F. M., 1987, Accelerator mass spectrometry for measurement of long-lived radioisotopes: *Science*, v. 236, p. 543-550.
- England, P., and Molnar, P., 1990, Surface uplift, uplift of rocks, and exhumation of rocks: *Geology*, v. 18, p. 1173-1177.
- Froggatt, P. C., and Lowe, D., 1990, A review of late quaternary silicic and some other tephra formations from New Zealand: their stratigraphy, nomenclature, distribution, volume, and age: *New Zealand Journal of Geology and Geophysics*, v. 33, p. 89-109.
- Gomez, B., Banbury, K., Marden, M., Trustrum, N. A., Peacock, D., and Hoskin, P., 2003, Gully erosion and sediment production: Te Weraroa Stream, New Zealand: *Water Resources Research*, v. 39, no. 7, p. ESG 3-1 to ESG 3-7.
- Gosse, J., and Phillips, F. M., 2001, Terrestrial *in situ* cosmogenic nuclides: theory and applicaiton: *Quaternary Science Reviews*, v. 20, p. 1475-1560.
- Graly, J., Bierman, P., and Reusser, L. J., 2010, Meteoric  $^{10}\text{Be}$  in soil profiles - A global meta-analysis: *Geochimica et Cosmochimica Acta*, v. 74, p. 6814-6829.
- Granger, D. E., Kirchner, J. W., and Finkel, R., 1996, Spatially averaged long-term erosion rates measured from in situ-produced cosmogenic nuclides in alluvial sediments: *Journal of Geology*, v. 104, no. 3, p. 249-257.
- Granger, D. E., Lifton, L. A., and Willenbring, J. K., 2013, A cosmic trip: 25 years of cosmogenic nuclides in geology: *GSA Bulletin*, p. doi: 10.1130/B30774.30771.

- Harris, S. E., and Mix, A. C., 2002, Climate and tectonic influences on continental erosion of tropical South America, 0-13 Ma: *Geology (Boulder)*, v. 30, no. 5, p. 447-450.
- Hatcher, R. D., 1978, Tectonics of the western Piedmont and Blue Ridge, southern Appalachians; review and speculation: *American Journal of Science*, v. 278, no. 3, p. 276-304.
- Hessell, J. W., 1980, The climate and weather of the Gisborne region: New Zealand Meteorological Service, Misc. Publ, v. 115, p. 29p.
- Hicks, D. M., Gomez, B., and Trustrum, N. A., 2000, Erosion thresholds and suspended sediment yields, Waipaoa River Basin, New Zealand: *Water Resources Research*, v. 36, no. 4, p. 1129-1142.
- Hooke, R. L., 1994, On the efficacy of humans as geomorphic agents: *GSA Today*, v. 4, no. 9, p. 224-225.
- , 2000, On the history of humans as geomorphic agents: *Geology*, v. 28, no. 9, p. 843-846.
- Judson, S., and Ritter, D., 1964, Rates of regional denudation in the United States: *Journal of Geophysical Research*, v. 69, no. 16, p. 3395-3401.
- Jungers, M., Bierman, P., Matmon, A. S., Nichols, K. K., Larsen, J., and Finkel, R., 2009, Tracing hillslope sediment production and transport with *in situ* and meteoric <sup>10</sup>Be: *Journal of Geophysical Research - Earth Surface*, v. 114, F04020, doi: 10.1029/2008FJ001086.
- Kettner, A. J., Gomez, B., and Syvitski, J. P. M., 2007, Modeling suspended sediment discharge from the Waipaoa River system, New Zealand: The last 3000 years: *Water Resources Research*, v. 43, no. W07411, p. doi: 10.1029/2006WR005570.
- Kirchner, J. W., Finkel, R., Reibe, C., Granger, D. E., Clayton, J., King, J., and Megahan, W., 2001, Mountain erosion over 10 yr, 10 k.y., and 10 m.y. time scales: *Geology*, v. 29, no. 7, p. 591-594.

- Kohl, C. P., and Nishiizumi, K., 1992, Chemical isolation of quartz for measurement of in-situ-produced cosmogenic nuclides: *Geochimica et Cosmochimica Acta*, v. 56, p. 3583-3587.
- Lal, D., 1991, Cosmic ray labeling of erosion surfaces; *in situ* nuclide production rates and erosion models: *Earth and Planetary Science Letters*, v. 104, no. 2-4, p. 424-439.
- Lal, D., and Peters, B., 1967, Cosmic ray produced radioactivity on the Earth, *in* Sitte, K., ed., *Handbuch der Physik*: New York, Springer-Verlag, p. 551-612.
- Marden, M., 2004, Future-proofing erosion-prone hill country against soil degradation and loss during large storm events: have past lessons be heeded?: *NZ Journal of Forestry*, p. 11-16.
- Marden, M., Arnold, G., Gomez, B., and Rowan, D., 2005, Pre- and post-reforestation gully development in Mangatu Forest, East Coast, North Island, New Zealand: *River Research and Applications*, v. 21, p. 757-771.
- Marden, M., Betts, H., Arnold, G., and Hambling, R., Gully erosion and sediment load: Waipaoa, Waiapu and Uawa rivers, eastern North Island, New Zealand, *in* *Proceedings Sediment Dynamics in Changing Environments 2008*, Volume 325, IAHS, p. 339-350.
- Matmon, A., Bierman, P., and Enzel, Y., 2002, Pattern and tempo of great escarpment erosion: *Geology*, v. 30, no. 12, p. 1135-1138.
- Matmon, A., Bierman, P., Larsen, J., Southworth, S., Pavich, M., and Caffee, M., 2003a, Temporally and Spatially Uniform Rates of Erosion in the Southern Appalachian Great Smokey Mountains: *Geology*, v. 31, no. 2, p. 155-158.
- Matmon, A., Bierman, P. R., Larsen, J., Southworth, S., Pavich, M., Finkel, R., and Caffee, M., 2003b, Erosion of an ancient mountain range, the Great Smoky Mountains, North Carolina and Tennessee: *American Journal of Science*, v. 303, no. 10, p. 972-973.
- Mazengarb, C., and Speden, I., 2000, *Geology of the Raukumara Area, Map 6*: Institute of Geological & Nuclear Sciences, 1 sheet 1:250,000, 260 pp, scale 1:250,000.

- Meade, R. H., 1969, Errors in using modern stream-load data to estimate natural rates of denudation: Geological Society of America Bulletin, v. 80, p. 1265-1274.
- Meade, R. H., 1982, Sources, sinks and storage of river sediment in the Atlantic drainage of the United States: Journal of Geology, v. 90, p. 235-252.
- Meade, R. H., and Trimble, S. W., 1974, Changes in sediment loads in rivers of the Atlantic drainage of the United States since 1900, Effects of Man on the Interface of the Hydrological Cycle with the Physical Environment, Volume Hydrol. Pub. 113, Internat. Assoc. Sci., p. 99-104.
- Menard, H. W., 1961, Some rates of regional erosion: Journal of Geology, v. 69, p. 154-161.
- Merchel, S., Arnold, M., Aumaitre, G., Benedetti, L., Boules, D. L., Braucher, R., Alfimov, V., Freeman, S., Steier, P., and Wallner, A., 2008, Toward more precise  $^{10}\text{Be}$  and  $^{36}\text{Cl}$  data from measurements at the  $10^{-14}$  level: influence of sample preparation: Nuclear Instruments and Methods in Physics Research B, v. 266, p. 4921-4926.
- Milliman, J., and Meade, R. H., 1983, World-wide delivery of river sediment to the oceans: The Journal of Geology, v. 91, no. 1, p. 1-21.
- Molnar, P., and England, P., 1990, Late Cenozoic Uplift of Mountain Ranges and Global Climate Change: Chicken or Egg?: Nature, v. 356, p. 29-34.
- Monaghan, M. C., Krishnaswami, S., and Turekian, K. K., 1986, The global-average production rate of  $^{10}\text{Be}$ : Earth and Planetary Science Letters, v. 76 (1985/86), p. 279-287.
- Montgomery, D. R., 1994, Valley incision and the uplift of mountain peaks: Journal of Geophysical Research, v. 99, no. B7, p. 13913-13921.
- National Research Council, 2010, Landscapes on the edge: New horizons for research on Earth's surface: The National Academies Press: National Research Council.

- Neary, D. G., Swift, L. W. J., Manning, D., and Burns, R. G., 1986, Debris avalanching in the Southern Appalachians; An influence on forest soil formation: *Soil Science Society of American Journal*, v. 50, p. 465-471.
- Niemi, N., Oskin, M., Burbank, D. W., Heimsath, A. M., and Gabet, E., 2005, Effects of bedrock landslides on cosmogenically determined erosion rates: *Earth and Planetary Science Letters*, v. 237, no. 3-4, p. 480-498.
- Nishiizumi, K., Imamura, M., Caffee, M., Southon, J., Finkel, R., and McAninch, J., 2007, Absolute calibration of  $^{10}\text{Be}$  AMS standards: *Nuclear Instruments and Methods in Physics Research B*, v. 258, p. 403-413.
- Nyffeler, U. P., Li, Y.-H., and Santschi, P. H., 1984, A kinetic approach to describe trace-element distribution between particles and solution in natural aquatic systems: *Geochemica et Cosmochemica Acta*, v. 48, p. 1513-1522.
- Pavich, M., Brown, E. T., Klein, J., and Middleton, R., 1984, Beryllium-10 accumulations in a soil chronosequence: *Earth and Planetary Science Letters*, v. 69, p. 198-204.
- Pavich, M., Brown, L. J., Harden, J., Klein, J., and Middleton, R., 1986,  $^{10}\text{Be}$  distributions in soils from Merced River terraces, California: *Geochemica et Cosmochemica Acta*, v. 50, p. 1727-1735.
- Pavich, M. J., Brown, L., Valette-Silver, J.N., Klein, J. & Middleton, R., 1985,  $^{10}\text{Be}$  analysis of a Quaternary weathering profile in the Virginia piedmont: *Geology*, v. 13, p. 39-41.
- Phillips, J. D., 1992, The source of alluvium in large rivers of the lower Coastal Plain of North Carolina: *Catena*, v. 19, p. 59-75.
- Phillips, J. D., 2003, Alluvial storage and the long-term stability of sediment yields: *Basin Research*, v. 15, p. 153-163.
- Phillips, J. D., 2006, Residence time of alluvium in an aggrading fluvial system: *Earth Surface Processes and Landforms*, v. 32, p. 307-316.
- Portenga, E. W., and Bierman, P. R., 2011, Understanding Earth's eroding surface with  $^{10}\text{Be}$ : *GSA Today*, v. 21, no. 8, p. doi: 10.1130.

- Reid, L. M., and Page, M. J., 2002, Magnitude and frequency of landsliding in a large New Zealand catchment: *Geomorphology*, v. 49, p. 71-88.
- Reusser, L. J., and Bierman, P., 2010, Using meteoric  $^{10}\text{Be}$  to track fluvial sand through the Waipaoa River basin, New Zealand: *Geology*, v. 38, no. 1, p. 47-50.
- Reusser, L. J., Graly, J., Bierman, P., and Rood, D., 2010, Calibrating a long-term meteoric  $^{10}\text{Be}$  accumulation rate in soil: *Geophysical Research Letters*, v. 37, no. 19, p. DOI: 10.1029/2010GL044751.
- Riebe, C. S., Kirchner, J. W., Granger, D. E., and Finkel, R. C., 2000, Erosional equilibrium and disequilibrium in the Sierra Nevada, inferred from cosmogenic  $^{26}\text{Al}$  and  $^{10}\text{Be}$  in alluvial sediment: *Geology*, v. 28, no. 9, p. 803-806.
- Safran, E. B., Bierman, P., Aalto, R., Dunne, T., and Whipple, K. X., 2005, Erosion rates driven by channel network incision in the Bolivian Andes: *Earth Surface Processes and Landforms*, v. 30, p. 1007-1024.
- Schaller, M., Blanckenburg, F. v., Hovius, N., and Kubik, P., 2001, Large-scale erosion rates from in situ-produced cosmogenic nuclides in European river sediments: *Earth and Planetary Science Letters*, v. 188, p. 441-458.
- Stone, J., 1998, A rapid fusion method for separation of beryllium-10 from soils and silicates: *Geochemica et Cosmochemica Acta*, v. 62, no. 3, p. 555-561.
- Stuiver, M., and Reimer, P. J., 1993, Extended  $^{14}\text{C}$  database and revised CALIB 3.0  $^{14}\text{C}$  age calibration program: *Radiocarbon*, v. 35, p. 215-230.
- Sullivan, C., 2007,  $^{10}\text{Be}$  erosion rates and landscape evolution of the Blue Ridge Escarpment, southern Appalachian Mountains [Masters of Science: University of Vermont, 66 p.
- Sullivan, C., Bierman, P., Pavich, M., Larsen, J., and Finkel, R., 2006, Cosmogenically derived erosion rates for the Blue Ridge Escarpment, southern Appalachian Mountains: *Geological Society of America - Abstracts with Programs*, v. 38, no. 7, p. 279.
- Syvitski, J. P. M., Vorosmarty, C. J., Kettner, A. J., and Green, P., 2005, Impact of Humans on the flux of Terrestrial Sediment to the Global Coastal Ocean: *Science*, v. 308, p. 376-380.

- Team, W. C. S. P., 1994a, Waipaoa Catchment Study: Literature Review, Palmerston North, Manaaki Whenua-Landcare Research.
- Trimble, S. W., 1974, Man-induced soil erosion on the Southern Piedmont 1700-1970: Soil Conservation Society of America, p. 180.
- Trimble, S. W., 1975, A volumetric estimate of man-induced erosion on the Southern Piedmont, *in* Agr., U. S. D., ed., Volume Present and Prospective Technology for Predicting Sediment Yields and Sources: Fort Worth, p. 142-154.
- Trimble, S. W., 1977, The fallacy of stream equilibrium in contemporary denudation studies: *American Journal of Science*, v. 277, p. 876-887.
- Trimble, S. W., and Crosson, P., 2000, U.S. soil erosion rates - Myth and reality: *Science*, v. 289, p. 248-250.
- Trodick, 2011, *in situ* and meteoric  $^{10}\text{Be}$  concentration of fluvial sediment collected from the Potomac River Basin [Masters: University of Vermont, 203 p.
- Usoskin, I. G., and al, e., 2005, Heliospheric modulation of cosmic rays: monthly reconstruction for 1951-2004: *Journal of Geophysical Research*, v. 110, p. A12108.
- Valette-Silver, J. N., Brown, L., Pavich, M. J., Klein, J., and Middleton, R., 1986, Detection of erosion events using  $^{10}\text{Be}$  profiles; example of the impact of agriculture on soil erosion in the Chesapeake Bay area (U.S.A.): *Earth and Planetary Science Letters*, v. 80, no. 1-2, p. 82-90.
- von Blackenburg, F., Hewawasam, T., and Kubik, P., 2004, Cosmogenic nuclide evidence for low weathering and denudation in the wet, tropical highlands of Sri Lanka: *Journal of Geophysical Research*, v. 109, p. 1-22.
- Walling, D. E., 1983, The sediment delivery problem: *Journal of Hydrology*, v. 65, p. 209-237.
- Walling, D. E., 1999, Linking land use, erosion and sediment yields in river basins: *Hydrobiologia*, v. 410, p. 223-240.

- Walling, D. E., Collins, A. L., and Sickingabula, H. M., 2003, Using unsupported lead-210 measurements to investigate soil erosion and sediment delivery in a small Zambian catchment: *Geomorphology*, v. 52, p. 193-213.
- Walter, R., and Merritts, D. J., 2008, Natural Streams and Legacy of Water-Powered Mills: *Science Magazine*, v. 319, no. 5861, p. 299-304.
- Whiting, P. J., 2006, Estimating TMDL background suspended sediment loading to Great Lake tributaries from existing data: *Journal of American Water Resources Association*, v. 42, no. 3, p. 769-776.
- Wilkinson, B. H., and McElroy, B. J., 2007, The impact of humans on continental erosion and sedimentation: *GSA Bulletin*, v. 119, no. 1.2, p. 140-156.
- Willenbring, J. K., and von Blackenburg, F., 2010, Meteoric cosmogenic Beryllium-10 adsorbed to river sediments and soil: Applications for Earth-surface dynamics: *Earth Science Reviews*, v. 98, p. 105-122.
- Wolman, G. M., 1967, A cycle of sedimentation and erosion in urban river channels: *Geografiska Annaler*, v. 49A, p. 385-395.
- Wolman, M. G., and Miller, J. P., 1960, Magnitude and frequency of forces in geomorphic processes: *Journal of Geology*, v. 68, no. 1, p. 54-74.
- You, C.-F., Lee, T., and Li, Y.-H., 1989, The partition of Be between soil and water: *Chemical Geology*, v. 77, no. 2, p. 105-118.
- Zhou, W., Priller, A., Beck, J. W., Zhengkun, W., Maobai, C., Zhisheng, A., Kutschera, W., Feng, X., Huagui, Y., and Lin, L., 2007, Disentangling geomagnetic and precipitation signals in a 80-kyr Chinese loess record of  $^{10}\text{Be}$ : *Radiocarbon*, v. 49, no. 1, p. 139-160.